Master's thesis

NTNU
Norwegian University of Science and Technology
Faculty of Engineering
Department of Geoscience and Petroleum

Ingeborg Pedersen Reigstad

# An investigation of sediment gravity flow deposits in a Mesozoic flood-dominated delta, Møre Margin, Norway

Master's thesis in Geology
Supervisor: Maarten Felix
December 2022

NTNU
Norwegian University of
Science and Technology

Ingeborg Pedersen Reigstad

# An investigation of sediment gravity flow deposits in a Mesozoic flood-dominated delta, Møre Margin, Norway

Master's thesis in Geology
Supervisor: Maarten Felix
December 2022

Norwegian University of Science and Technology
Faculty of Engineering
Department of Geoscience and Petroleum

NTNU
Norwegian University of
Science and Technology

# Abstract

The easternmost part of the Møre Margin was subject to extensive fault block rotation and faulting during the Mesozoic. As a result of this, coarse grained fan deltas developed in shallow water basins in the area. In 1988, IKU drilled four shallow stratigraphic cores through one of these shallow water deltas of uppermost Triassic to upper Cretaceous age off the coast of Kristiansund, at the Møre Margin. The deltaic deposits of core 6206/02-U-01 were found to contain sediment gravity deposits (turbidites and debrites). These deposits have been re-evaluated in this work based on newer understanding of flow processes developed in the decades since the original investigation.

Through logging of the cores, optical microscopy of 22 petrographic thin sections, and element measurements at 10 cm intervals using a portable XRF, an improved interpretation of the delta evolution and the relevant processes is proposed.

Low density turbidity currents, high density turbidity currents, mudflows, grain flows, slumping, dense to dilute flows, hybrid event flows and hyperpycnal flows are all described and interpreted in a flood-dominated deltaic setting. The flow transformation processes described in this work include dense to dilute flow transformation and hybrid event transformation.

A decrease in fluvial input through time is interpreted based on the lack of event beds and a decrease in concentrations of elements used as proxies to indicate terrestrial input, above 98.3 m depth. It is found that the sediment gravity flows and flow transformation processes are directly linked to fluvial input in this type of delta.

In the literature, hybrid beds are only documented in mid- to distal fan systems, but this work has shown that such beds can be found in deltaic deposits too. Evolution of hyperpycnal flows by either entrainment of mud from the seafloor or deceleration of muddy hyperpycnal flows are proposed to explain the formation of hybrid beds in a deltaic setting.

# Sammendrag

Den østligste delen av Møre-Marginen gjennomgikk utbredt forkastningsasktivitet og blokkrotasjon i løpet av mezosoikum. Det utviklet seg grovkornede viftedeltaer i grunne sedimentbasseng. I 1988 gjennomførte Institutt for kontinentalsokkelundersøkelser (IKU) fire grunne boringer av grunnmarine delta sørvest for Kristiansund, hvor de penetrerte et delta med avsetninger fra tidligste trias til eldre kritt. Kjerne 6206/02-U-01 vil være fokuset i denne avhandlingen.

En oppdatert tolkning av deltautviklingen og de relevante strømningsprosessene presenteres basert på logging av kjernen, optisk mikroskopering av 22 petrografiske tynnslip, samt grunnstoffsmålinger ved bruk av pXRF i 10 cm intervaller.

Turbidittstrømmer, debrisstrømmer, leirstrømmer, kornstrømmer (grain flows), slumping, «dense to dilute» strømmer, hybridavsetninger og hyperpyknale strømmer er beskrevet og tolket i et flom-dominert delta. Strømningstransformasjonene som beskrives i denne studien inkluderer strømingstransformasjon for «dense to dilute» strøm og hybridavsetninger.

Det observeres en nedgang i fluvial innvirkning over tid, basert på fraværet av hendelsesstrømmer, samt at de kontinentalt deriverte proksiene viser en reduksjon i konsentrasjon over 98.3 m. Resultatene viser at sedimentgravitasjonsstrømmene og strømningstransformasjon er direkte relatert til fluvial input i denne typen delta.

Tidligere har hybridavsetninger kun vært dokumenterte i midt- til distale viftesystemer. Denne studien viser at slike avsetninger også kan oppstå i deltaer. Utviklingen av hyperpyknale strømmer, enten ved inkorporering av leire erodert fra havbunnen, eller deakselerasjonen av leirholdige hyperpyknale strømmer, er her foreslått som forklaringer på dannelsen av hybridavsetninger i et delta.

.

# Acknowledgements

This thesis marks the end of my MSc degree at the Norwegian University of Science and Technology. The work was carried out with vital support and guidance from my supervisor Maarten Felix at the Norwegian University of Science and Technology (NTNU). After a rollercoaster concerning results, motivation, and my health, I am relieved and happy that everything came together in the end.

Maarten, I am thankful for your patience, humour, and ability to change plans when things don't go as we thought they would. Where others grow tired of their thesis, you have let me evolve my project into something of my own, and for that, I am grateful. With your feedback and reassuring words, I am happy with the result and proud of what we managed to present.

I want to thank Atle Mørk for his help and guidance and for making me coffee at Dora, and Mai-Britt Mørk for input on my project, access to thin sections, and her willingness to share her knowledge on clays. I would also like to thank the friendly people at Berglaboratoriet who helped me figure out the pXRF. I would also thank my fellow geostudents at NTNU for lifting my spirits, long coffee breaks, and endless laughs through these past five years.

My time as a student in Trondheim would not have been the same without Symforch and Salongorkesteret. My fellow musicians have given me a much-needed distraction from my studies, and we have created wonderful moments and memories over the past five years.

I want to thank my family for believing in me, giving me feedback, and always ensuring I kept my head above water.

Finally, I would like to thank Ola for supporting me through the ups and downs and always being there for me.

# Table of Contents

# List of Figures

# List of Tables

# 1 Introduction

Since the 1960s, multiple types of sediment gravity currents have been defined, such as the Bouma sequence (Bouma, 1962; Allen, 1985), Lowe's high density turbidity current sequence (Lowe, 1982) and the hybrid event bed sequence (Haughton et al., 2009), which are now well recognized in the research community. Haughton et al. (2009) describe hybrid beds as flows which show transformation from turbulent flows to a cohesive, laminar flow. Felix and Peakall (2006) describe dense to dilute flow transformation as laminar flows transforming into turbulent flows through dilution.

Some bed types are confined to a specific depth interval, e.g., hybrid event beds, while others, such as turbidites are known to occur at different depths. The established interpretation of hybrid beds is as distal fan deposits (Fonnesu et al., 2018; Haughton et al., 2009; Pierce et al., 2017; Talling, 2013) or mid-fan (Fonnesu et al., 2018; Hussain et al., 2020) deposits in a larger, deeper marine environment. For a hybrid bed to form, the flow must have travelled a significant distance to either erode enough mud or slow down enough for the flow to transform (Haughton et al., 2009). Since the recognition of hybrid bed as an established sequence, the deposit has been used as an indication for mid- to distal fan environments. Deltaic deposits show a great variety of sediment gravity flows, which have been investigated thoroughly over the past decades. However, hybrid beds have not been described in deltaic deposits.

Preliminary investigation of core 6206/02-U-01 indicated hybrid beds and other signs of flow transformations in deposits described by Smelror et al. (1994) as deltaic. Smelror et al. (1994) suggest a distal fan delta overlain by prodelta deposits and open marine, outer shelf deposits. They describe the deposits as debrites and turbidites. In the decades since this work was done, different types of gravity flows deposits have been recognised and the core is re-evaluated based on these newer works.

This thesis is a thorough investigation of core 6206/02-U-01 from the Møre Margin, southwest of Kristiansund (figure 1). The core penetrated lower Jurassic sediments, overlain by the lower Cretaceous Lange formation and the upper Cretaceous Kvitnos formation (Smelror et al., 1994). The core was one of four cores drilled by IKU (later renamed Sintef) in 1988, and Smelror et al. (1994) gave a thorough description of the cores and the depositional environment and dating of the core.

In the current work, the core was investigated using logging, thin sections and pXRF analysis. The latter method gives the opportunity to see changes in 40 chemical elements

in the sediments. These elements can be used as proxies for environmental changes, e.g., terrestrial input or lack thereof, oxygen conditions and palaeoproductivity. All these environmental indicators contribute to the determination of the dominance of fluvial versus marine processes.

The aim of this study is to get a deeper understanding of the different flow processes and their depositional environments and the evolution of the delta in question.

# 2 Background

## 2.1 Geological background

The Møre Basin is situated off the coast of the north-western part of the Norwegian coastline (see Figure 1). In the eastern part of the Møre Basin, the Slørebotn Subbasin is separated from the main basin by a row of structural highs, amongst other the Gossa High. The Slørebotn Subbasin terminates in the Møre Margin to the east, and in the Frøya High towards the north (Blystad et al., 1995).

The Norwegian continental shelf has undergone three main rifting periods (Brekke et al., 2001). The first lasted from Early Carboniferous to Middle Triassic times, the second lasted from the Middle Jurassic to the Late Cretaceous and the last phase lasted from Latest Cretaceous to Eocene times. The Møre Basin is affected by the NE-SW trending Møre-Trøndelag Fault Complex, and the area is structurally complex with rotated fault blocks of pre-Cretaceous age (Smelror et al., 1994).

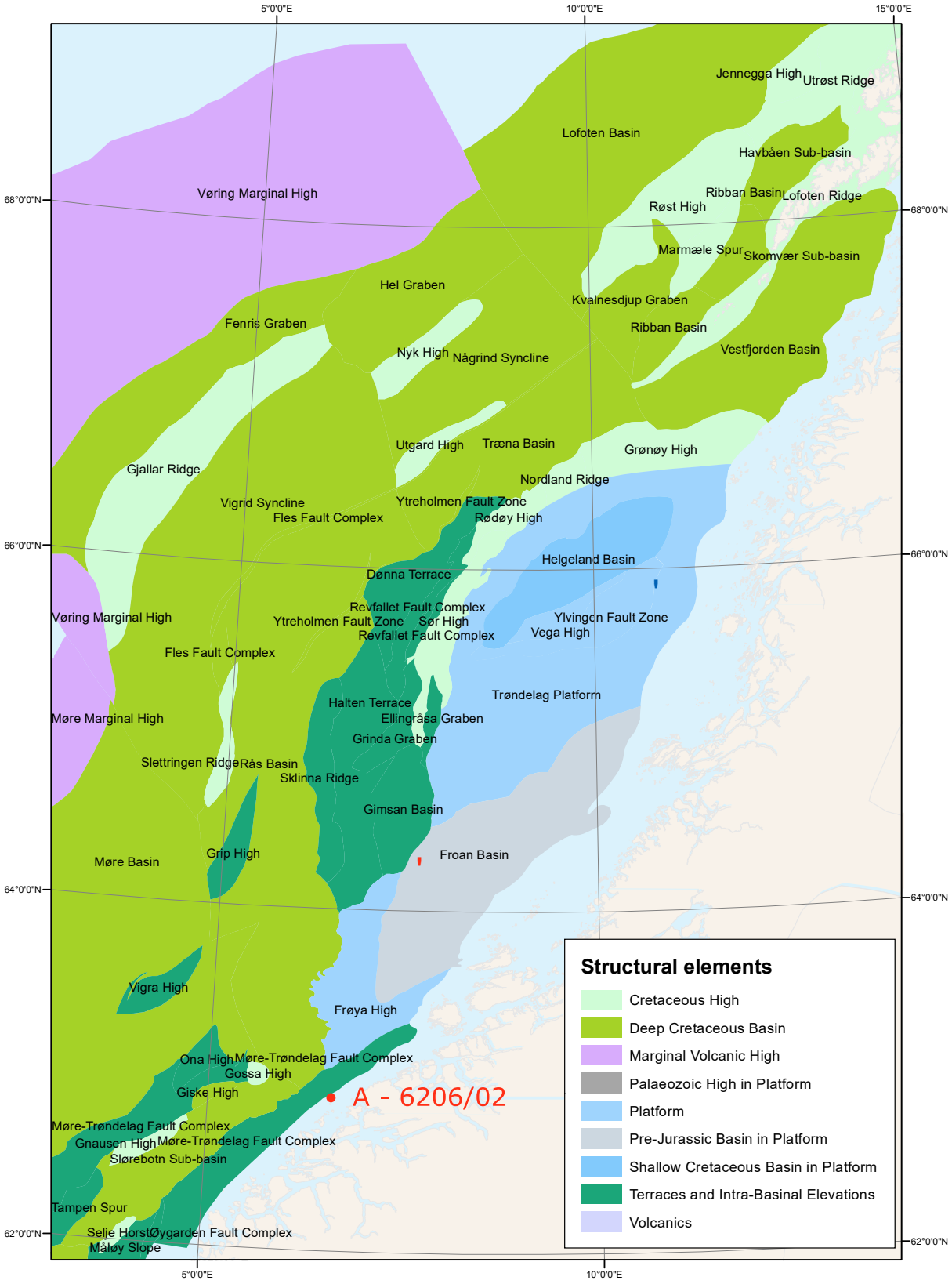


Figure 1: Geological map over the Norwegian Sea with major structural elements. The cores drilled by IKU are indicated. From Halland et al. (2014).

## 2.2 Pre-Triassic structural and depositional evolution

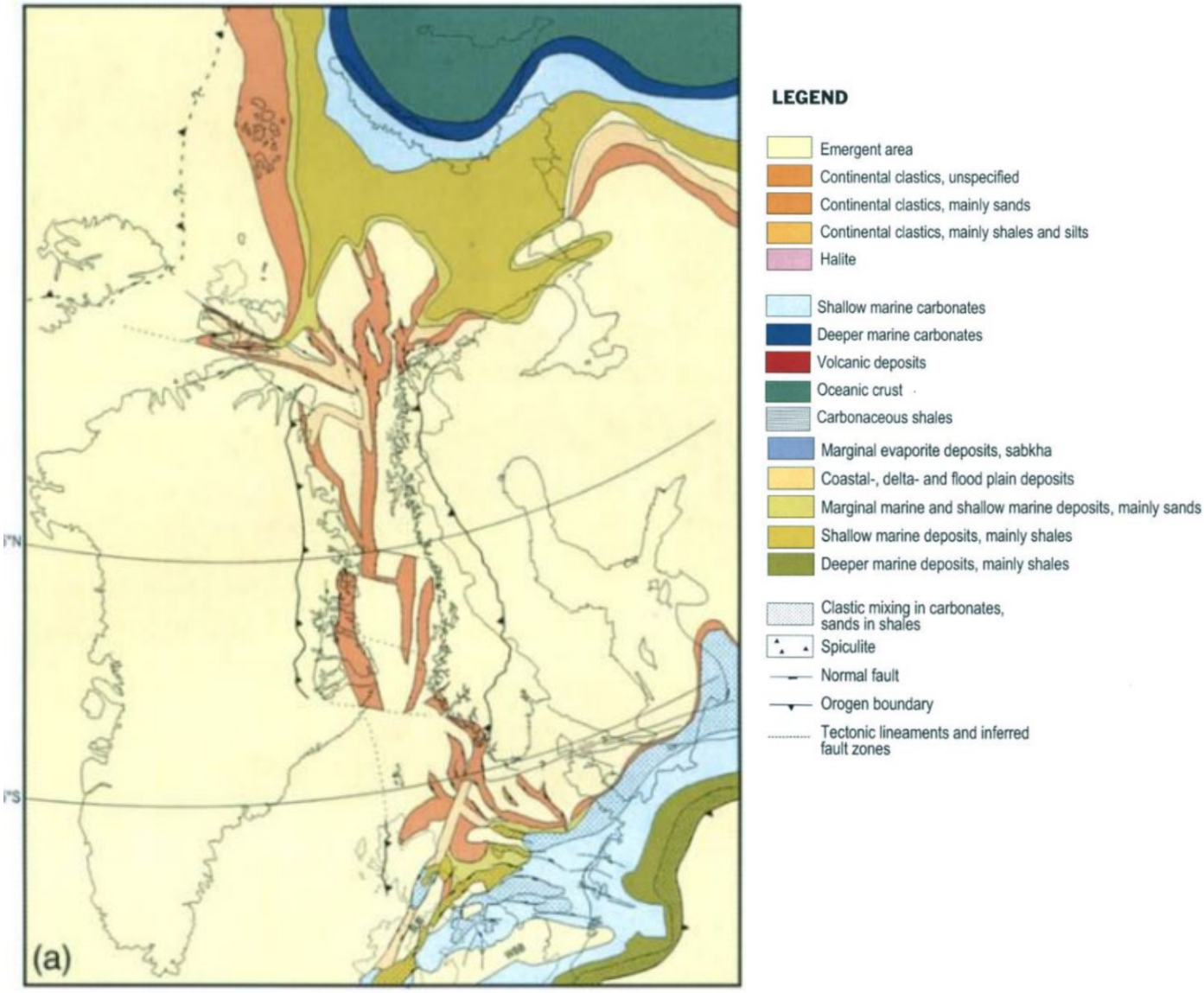


Figure 2: Palaeogeographic reconstruction of the Early Visean. Colour legend for all palaeogeographic maps is shown to the right of the map. From Brekke et al. (2001).

During the first of the main rifting periods described by Brekke et al. (2001), the Norwegian continental shelf was dominated by N-S to NE-SW trending normal faults and lineaments such as the Møre Trøndelag Fault Complex (Figure 2). These faults have since been reactivated several times and are the cause of the NE-SW trending basins and fault complexes in the study area (Blystad et al., 1995; Brekke et al., 2001; Jongepier et al., 1996). This was followed by rapid subsidence and a transgression which caused several basins to form between Norway and Greenland (Figure 3).

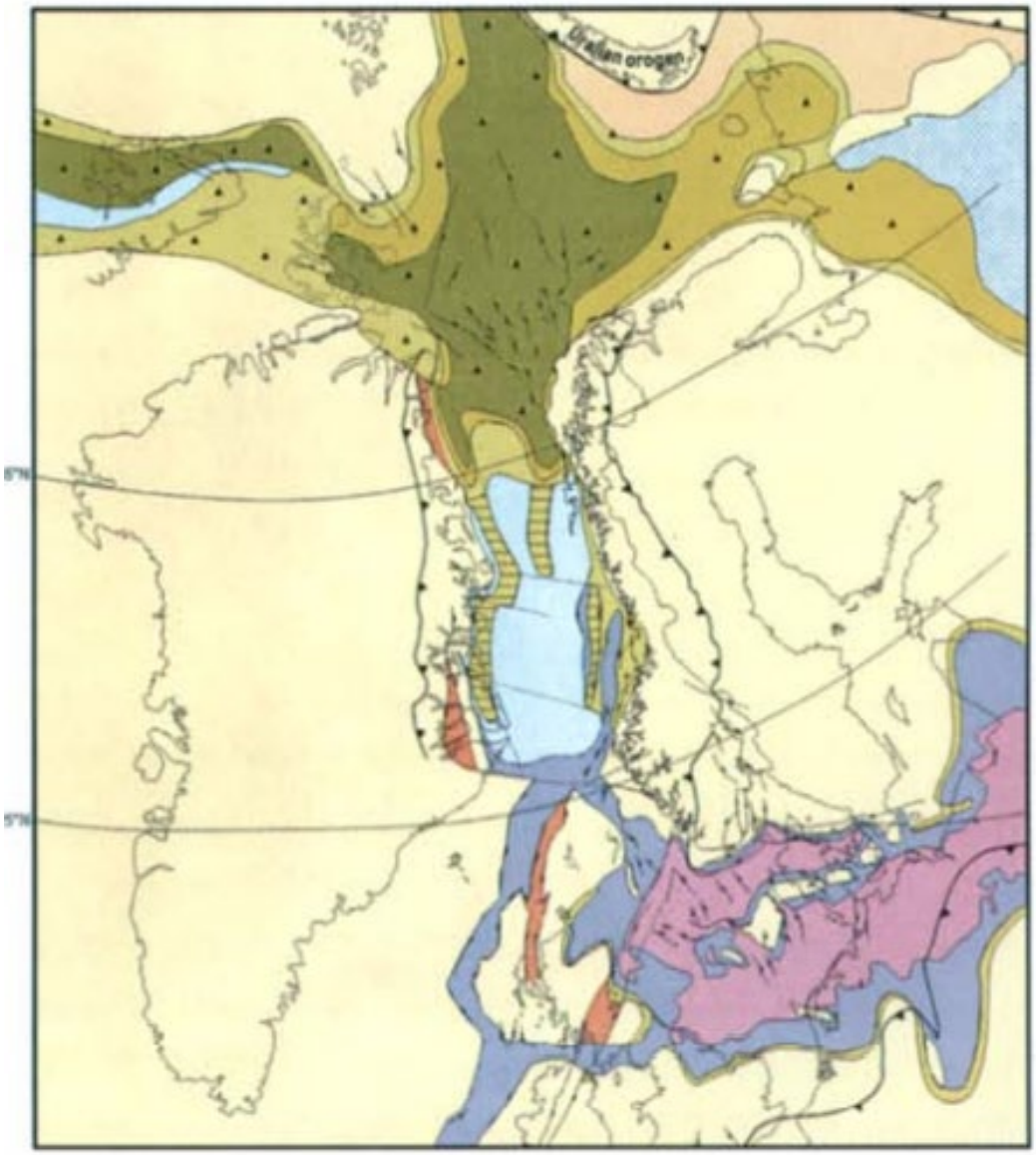


Figure 3: Palaeogeographic reconstruction of the late Kazanian – early Tatarian times. Colour legend for all palaeogeographic maps is shown in figure 2. From Brekke et al. (2001).

The Early and Middle Triassic was dominated by thermal relaxation and extension, with extensive continental alluvial and fluvial deposits (see Figure 4Figure **4**: Palaeogeographic reconstruction of the Middle Triassic to the left and Upper Triassic to the right. Colour legend for all palaeogeographic maps is shown in figure 2. From Brekke et al. (2001).

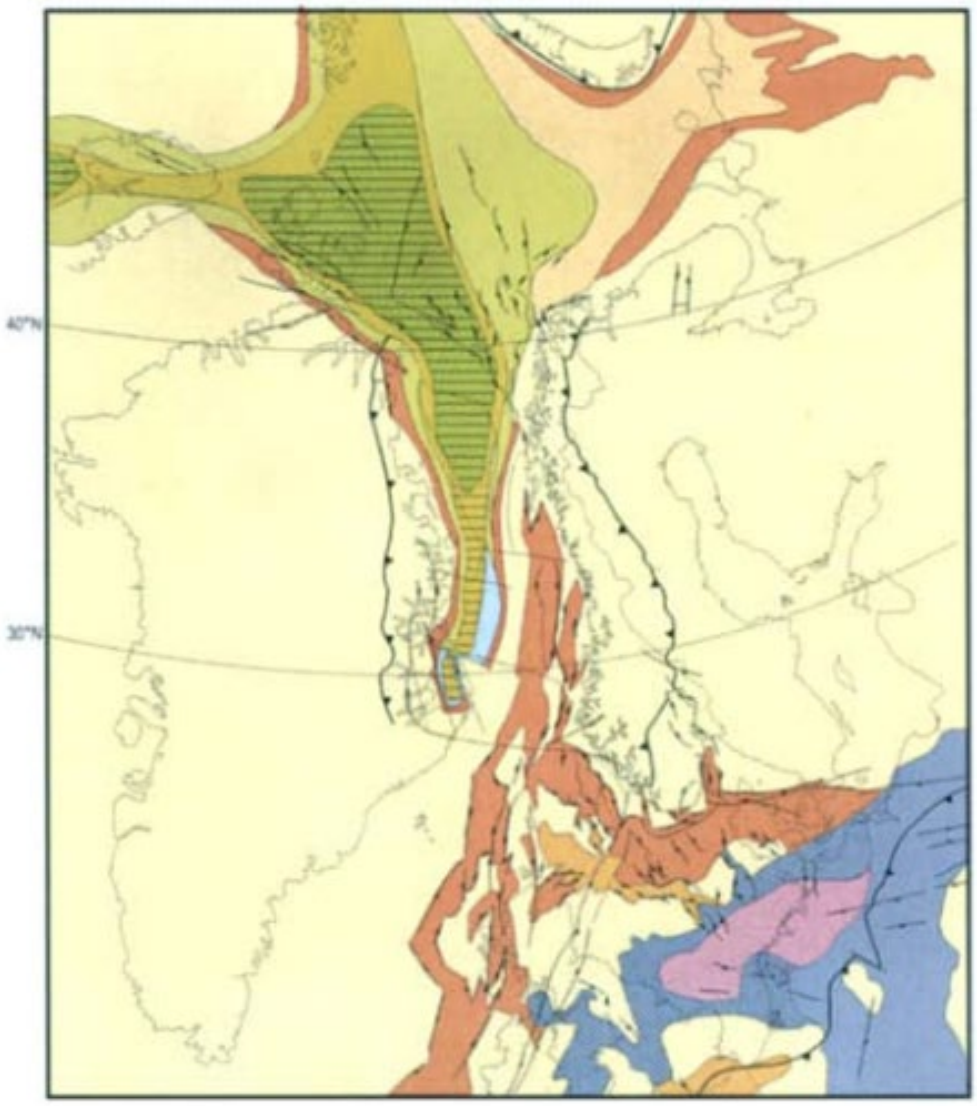

Figure 4: Palaeogeographic reconstruction of the Middle Triassic to the left and Upper Triassic to the right. Colour legend for all palaeogeographic maps is shown in figure 2. From Brekke et al. (2001).

## 2.3 Upper Triassic –Middle Jurassic

A mega fining upwards sequence of Middle Triassic age is found adjacent to the Gossa high, which could be an indication of waning tectonic activity in the area throughout the Middle Triassic (Jongepier et al., 1996). The entire Triassic sequence is missing from the Gossa High, where Bathonian sediments lie directly on top of metamorphic greenstones. The Early and Middle Jurassic were dominated by thermal uplift from doming in the North Sea and southern Norwegian mainland (Brekke et al., 2001). The doming was most intense in the Møre and Vøring Basins in the Middle Jurassic (Figure 5).

For the specific system this thesis focusses on, Smelror et al. (1993) suggest an alluvial fan environment in the Early Jurassic. In the Lower to Middle Jurassic, Smelror et al. (1993) present evidence of an approaching shoreline with increasing marine influence in the system. Jongepier et al. (1996) agree with Smelror et al. (1993) and interpret an arid alluvial environment with fans and alluvial plain sediments in a complex topography consisting of local highs and lows. According to Mørk et al. (2003), the alluvial fans show a complex mineralogical evolution that could be explained by deposition from tectonically induced mass flows over a short time span. By investigating clay minerals, Mørk et al. (2003) suggest a transition from arid in the Triassic to a more humid climate towards the latest Triassic/early Jurassic.

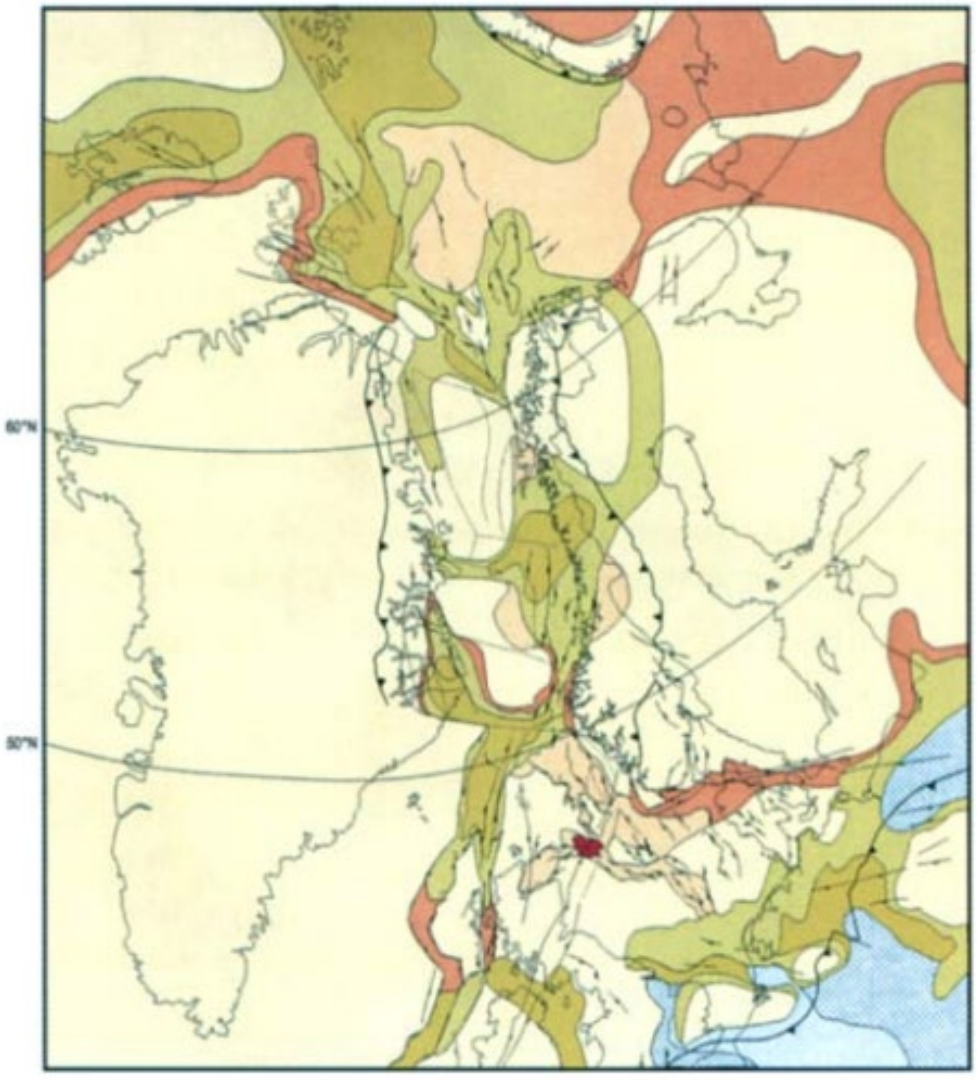

Figure 5: Palaeogeographic reconstruction of the Bajocian. Colour legend for all palaeogeographic maps is shown in figure 2. From Brekke et al. (2001).

## 2.4 Bathonian – Tithonian

The second phase of rifting in the North Sea and Norwegian-Greenland Sea, lasting from Middle Jurassic to Late Cretaceous, caused the creation of the new Atlantic Ocean. The area was subject to extension from the Middle Jurassic until the Earliest Cretaceous (Brekke et al., 2001), leading to subsidence of basinal areas and accumulation of sediments, while uplift and erosion dominated the local highs (Figure 5). In the Middle to Late Jurassic, several basins developed on the continental shelf (Figure 6), including the Møre Basin and the Slørebotn Subbasin. The eastern margin of the Møre basin underwent flexuring and faulting, resulting in thinning of the crust (Blystad et al., 1995). Extensive erosional surfaces and the lack of pre-Bathonian Jurassic sediments suggest significant uplift of the study area, possibly due to flexure.

The Slørebotn subbasin underwent a major transgression in early to middle Bathonian times, which led to sediments starting to accumulate once more in a marginal marine environment. Sediment sequences with sandstones, siltstones, claystones, coal and conglomerates suggest a coastal plain environment with a humid climate in the Bathonian (Jongepier et al., 1996). Deposition of coarse material directly on the Hitra Fault scarp indicates movement along the fault with syndepositional sedimentation in the Middle Jurassic, suggesting a new period of rifting. Another incomplete mega fining upwards sequence of Upper Jurassic age could be explained by tectonic pulses from hinterland uplift, with waning tectonic activity. The general trend is a more proximal depositional environment towards the west. From the late Middle Jurassic to Upper Jurassic, the depositional environment changed from subaerial coastal plain to marine anoxic. As extension accelerated, fault block rotations increased, and the rotations climaxed in the Tithonian, before the activity waned (Jongepier et al., 1996).

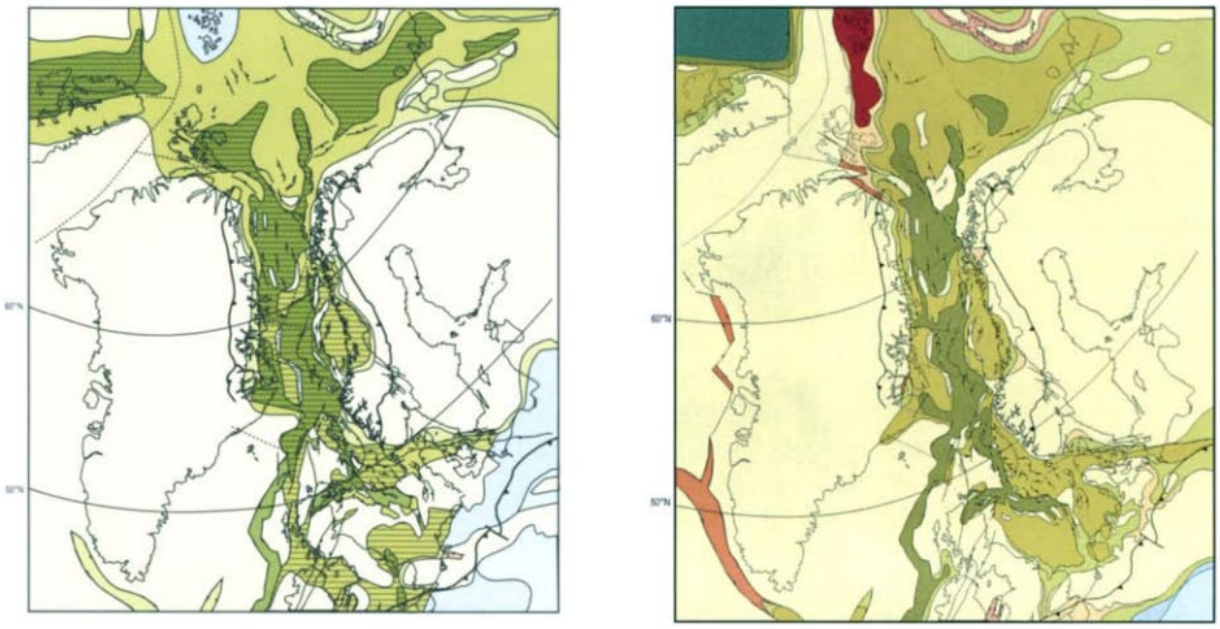

Figure 6: Palaeogeographic reconstruction of the late Oxfordian to early Kimmeridgian in the left figure, and of the Barremian in the right figure. Colour legend for all palaeogeographic maps is shown in figure 2. From Brekke et al. (2001).

## 2.5 Cretaceous

The rifting continued throughout the earliest Cretaceous (Brekke et al., 2001), with basins forming and shallow marine sands surrounding them (Figure 6). The increasing marine influence continued in the early Cretaceous, when the Sløre botn Subbasin was mainly oxic with occasionally suboxic conditions. The western part of the subbasin underwent significant subsidence, while the eastern part does not appear to have done the same (Jongepier et al., 1996). The thin lower Cretaceous section may suggest a shallow platform with occasional subaerial or subaqueous erosion. The deposition was dominated by turbiditic activity on an unstable slope and suspension fallout. Jongepier et al. (1996) suggest a deep marine fan system, as the result of a relative sea level fall or due to tectonics. As the rifting ceased, the area underwent thermal relaxation with uniform subsidence of the basin. There is evidence that there were major active faults until Turonian times.

## 2.6 Previous work on the cores

In 1988, IKU drilled four shallow stratigraphic cores (6206/02-U-01, 6206/02-U-02, 6206/02-U-03, 6206/02-U-08) SW of Kristiansund. Smelror et al. (1994) divide the Jurassic sediments into units A, B and C, and correlate these between the cores. All units are described by Smelror et al. (1994), however only unit C is relevant for this thesis.

Unit C, named Early Jurassic sandstone, is found in core 6206/02-U-01 (herein called core 1) in the interval 179.8 m – 98.3 m, in core 2 from 85 – 73 m and in the entire core 8. In core 1, this unit has several erosive cycles of graded sandstones, interbedded with silty claystones and gravel. The unit is generally poorly consolidated and shows an overall fining upward trend with gravel-rich sediments in the bottom part of the core, and an increasing amount of sand and silt higher up in the unit. Smelror et al. (1994) interpret unit C in core 1 as a braid plain with deposition mainly taking place in flowing water. Palaeontological analysis shows marine influence and calcite cemented horizons indicate a foreshore setting, but an upward decrease in beach rock deposits with a simultaneous increase in soil horizons, indicate a regression. The general environment is interpreted as delta front/lower delta of a braided delta or fan delta (Smelror et al., 1994).

According to Smelror et al. (1994), the Cretaceous deposits in core 1 are correlated to the Lange Formation and the Kvitnos Formation which are again divided into subunits. The Lower Cretaceous Lange Formation is subdivided into three subunits. Subunit 1 (98.3 m – 90 m) contains chaotic facies comprising of clasts and greyish mudstone. The flow mechanism is thought to have been mass gravity flows, specifically debris flows and turbidity currents, on an inner shelf or prodelta with suspension fallout in-between flows (Smelror et al., 1994). Subunit 2 (90 m – 79.5 m) is a glauconite-rich fine to medium sandstone with horizontal lamination that changes into large scale cross lamination with strong bioturbation in the upper parts of the subunit. The depositional environment is interpreted as transgressive marine. Marine coastal sandstones transitioned into shelf deposits, at the same time as the sedimentation rate, bioturbation and glauconitization decreased (Smelror et al., 1994). Subunit 3 (79.5 – 76 m) is similar to subunit 1, with heterogenous mudstones containing clasts. This subunit might be indicative of a regression. The upper boundary of subunit 3 is a sharp hiatus of 2 My (Smelror et al., 1994).

The Upper Cretaceous Kvitnos Formation is divided into two subunits by Smelror et al. (1994). Subunit 1 (76 – 63 m) overlies a hiatus that is the upper boundary of subunit 3 in the Lange Formation. It is a calcareous greyish black laminated shale with some silt and dolomite/ankerite laminations. There are bioturbated intervals, and some thin

intervals of medium grained, bioturbated glauconitic sandstone and conglomerate with pebbles. The depositional environment is interpreted as outer shelf (Smelror et al., 1994). Subunit 2 (63 – 54.9 m) is an upward coarsening sequence, with a sandy, calcareous laminated shale. The sand is mostly biogenic silica, and there are some erosive coarse-grained pebbly glauconitic beds (Smelror et al., 1994). These deposits indicate varying energy conditions, which may be due to storm or other current-generating events in a sediment starved shelf area. There is an overall gradually decreasing sedimentation rate upwards. This subunit is interpreted as an outer shelf to open marine environment (Smelror et al., 1994).

Jongepier et at. (1996) investigated the structural and stratigraphic development in the area. They described structural elements and the change in geological history by using both the IKU cores and other cores (6305/3, 6305/12, 6306/10). They disagree with Smelror et al. (1994) regarding the dating of unit B and C. According to Jongepier et al. (1996), there is only weak evidence for Smelror et al.'s dating (Unit B: Pliensbachian-Toarcian, Unit C: Late Toarcian – Aalenian), as the palynoflora used is dominantly continentally derived spores and pollen, in addition to sparse diagnostic taxa. Instead, they suggest a Bathonian age for both units B and C.

Mørk et al. (2003) investigated the stratigraphic and geographic variations in the composition of the rocks in the North Sea, with the aim to predict offshore rock properties. The paper focuses on identifying clay minerals in the cores, which were used to interpret the climate and depositional environment. The Lower Triassic is dominated by mica, chlorite, a mixed clay, and feldspar while the Uppermost Triassic and Lowermost Jurassic show extensive kaolinite formation. This change indicates a transition from an arid climate to a more humid climate where the sediments are more prone to weathering (Mørk et al., 2003). Kaolinite dominates throughout the Lower and Middle Jurassic deposits but is replaced by smectite-rich mixed clay laminae in the Upper Jurassic deposits. The mixed clay reflects an increased marine influence with several sediment sources and therefor mixing, combined with a more arid terrestrial climate seen across southern Eurasia. The smectite-rich mixed clay is also interpreted to have been influenced by increasing volcanism in the North Sea (Mørk et al., 2003).

# 3 Methodology

Based on core logging, the different flow processes and transformations were determined and described. By combining the logs, suggested flow processes, pXRF measurements and observations from the thin sections, depositional environments and environmental changes were suggested.

## 3.1 Core logging

Core 6206/02-U-01 was logged at a scale of 1:20, see appendix 1. Both the display half and the working half of the core were investigated using a hand lens and stereo microscopy where necessary. The description of the core consists of observations of lithology, grain size, sedimentary structures, bedding, fossils, bioturbation and colour.

## 3.2 Optical microscopy

Twenty-two petrographic thin sections from various core depths (see Table 1) were used. These thin sections are the same as described in Mørk et al. (2003). The thin sections were investigated using an optical microscope with the main aim being to identify minerals and to describe the textural composition and maturity of the rock.

Table 1: Table showing the number of the thin section and the depth in the core it relates to. Thin sections

| Thin section number | Depth (meter) |
|---|---|
| 1 | 57.71 |
| 2 | 57.89 |
| 3 | 58.38 |
| B1 | 73.82 |
| 4 | 81.64 |
| 5 | 83.82 |
| 6 | 84.49 |
| 7 | 88.44 |
| B2 | 88.84 |
| B3 | 91.84 |
| 8 | 92.31 |
| 9 | 99.03 |
| 10 | 105.08 |
| 11 | 105.12 |
| 12 | 105.18 |
| 13 | 105.22 |
| 14 | 119.82 |
| 15 | 121.89 |
| 16 | 135.88 |
| 18 | 152.95 |
| 19 | 171.86 |

## 3.3 pXRF analysis

To investigate elemental proxies in the core, a portable XRF (herein referred to as pXRF) was used. The core was analysed using a Thermo Scientific Niton XL3t 600 XRF GOLDD Analyzer in the Mining Cu/Zn mode. In this analyzer, a source produces an X-ray that is pointed at the core surface (ThermoFisher, 2018). The energy in the beam causes inner-shell electrons of the atoms in the sample to eject, while the outer-shell electrons fill the vacancies. This process emits fluorescent x-rays, which are detected and processed by the tool.

The result are spectral data which are shown as a composition analysis (ThermoFisher, 2018). The precision of each element is two times the standard deviation for the measurement. If the tool cannot detect levels of an element that is at least 1.5 times the

precision, the result is shown as <LOD (below the limits of detection). The tool registers 40 elements given in percentages, where 20 elements (Nd, Pr, Ce, La, Ba, Th, Zr, Sr, Rb, Zn, Cu, Fe, Ti, Ca, K, Al, P, Si, Cl and S) showed measurable results for the investigated core and 20 elements were always below the limit of detection or had very few measurements (Sb, Sn, Cd, Ag, Mo, Nb, Y, U, Bi, Au, Se, As, Pb, W, Ni, Co, Mn, Cr, V and Mg).

Figure 7: Setup of the pXRF during scanning of the core.

The measurements were taken at an interval of 10 cm throughout the entire core. The sample time was a minimum of 120 seconds, but some measurements exceeded the sample time. This does not affect the measurements to a significant degree.

The main advantage of using a pXRF, rather than stationary XRF is that it is a non-destructive analysis. The measurements can be done on the cores as is, rather than having to take samples from the core to be crushed. As several of the elements works as proxies for the same environment, a multiproxy evaluation of the cores will result in a better understanding and safer results (Algeo and Maynard, 2004; Tribovillard et al., 2006).

# 4 Results, event bed descriptions and interpretation

## 4.1 Core logging

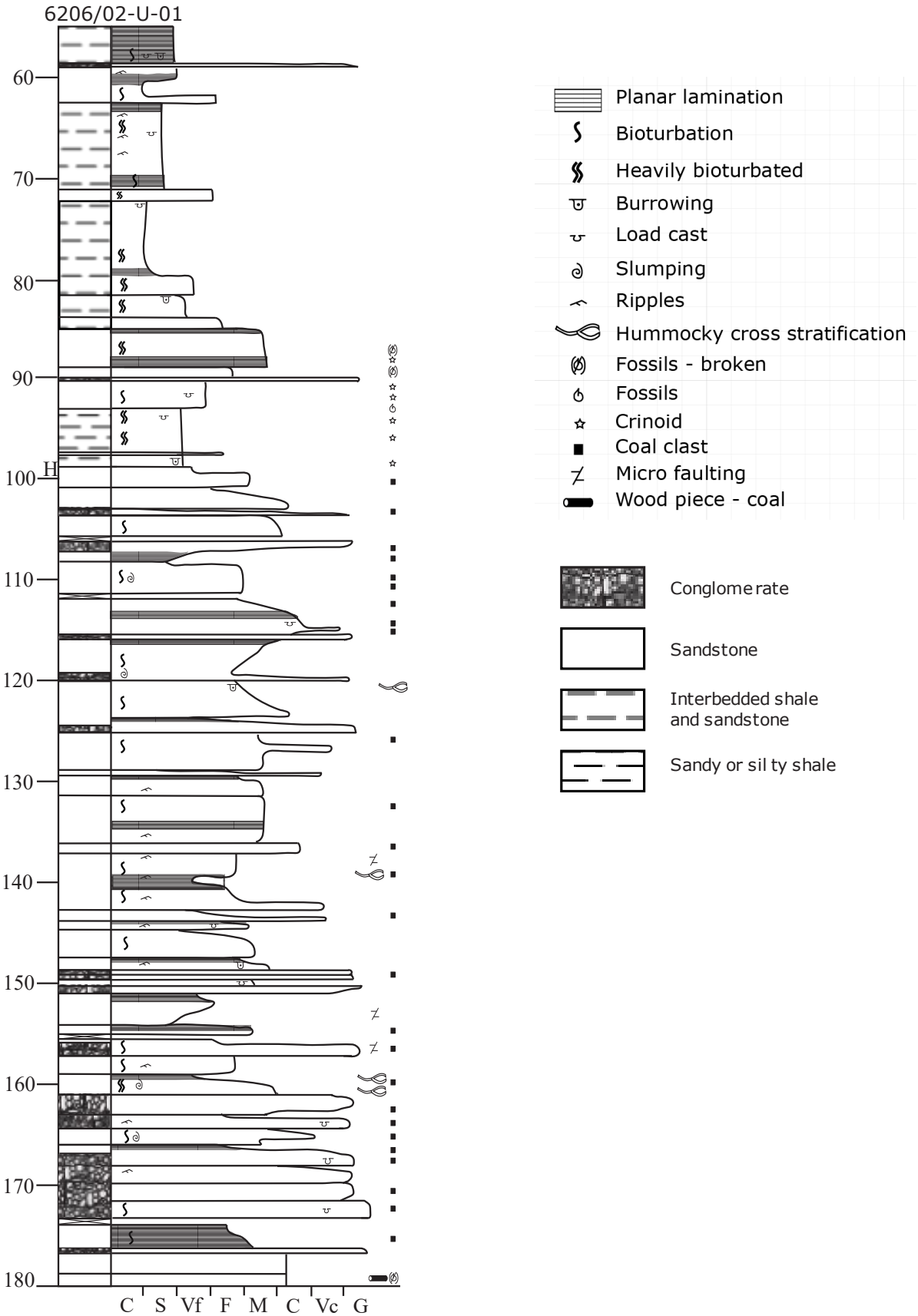


Figure 8: A log showing core 6202/02-U-01 with lithology, structures and observed fossils.

### 4.1.1 Overall core description

The complete log at 1:20 scale is shown in appendix 1, while a summary is shown in Figure 8.

A hiatus of 80 My at 98.3 m depth (Smelror et al., 1994) acts as a boundary between the lower part of the core and the upper part. In the lower part of the core, event beds are abundant, and are described in chapter 4.3. The upper part shows mainly low density turbidites (chapter 4.3.1.1) and hemipelagic deposition.

The core shows an overall fining up, where the bottom part is dominated by coarse sandstones and conglomerates while the upper part consists of mudstone to fine sandstone. An increase in bioturbation is also observed. The sandstones in the lower part are generally more argillaceous than in the upper part, see appendix 1. This is also observed in thin sections 9, 10, 11, 12, 13, 14, 15, 16, 18, see Table 1

Glauconite is observed in several intervals throughout the upper part of the core (example in Figure 36), in addition to one interval below 98.3 m, at 101.14 m, see Figure 9. Glauconite is identified and logged based on core observation and optical microscopy. Glauconite is only observed in event beds in the core. In modern settings, glauconite formation occurs in the subsurface of marine environments (Chamley 2001; Hesse and Schacht 2011; Velde 2014), and is restricted to zones of low deposition rate (Velde, 2014). This indicates that the glauconite has formed further up the slope, and later been flushed out into the delta during gravity current events.

Figure 9: Core photo of glauconitic sand in an event bed at depth 101.18 - 101.14 m.

Hummocky cross stratification is observed in several beds throughout the core, see Figure 10-12. This structure indicates storm deposits and is preserved in the zone above storm weather wave base and (normally) below fair-weather wave base. Smelror et al. (1994) describe these structures as large-scale cross stratification, but hummocky cross stratification is a possible interpretation of this structure, and fits into the suggested depositional environment.


Figure 10: Core photo of hummocky cross stratification observed at depth 158.77 m. The increasing inclination on the lamination up the bed is characteristic for hummocky cross stratification.

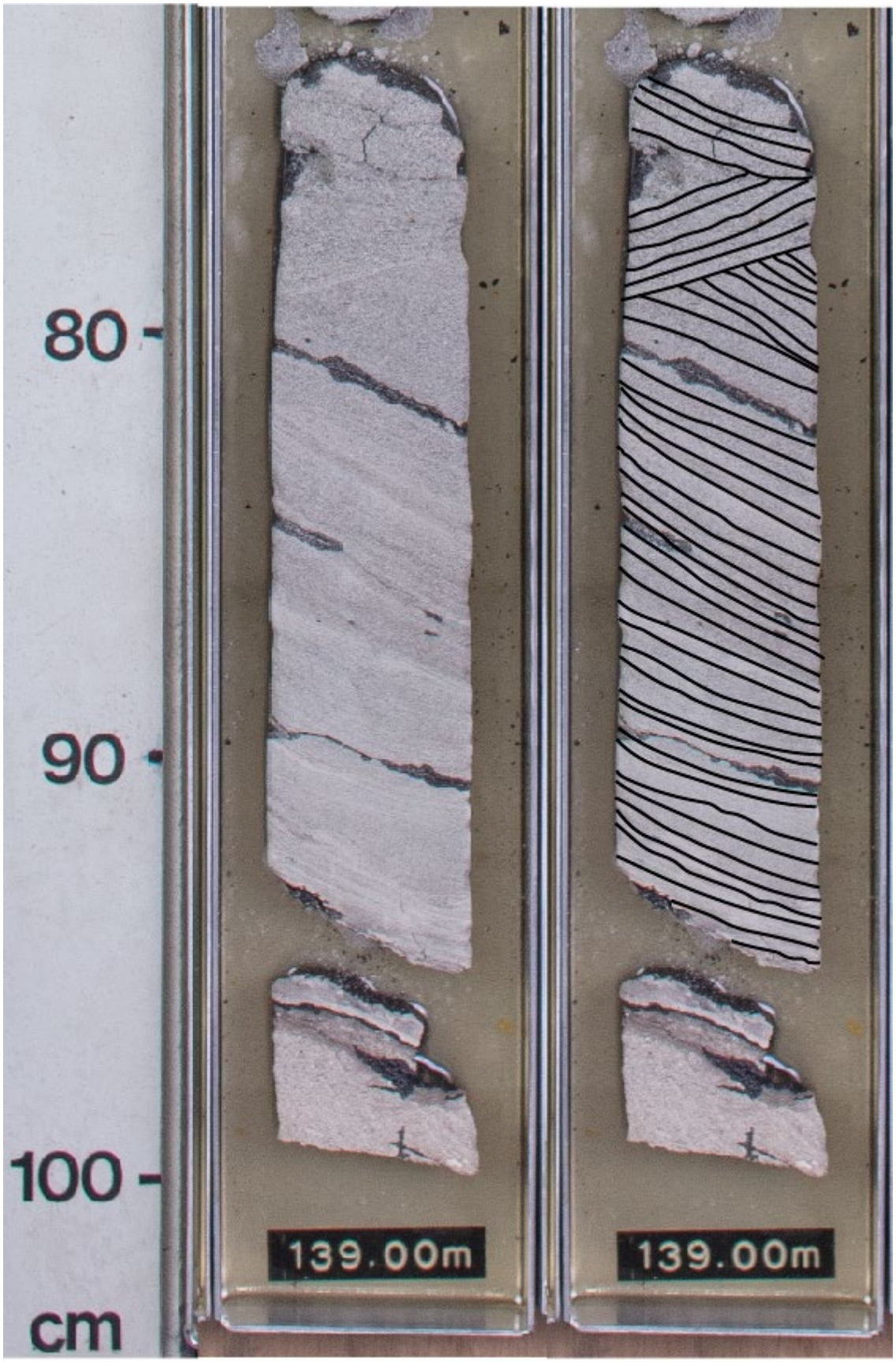


Figure 11: Core photo of hummocky cross stratification with changing angular lamination indicated.


Figure 12: Core photo of hummocky cross stratification with increasingly steep lamination.

### 4.1.2 Fossils and bioturbation

Both fossils and bioturbation are observed throughout the core, and microfossils are observed in thin sections 1 and 2 (see Table 1 for depths in core). In the lower part of the core, coal and bioturbation are abundant, along with some broken shells. Bioturbation continues in the upper part of the core, and crinoids are observed in the bottom 20 metres of the upper part of the core. In the thin sections, bivalves, coral fragments and fusulinids are observed, and possibly a type of sea sponge. All observed fossils are marine fossils, with the exception of coal, which is land-derived.

For bioturbation to occur, oxygen must be present, and there must be some time in between the events for organisms to bury in the sediments. As the bioturbation to a varying degree destroys the sedimentary structures, it is difficult to determine the original depositional mechanism.


Figure 13: Core photo of burrowing and bioturbation at depth 81.55 m.

Figure 14: Core photo of a horizontal burrow at depth 92.77 in a concretion.

Coal is found mainly in the lower part of the core and appears as both larger clasts up to four cm, specs, flakes and as lamination. Darker discolouration in coal-rich intervals indicates very fine coal fragments mixed into the sediments, as observed in thin sections. The coal is confined to event beds and is interpreted to have been transported by the river during flooding events. One of the coal clasts is identified as a wood piece (see Figure 15).

Figure 15: Core photo showing a piece of wood turned into coal. The piece of wood is 3 cm thick at depth 179.58-61 m.

## 4.2 Element analysis of the cores

In this chapter, the element measurement results are described, based on their use as proxies. First, the relevant literature will be introduced for the proxy, followed by a description of the elemental measurements, and then an interpretation of the proxy. The elements which are identified in the literature as proxies for similar environments are described together. The proxies are therefore grouped in proxies for palaeoproductivity (Ba, P and Ca), continentally derived sediments (Al, K, Rb, Zn, Cu, Ti, Th, Zr, Nd, Pr, Ce and La), marine influence (S, Sr and Ca) and oxygen conditions (Fe), in addition to silicon and chlorine. The different proxies are also compared to each other, e.g., proxies for continentally derivation and marine influence, to give an overall interpretation of the changes in the depositional environment.

### 4.2.1 Silicon

Silicon is the most dominant element in this core, with a concentration ranging mainly between 10 and 25%, see Figure 16. The silicon concentration shows a slight reduction in the top 20 m of the core. Silicon is high in sand and conglomerate rich beds, due to quartz sand, see appendix 1.

High concentrations of silicon match event beds, see appendix 1, which from core observations are clearly sand-rich. The number of event beds decreases towards the top of the core, and therefore silicon concentration decreases.

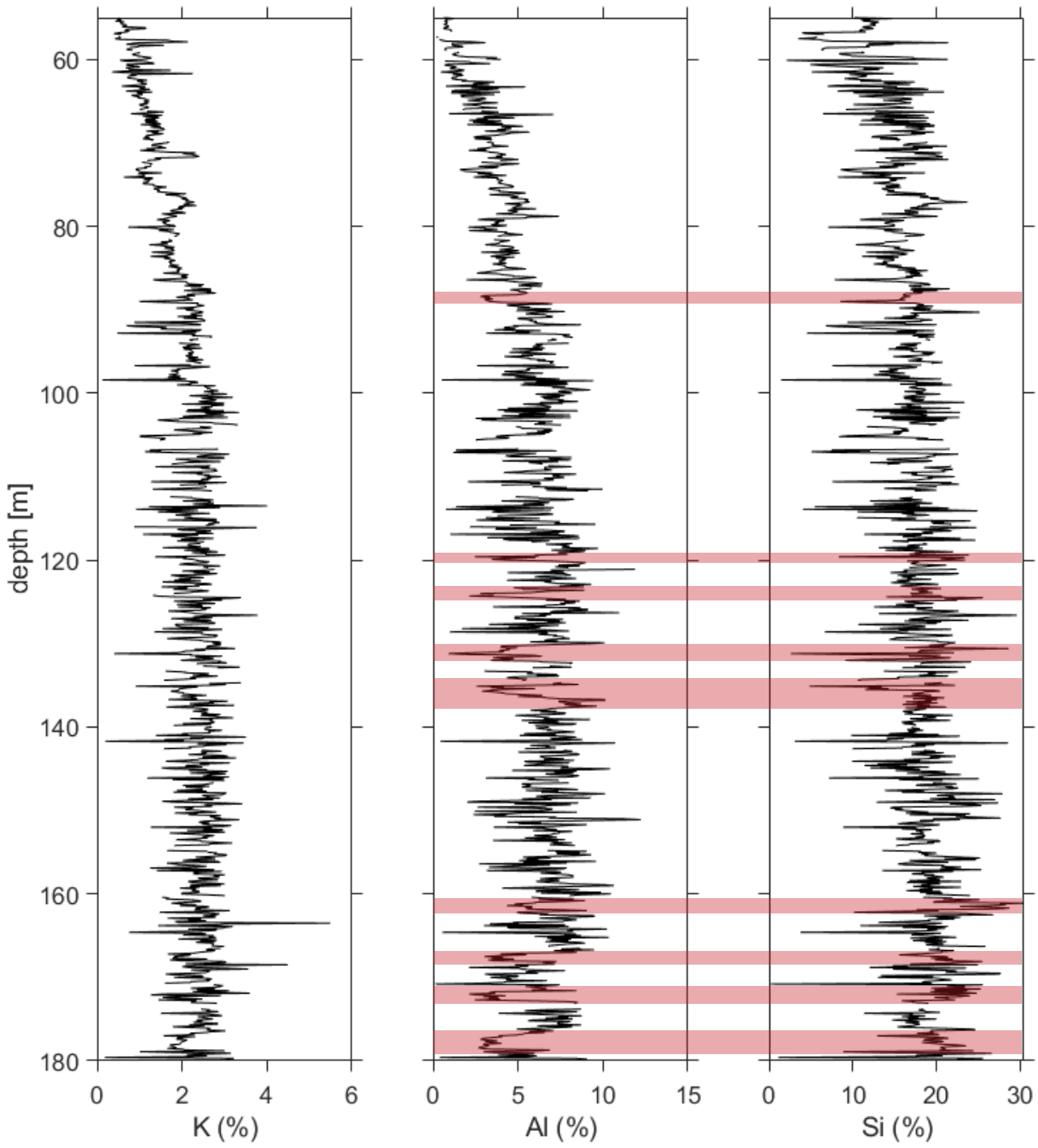


Figure 16: Elemental measurements of K, Al and Si. The major differences between the Al measurements and Si measurements are marked in red.

### 4.2.2 Palaeoproductivity

The three measured elements barium, phosphorus and calcium can be used as proxies for palaeoproductivity (Alego and Maynard, 2004; Tribovillard et al., 2006). Barium is absorbed by organisms and stored in skeletal and organic debris (Calvert and Pedersen, 2007). However, barium is prone to diagenetic alterations and unreliable for interpreting palaeoproductivity in oxic deposits (Tribovillard et al., 2006). Phosphorus is a macro nutrient for algae (Calvert and Pedersen, 2007). Calcium is the main component of both carbonate cement and skeletal debris and can indicate carbonate cementation or calcareous shells and fossils in the deposits.

The calcium concentration is relatively constant in the lower part of the core (Figure 17), except for some spikes. Phosphorus shows very low concentrations in the lower part of the core. Both phosphorus and calcium show an increase in concentration from 98.3 m up through the core, see Figure 17, coinciding with the previously mentioned hiatus. Barium shows a decreasing trend throughout the core, with the exception of some spikes, which match conglomeratic layers in the core. A significant spike at 71.6 m matches inversely with the calcium concentration. Spikes in the calcium concentration match well cemented beds in the core (appendix 1 and Figure 18). Calcite cement is observed in thin sections, which explains the spikes.

As barium is unreliable as a proxy in this study due to the oxic conditions indicated by the bioturbation throughout the core, the interpretation is based on phosphorus and calcium concentrations. The spikes in calcium in the lower part of the core, as well as the spikes between 100 m and 80 m match with observed calcite cemented beds or carbonate concretions (see appendix 1). The general increase in calcium above 98.3 m coincides with an increase in the number of fossils, as observed in both the core (appendix 1) and in thin sections 1 and 2. Both phosphorus and calcium concentrations increase towards the top of the core, indicating an increased marine influence and marine productivity.

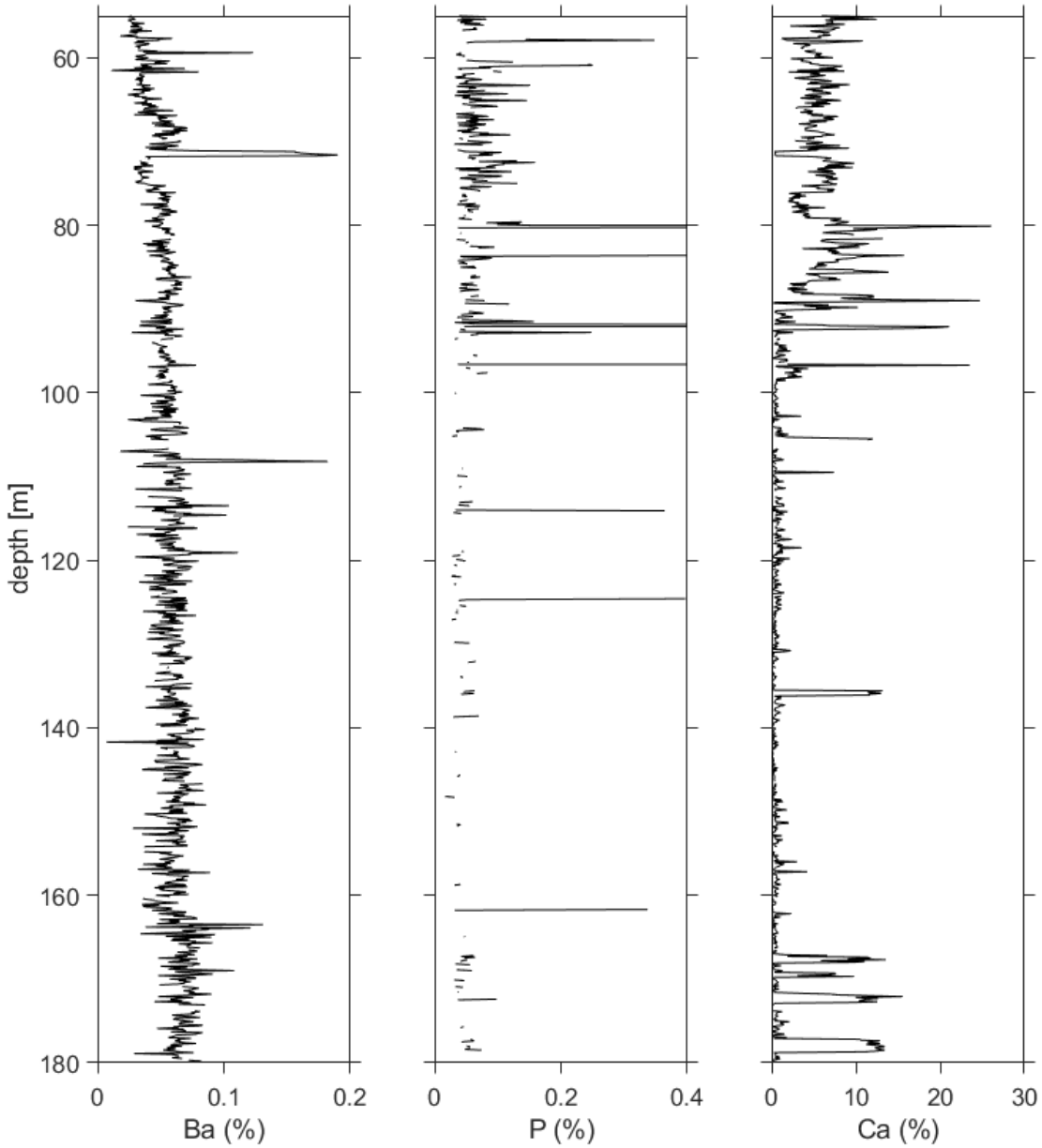


Figure 17: Elemental measurements of Ba, P and Ca. These elements are used as proxies for palaeoproduction.

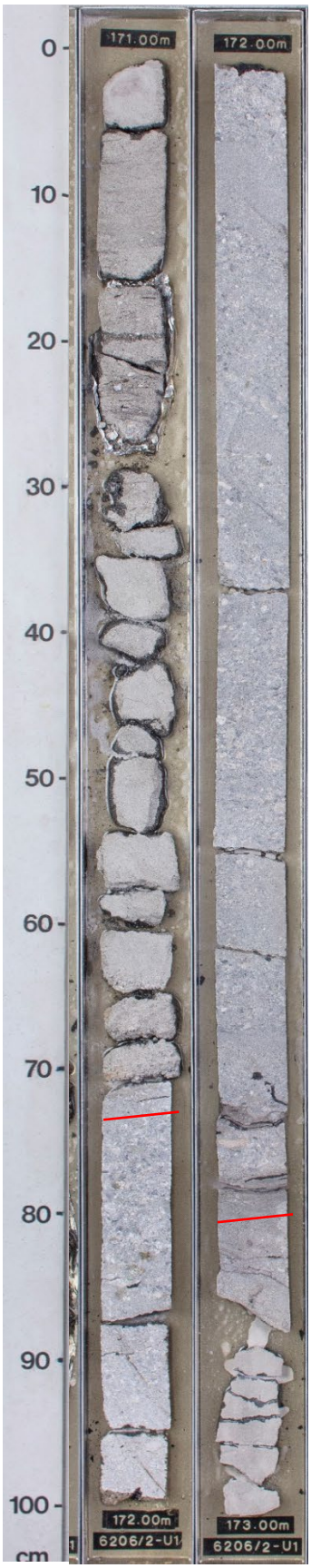


Figure 18: Core photo of a well cemented bed. The upper (left core section) and lower boundary (right core section) are marked in red.

### 4.2.3 Proxies for continentally derived material

Several of the measured elements can be used as an indicator for continentally derived sediment influx in the delta.

#### 4.2.3.1 Proxies for fine fraction of continentally derived sediments

Elements which are enriched in the finer fraction of continentally derived material can be used as a proxy for terrigenous derived deposits. Aluminium and potassium are components of several clay minerals, such as kaolinite (Poulsen et al., 2007; Turner et al., 2015). Copper and zinc can readily substitute into clays, and therefore be enriched in detrital fine fraction sediments (Poulsen et al., 2007) and rubidium substitutes readily for potassium in micas (Calvert and Pedersen, 2007).

For all elements in Figure 19, the concentration varies more in the bottom part of the core, where the deposition contains many event beds, than in the upper part of the core, where there are fewer event beds. All elements in Figure 19 show a decrease from 93.3 m towards the top of the core. The rubidium concentration is close to the limit of detection of the measuring tool but show the same trend as the other elements in Figure 18. The copper concentration is dominated by a few clear spikes in the lower part of the core, while the spikes disappear, and the values are very low in the upper part of the core.

The reduction in aluminium and potassium in the upper part of the core indicate a reduction in continentally derived clays in the deposits. A higher concentration, especially the sharp spikes in the copper concentration could be explained by detrital copper-rich grains and pebbles. The decreased concentrations in the upper part of the core, therefore, indicate a reduction in continentally derived sediments. The reduction of rubidium in the upper part of the core may indicate a reduction in micas in the sediments, which is also observed in the core, where sandstones below 98.3 m are generally more argillaceous than above, see appendix 1. The proxies all show a decrease in continentally derived fine sediment from 98.3 m and up, compared to the bottom part of the core.

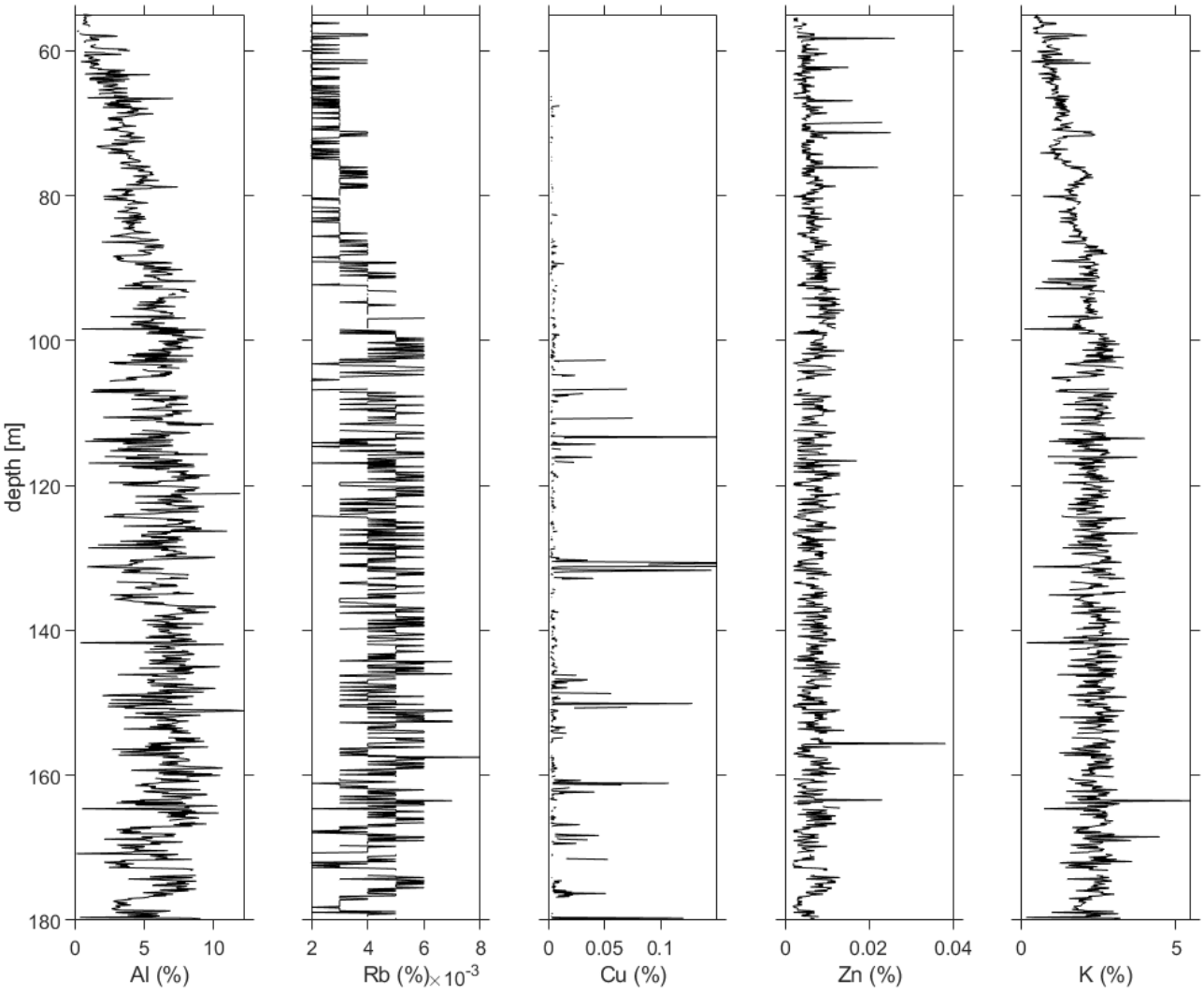


Figure 19: Elemental measurements of Al, Rb, Cu, Zn, K. These elements are used as proxies for the finer fraction of continentally derived sediment.

#### 4.2.3.2 Heavy minerals

Elements such as titanium (Calvert and Pedersen, 2007), thorium and zirconium are all related to heavy minerals, which are detrital minerals. Calvert and Pedersen (2007) used titanium as a proxy for input of coarse-grained sediments, while Bianchette et al. (2016) used titanium as a proxy for provenance in terrigenous sediments. Turner et al. (2016) stated titanium and zirconium to be associated with continentally derived sediments. Poulsen et al. (2007) related titanium oxide, thorium and zirconium to heavy minerals. They are therefore proxies for continentally derived material, as opposed to sediments of marine origin.

Figure 20 shows that titanium, thorium and zirconium all decrease in concentration towards the top of the core. The zirconium concentration shows some extreme spikes, which matches with very coarse sand or conglomeratic beds, see appendix 1. Thorium is barely above the limit of detection, but it is possible to observe the same trend as titanium and zirconium. Spikes in the thorium concentration match spikes in the zirconium concentration. Spikes in the titanium concentration coincide with thicker conglomeratic beds, see appendix 1.

The spikes in the concentrations of titanium, thorium and zirconium all appear in coarser sediments, and the elements are used in the literature as proxies for continentally derived material. The cause of the spikes is interpreted to be individual clasts with higher levels of heavy minerals, and therefor continentally derived material. The coarser beds seem to be land derived.

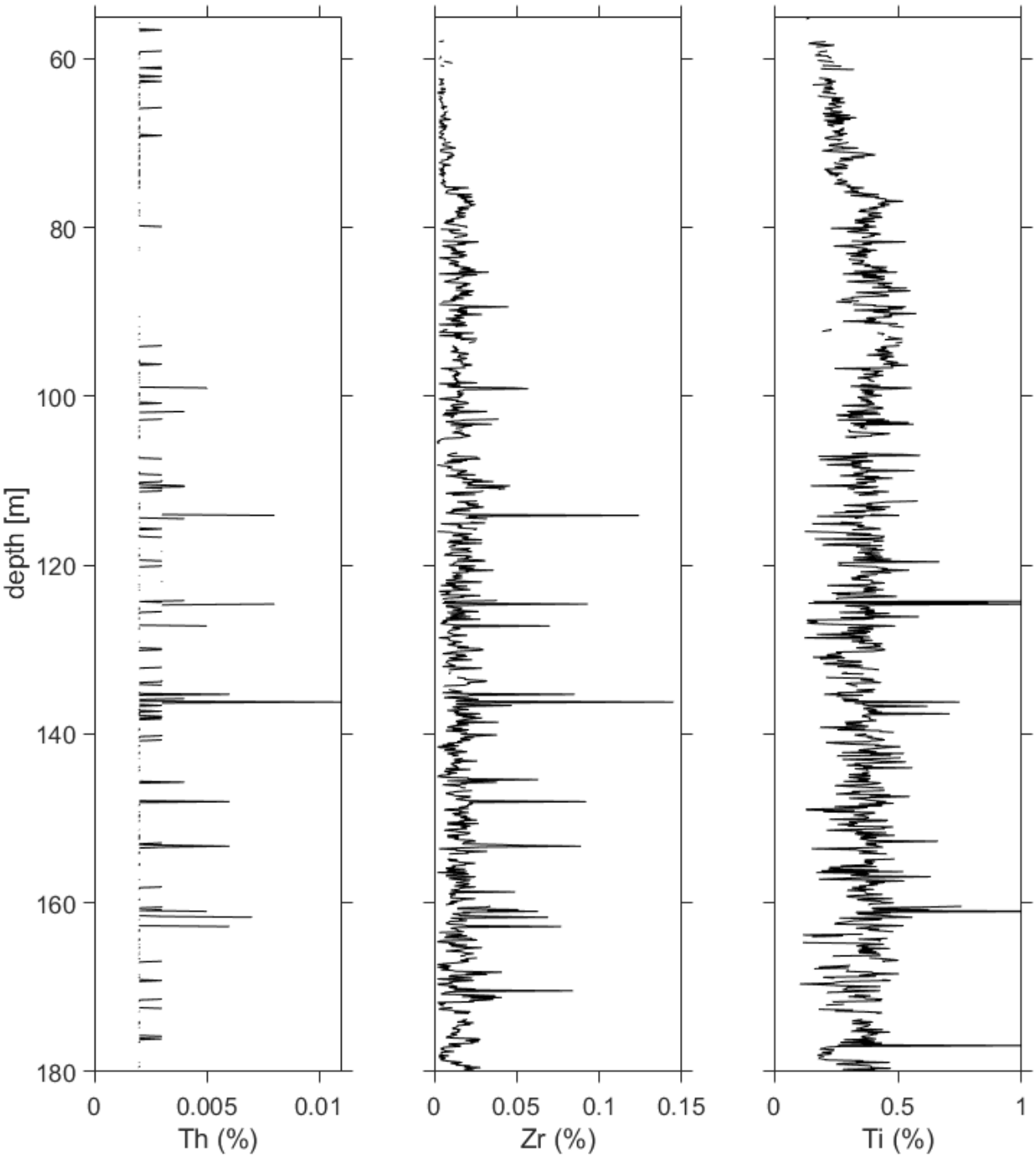


Figure 20: Elemental measurements of Th, Zr, Ti. These are used as proxies for continentally derived sediments.

#### 4.2.3.3 Rare Earth Elements (REEs)

Rare earth elements (REEs) have been linked to detrital, continentally derived material in marine settings (Tanaka et al., 2007).

All the measured REEs (Neodymium, praseodymium, cerium and lanthanum) show a similar concentration development throughout the core (see Figure 21) and show a slightly higher concentration in sandy intervals of the core. The spikes are tied to beds with a grain size ranging from medium sand to conglomeratic beds, see appendix 1. The overall trend for REE concentrations in the core shows constant values.

The large spikes at depth 114.6 m coincide with a spike in zirconium, which is interpreted as the effect of an individual high concentration clast. It is therefore assumed that the higher concentrations in REEs are a result of individual clasts as well. The lack of an overall change in the trend, contrary to what is observed in other proxies, implies that there is still some amount of sediment derived from land in the upper part of the core.

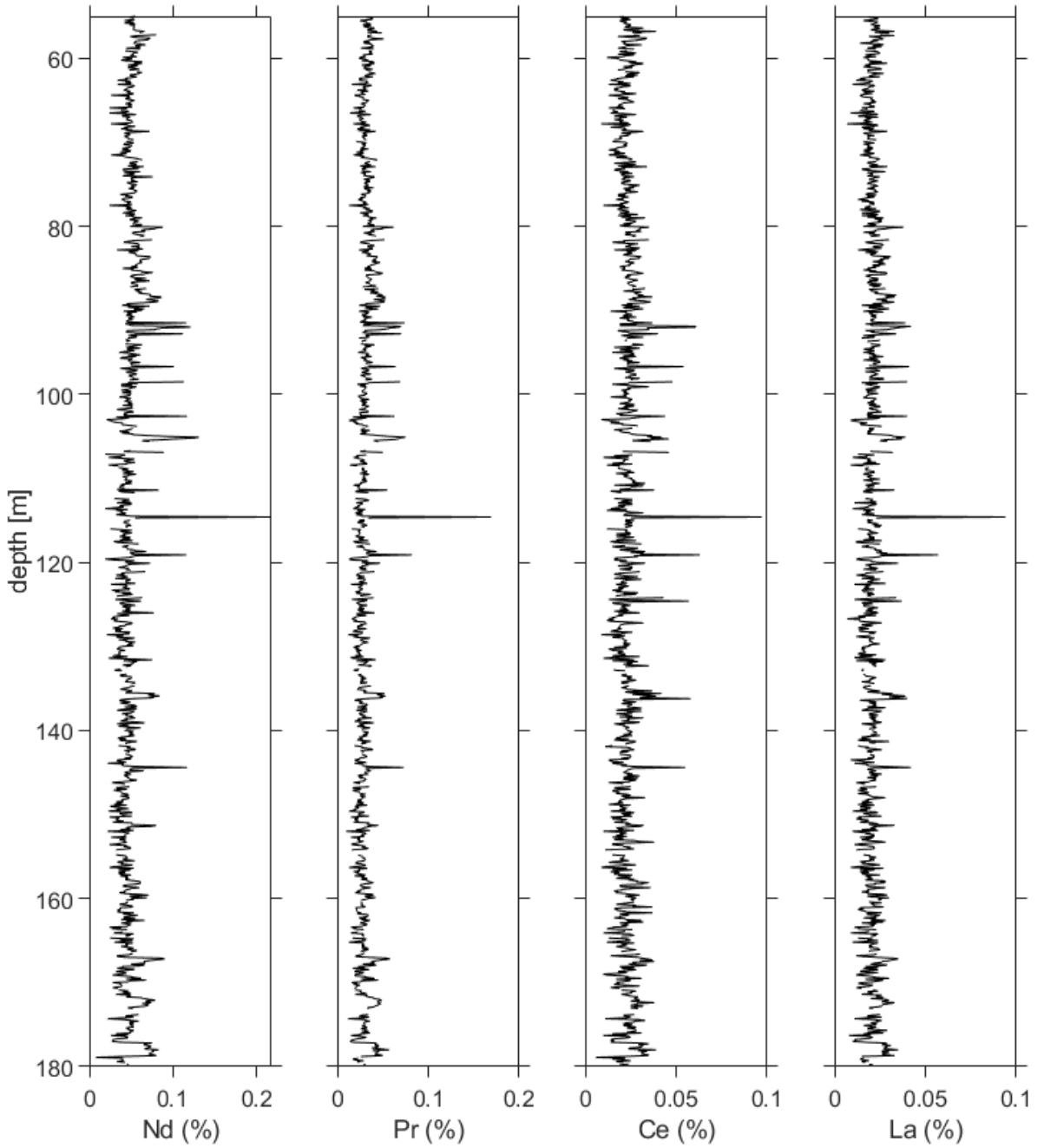


Figure 21: Elemental measurements of Nd, Pr, Ce, La.

### 4.2.4 Proxies for marine influence

The elements strontium, sulphur and calcium are enriched in marine sediments and seawater, which makes them good proxies for marine influence, as opposed to fluvial input in the delta (Bianchette et al., 2016). Sulphur is preserved in marine deposits under anoxic conditions, but not under oxic conditions (Calvert and Pedersen, 2007).

The general trend of the strontium concentration changes in the same way as the calcium concentration throughout the core, but with fewer spikes, see Figure 22. Both elements show a constant concentration up till 98.3 m, where the concentrations increase towards the top. Sulphur does not follow this trend and shows no clear trend.

The increase in calcium and strontium concentration from 98.3 m and up indicate increased marine influence in the upper part of the core. The interpretation of sulphur is left for the section below related to oxygen condition proxies.

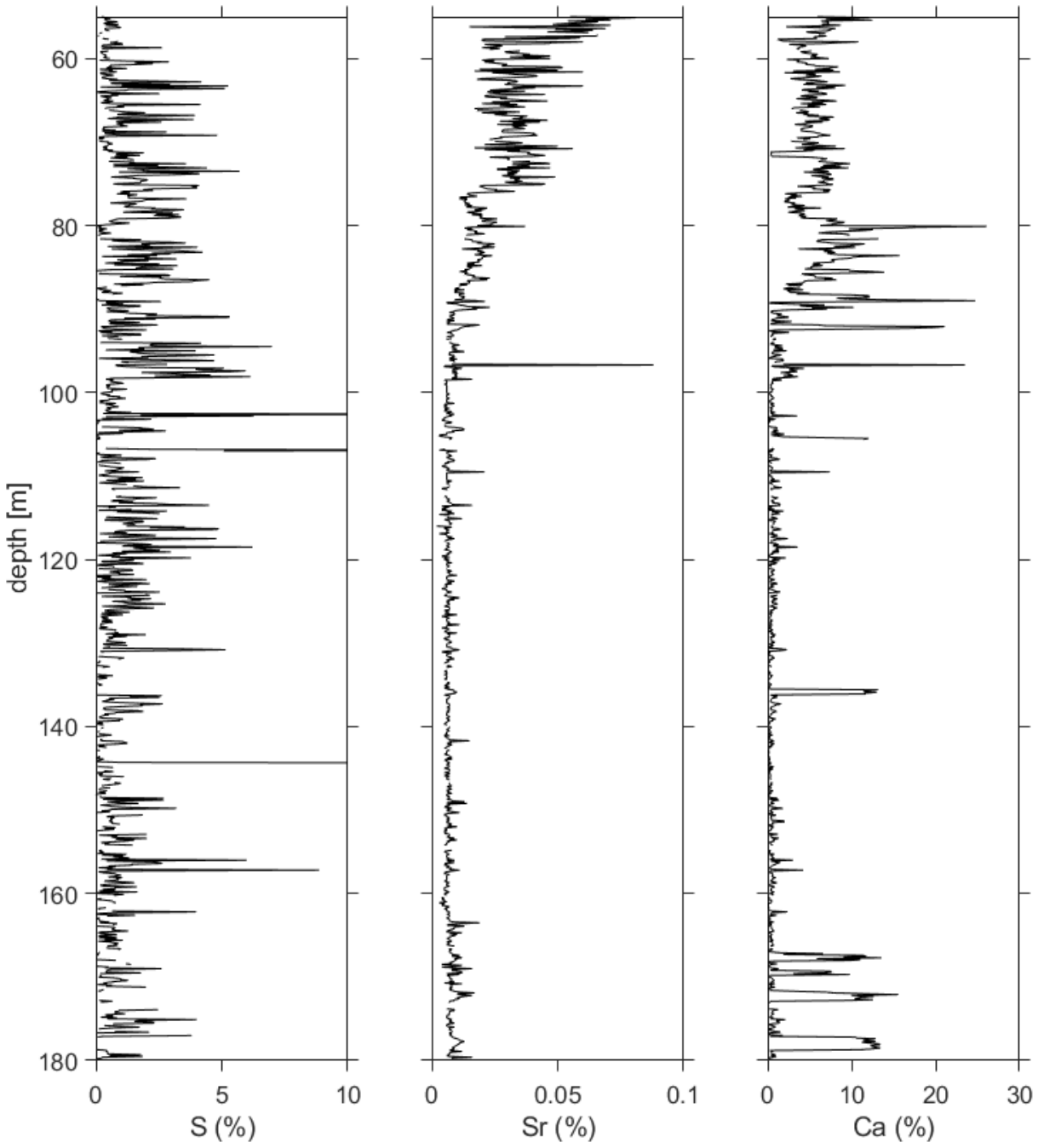


Figure 22: Elemental measurements of S, Sr, Ca. These elements are used as proxies for marine influence.

### 4.2.5 Proxies for redox conditions

Iron is a part of several observed minerals and is found in several proxy compounds in the core. Pyrite ($FeS_2$) and Siderite ($FeCO_3$) are two of the most important iron compounds in this core. Pyrite nodules ($FeS_2$) and grains are observed several times throughout the core, see appendix 1. The sulphur concentration shows some cyclicity (Figure 25), which could indicate a diagenetic effect in periods. The major spikes (up to 22% sulphur concentration) seen in the graph are caused by pyrite nodules and coincide with a high iron concentration as well (appendix 1).

The highest iron concentration measured in the core (36%) matches a significant peak in calcium concentration, which is an indication of a siderite rich interval. This interval is a well cemented coarse sand bed that is getting increasingly browner towards the top of the bed, see Figure 23. There are several other high iron concentration peaks which coincide with well cemented, browning up beds. These brown beds are a good indication of siderite cementation. Some concretions (see Figure 24) show an iron content of up to 33% but no spike in calcium concentration.

Siderite cementation, indicated by spikes in the iron concentration, indicate pore water flowing through the sediments post deposition. However, the trend of the iron concentration is constant, which matches the widespread observations of bioturbation in the core, see chapter 4.1.2, and interpreted fully oxic conditions throughout the core.


Figure 23: Core photo showing well cemented bed with increasing browning to the top, interpreted as siderite cemented bed.

Figure 24: Core photo showing iron concretion at depth 73.81-73-83. The interval is 2 cm thick.

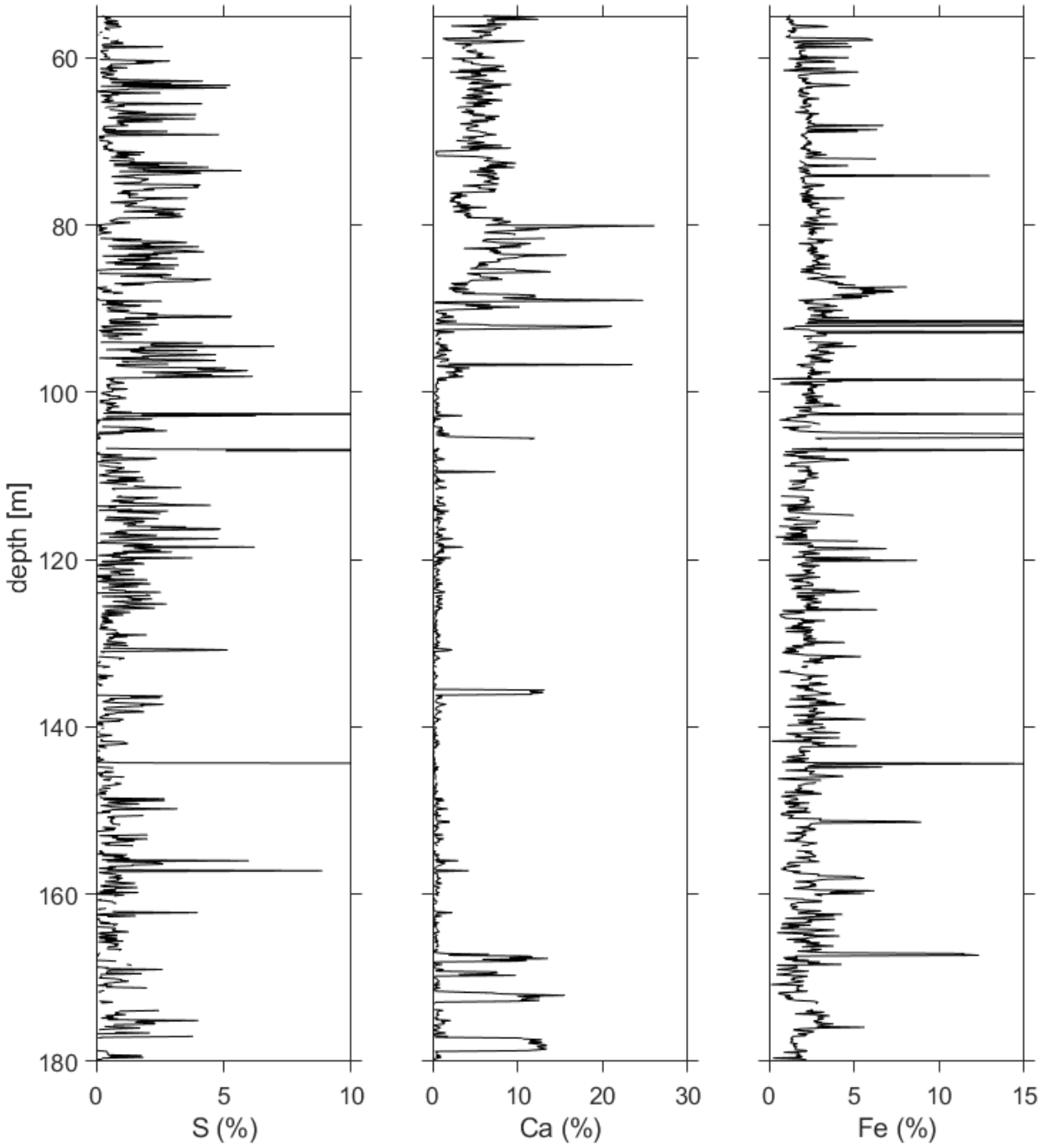


Figure 25: Elemental measurements of S, Ca, Fe.

### 4.2.6 Chlorine

The chlorine concentration is highest in two segments of the core (148.9 to130.9 m and 117.3 to 102.8 m), see Figure 26. These two segments do not stand out from any other parts of the core in terms of texture, colour, structures, flow types etc., see appendix 1. Nor are they marked by higher or lower concentrations in the other measured elements. The high chlorine concentration is therefore assumed to be due to high chlorine concentration in individual clasts.

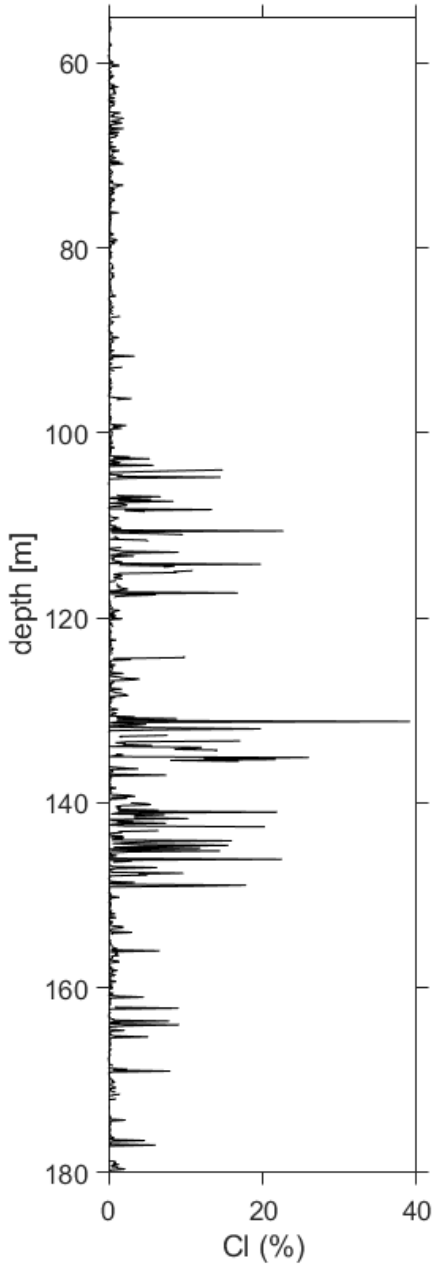


Figure 26: Elemental measurements of Cl.

## 4.3 Event bed descriptions

Previous studies have given thorough descriptions of facies, facies associations and sequences of flow deposits, which at this point are well established and recognized by the research community. This thesis will therefore not go into a traditional facies description and later arrange them in facies associations; instead, the different observed flow type deposits will be described, as also done by e.g. Talling (2013), Pierce et al. (2018), Fonnesu et al. (2018) and Hussain et al. (2020). Throughout this thesis, the term bed will refer to an event bed, here defined as a deposit of any short-lived sediment gravity flow. The different flow types can all be sorted on a spectrum where the two end members are turbidity current and debris flow (Felix et al., 2009).

### 4.3.1 Turbidites

Turbidity currents are currents in which fluid turbulence supports and transports the sediments as both bedload and suspension load (Haughton et al., 2009; Mulder and Alexander, 2001). An ideal turbidite as described by Bouma is shown in Figure 27. Turbidity currents can be subdivided into low- and high-density turbidity currents as described below.

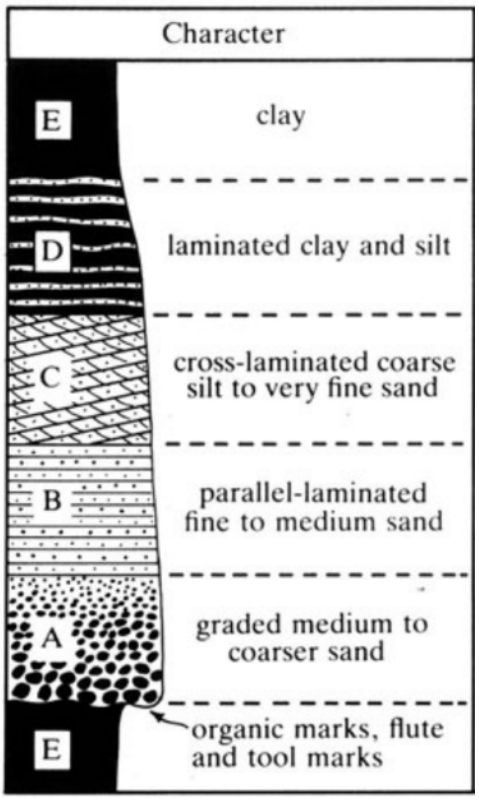


Figure 27: Diagram showing the ideal Bouma sequence with description of the deposits. From Allen (1985).

#### 4.3.1.1 Low density turbidite

Low density turbidites show a fining up sequence described by Bouma (1962), and consist of massive sandstone, planar laminated sandstone, rippled sandstone and laminated to massive clay. The facies in the Bouma sequence are often stacked two or three in the observed event beds, and no complete Bouma sequence has been observed in the core.

##### 4.3.1.1.1 Description

The thickness of the beds changes up through the core. Below 98.3 m, the turbidite beds are up to 20 cm thick, often with $T_A$ overlain by either planar laminated ($T_B$) and/or rippled sandstones. Some of the turbidites fine up into $T_E$, which is indistinguishable from hemipelagic mud.

Above 98.3 m the turbidites are much thinner (up to a few mm) in siltstone and mudstone dominated deposits. Sandy laminae are visible in intervals throughout this part of the core, indicating that some of the turbidity currents had the capacity to transport sand, while others have had a lower competence and were only able to transport silt and mud. One segment (Figure 28) shows a concretion containing low density turbidites, which shows the uncompacted turbidites. Here the turbidites are 0.5-1 cm thick and show a clear fining up sequence. Some sand ripples are observed at small scale in this part of the core, creating thin horizontal sand layers with a rippled texture, see Figure 29.

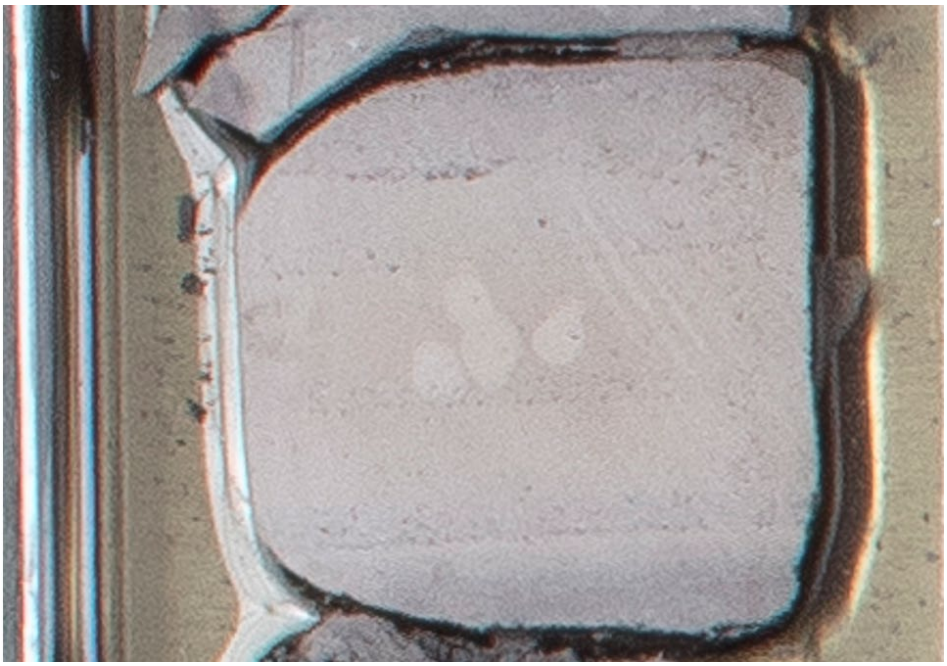

Figure 28: Core photo showing concretion with uncompacted turbidites stacked on top of each other. The concretion is 4.5 cm thick and at depth 63.24 - 63.29 m.

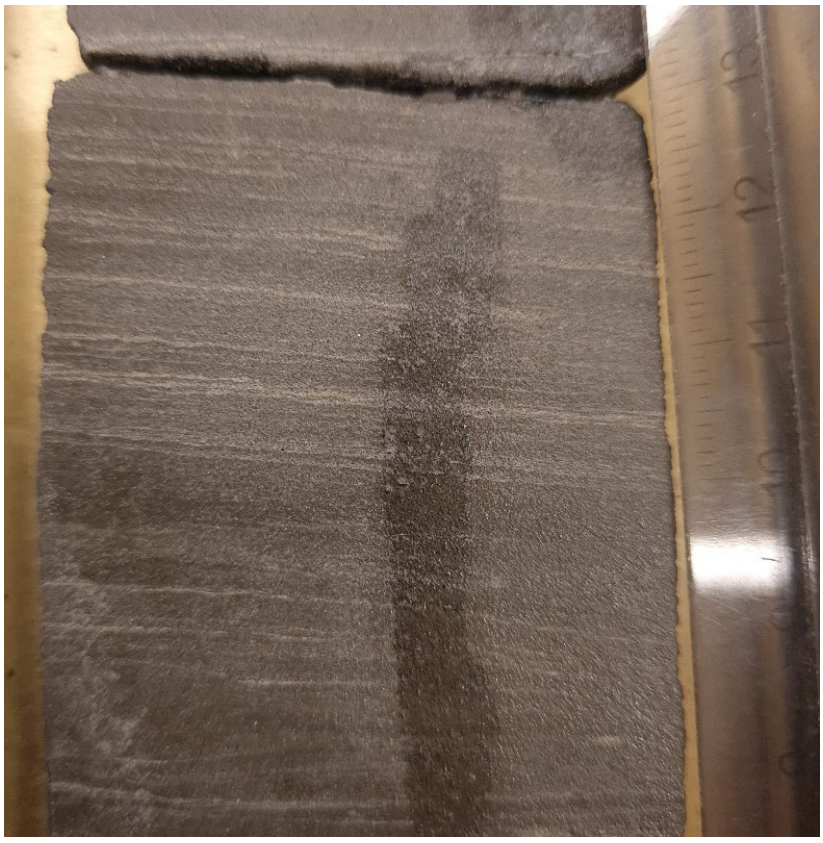

Figure 29: Core photo showing very small sandy ripples in a muddy deposit. The crack in the upper part of the photo is at depth 60.87 m. Ruler for scale.

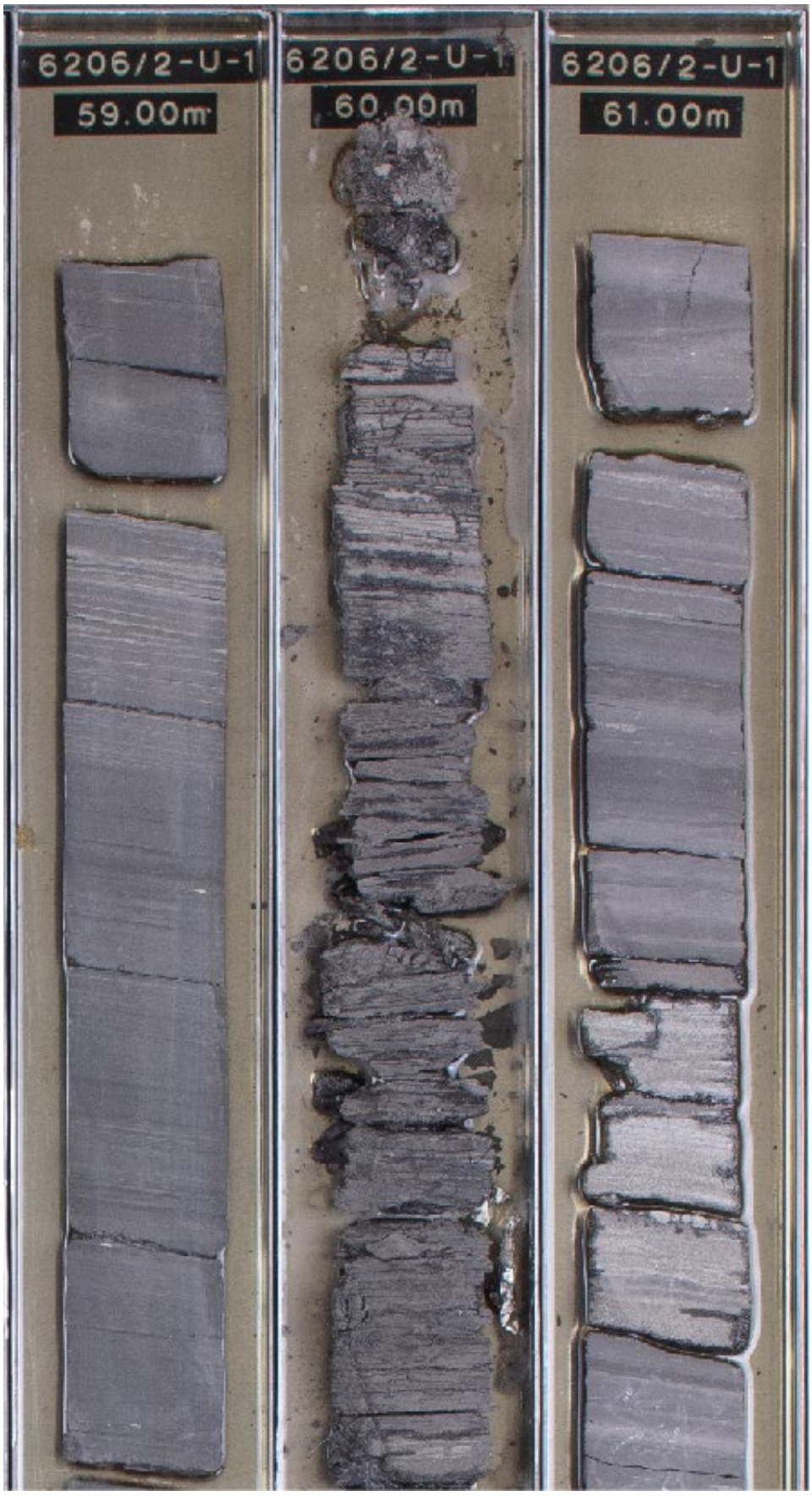


Figure 30: Core photo showing examples of thin turbidites and sandy laminae. The metal treys are 7.5 cm in width.

The low density turbidite is the result of a completely turbulent, low concentration, non-cohesive flow. The fining up trend indicates a decelerating flow, as described by Lowe (1982).

#### 4.3.1.2 High density turbidite

Lowe (1982) describes high density turbidites and their transportational and depositional characteristics and proposes a description and a model based on grain size and structures in the deposit. An ideal high density turbidite is shown in Figure 31 and Figure 32 with a low density turbidite on top. In general, high density turbidites have a higher concentration and the grains are suspended based on concentration effects while low density turbidites have a lower concentration and the sediments are supported by the turbulence in the flow (Lowe, 1982).

The higher concentration gives the flow the capacity to transport pebbles, and deposit coarser and thicker beds (Haughton et al., 2009). The deposit also shows more traction structures than low density turbidites as explained by Lowe, who found that the concentration is the highest at the base of the flow (Felix and Peakall, 2006; Lowe, 1982). This near-bed high concentration part of the flow might be weakly turbulent or close to laminar shear layers (Hiscott, 1994b; Talling, 2013). As the turbidity current wanes, the capacity decreases and the sediments deposit, which can occur in a rapid manner (Hiscott, 1994a).

It is worth noting that Lowe's (1982) $S_3$ equals Bouma's (1962) $T_A$, and that a high-density turbidity current commonly transforms into a low-density turbidity current.

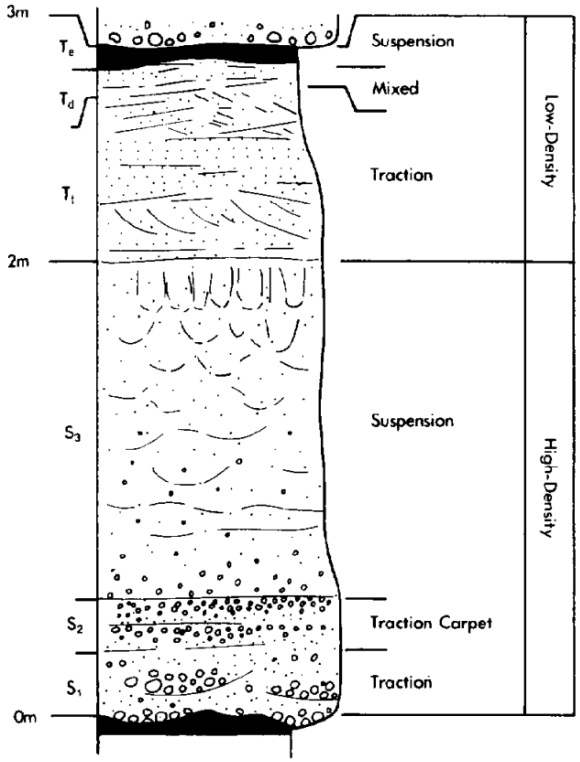


Figure 31: Sketch showing the Lowe sequence with suggested depositional mechanism of a sandy high density turbidite. From Lowe (1982).

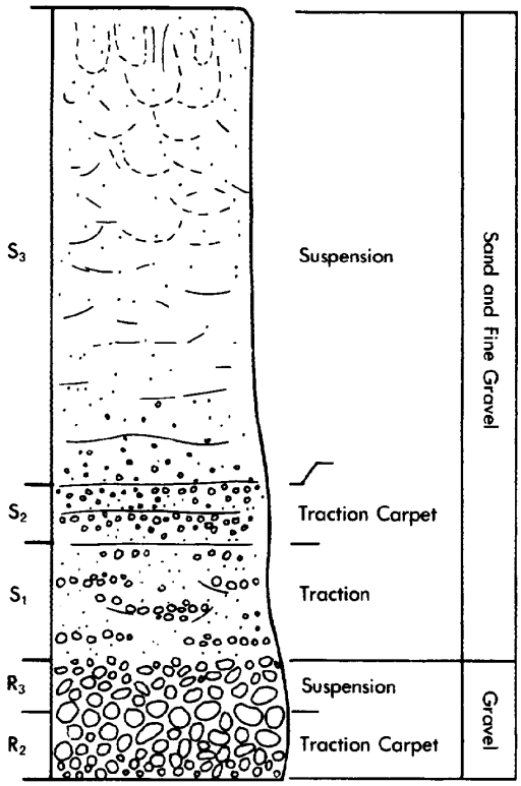


Figure 32: Sketch showing the Lowe sequence of a gravelly high-density turbidity current with suggested depositional mechanism. From Lowe (1982).

Turbidites can be initiated by several different processes. Hyperpycnal flows often occur in inertia-dominated deltas. These flows can turn into turbidity currents and show a more complex flow evolution than surge-type turbidites. These hyperpycnal turbidites show an inverse grading at the base, representing the waxing flow, followed by a normally graded deposit as the flow wanes. If the deposits show massive or parallel laminated sandstones, it may indicate a more sustained flow (Bhattacharya, 2006).

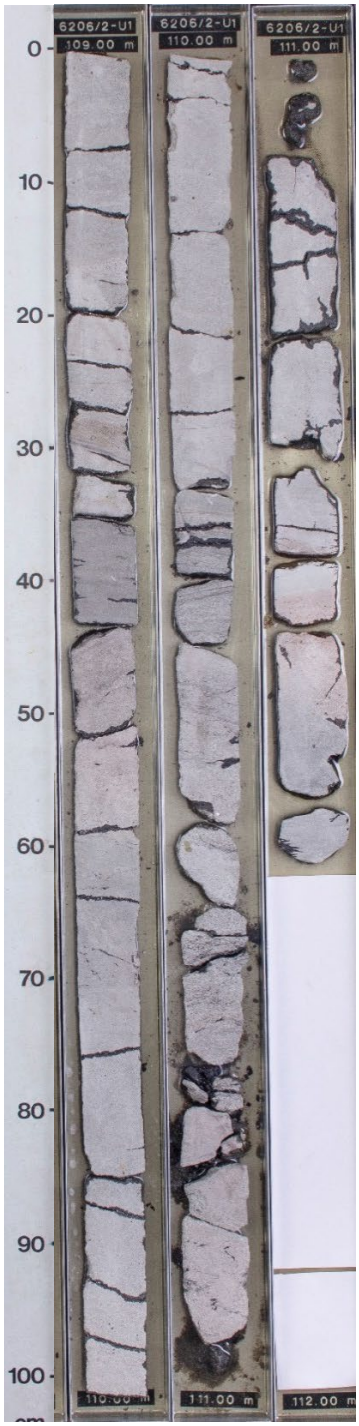


Figure 33: Core photo of quasi-steady turbidite (between red lines) and river run off (from middle red line to blue line) resulting in a hyperpycnite.

Storms and other disturbances of the sediment further up in the delta may cause sediments to destabilize and flow down the slope before being redeposited.

#### 4.3.1.2.1 Description

The thickness of the beds is up to 2 m, with several high density turbidites stacked on top of each other, indicating a pulsating influx of sediment. The boundaries between these pulses varies between sharper erosive boundaries and more gradual and undefinable transitions and variations in grain size, see Figure 34. The pulsating behaviour could be due to pulsating fluvial input and be related to hyperpycnites (see chapter 4.5).

In this core, the high density turbidites often have an erosional basal layer consisting of coarse sand to gravel (S1 or R2/R3), which is observed as either normally graded or inversely followed by normally graded deposits. Some R2/R3 deposits show larger clasts of clay or coal (see figures Figure 35 and Figure 37). R3 is overlain by coarse to gravelly sediments with traction structures (S1 or S2) as well as a general fining up sequence from coarse sand/gravel into massive sandstone (S3/T1). One bed comprises of several pulses of fining up massive sand ($T_A$), often with conglomeratic intervals. Some of the beds fine up into planar lamination ($T_B$), or rippled sandstone ($T_C$) which again is overlain by planar lamination ($T_D$).

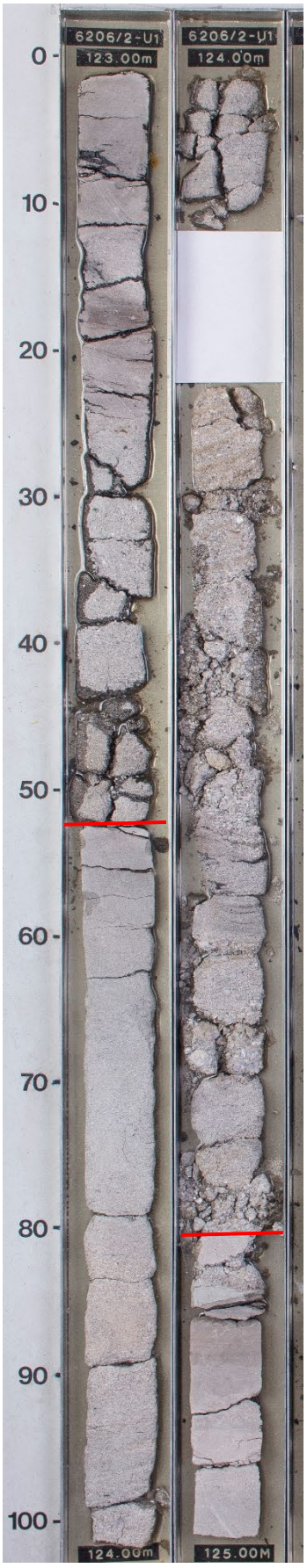


Figure 34: Core photo showing pulsating high density turbidites between the red lines.


Figure 35: Core photo showing high-density turbidites with larger clasts transported in the basal layer of the flow.

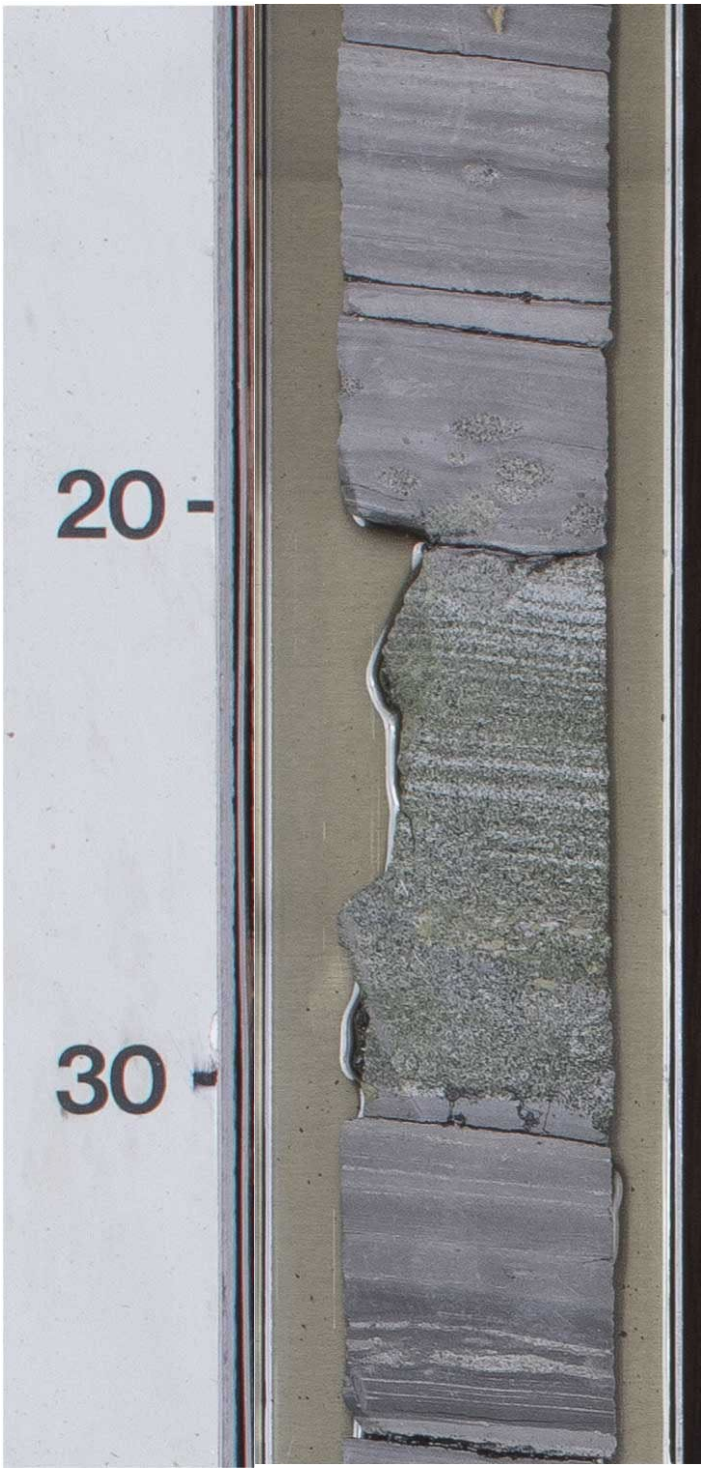


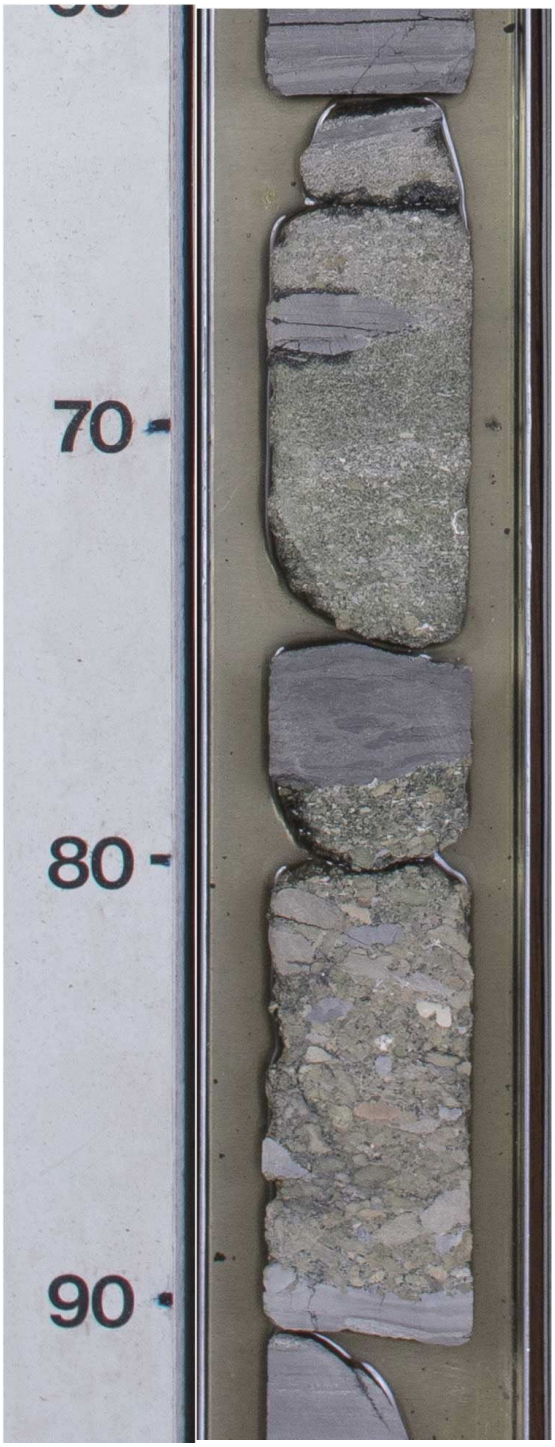


Figure 36 (Left): Core photo showing a glauconite-rich high-density turbidite with burrowing of the green sand above the upper boundary of the event bed. The deposit's lower boundary is at 56.30 m depth.

Figure 37 (Right): Core photo showing a glauconite-rich high-density turbidite with a large mud clast in the middle of the deposit. The lower boundary of the event bed is at 57.89 m depth.

### 4.3.2 Debrites

Debris flows are mainly laminar, non-Newtonian flows (Leeder, 2011), which can be subdivided with the two end members being mudflow and grain flow. What separates a debris flow from a turbidity current is the process of deposition, where turbidites deposit grain by grain or layer by layer on top of each other, while debrites show en masse freezing (Haughton et al., 2009).

#### 4.3.2.1 Mudflow deposits

A mudflow is a cohesive density flow with little to no coarse material (Mulder and Alexander, 2001). Mulder & Alexander (2001) defines a mudflow to be a cohesive flow with less than 5% gravel by volume and more mud than sand in the deposit. Mudflows have the capacity to carry pebbles and coarse sand due to the matrix strength caused by the large amount of cohesive mud (Tamura and Masuda, 2003). The transportational mechanism is plug flow, and the depositional mechanism is en masse deposition, which result in a chaotic bed with some possible shearing towards the top and the bottom of the deposit (Mulder and Alexander, 2001).

##### 4.3.2.1.1 Description

The mudflow deposits in the core generally have a high mud content with some mud clasts and coarser grains scattered throughout the deposit. Deposit thickness varies from 3 to 20 cm and the deposits show a wide range of grain sizes. These deposits have a messy texture due to the cohesiveness of the mud, see Figure 39, Figure 40 and Figure 41, and grains ranging from fine sand to pebbles are observed in several of the flows. Mud clasts are common and in the upper 45 m of the core, and the clasts range from mudstone, which is similar to the dark grey matrix, to clasts of glauconite. The clast shape is often elongated in a horizontal direction, some being angular, and others being rounded at the edges which may occur during transport.

Figure 38 (left): Core photo showing an example of a debris flow with clasts, varying texture and grain size.

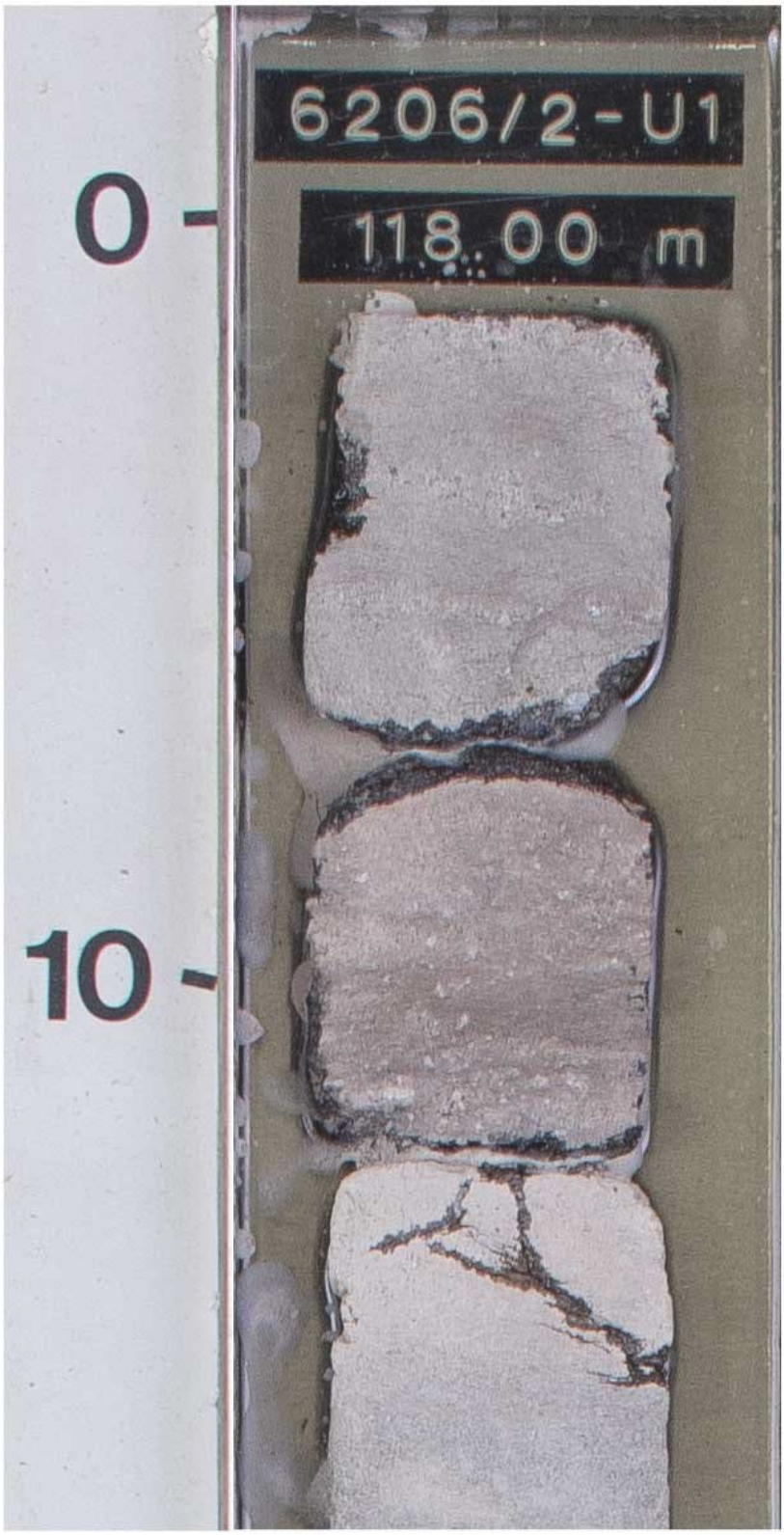


Figure 39: Core photo showing a discoloured mudflow deposit. The lower boundary of the deposit is at 118.12 m depth.

Figure 40: Core photo showing a mudflow with glauconite-rich sandy patches and mud clasts in a chaotic deposit. The base of the flow in the bottom of the photo at depth 58.31 m. The width of the metal tray the core lies in is 7.5 cm.


Figure 41: Core photo showing a mudflow with clasts of siderite, and pebbles. The top of the photo is at 92.82 m depth, and the deposit is 18 cm thick.

#### 4.3.2.2 Grain flows

Grain flows are cohesionless gravity flows which are supported by grain-to-grain collisions (Lowe, 1976), and thus friction-controlled as stated by Leeder (2011) and Mulder and Alexander (2001). The grain-to-grain interaction creates dispersive pressure, which supports the particles in the flow (Lowe, 1976). The flow is non-cohesive but is deposited due to en-masse freezing and the resulting deposit lacks sedimentary structures. The base of grain flow deposits might be erosional, followed by massive sand or gravel deposits which can be inversely graded if the concentration is high enough (Mulder and Alexander, 2001). These deposits might resemble $T_A$ or the Lowe sequence, as described in high density turbidity currents.

##### 4.3.2.2.1 Description

The beds observed in the core are 10-40 cm thick, massive sandstone beds. Some inverse grading at the bottom of the bed is observed, but there is no normal grading above this, which differentiates the deposits from $T_A$. The deposit is texturally immature with a varying grain size from silt up to very coarse sand. Both the upper and lower boundary are sharp.

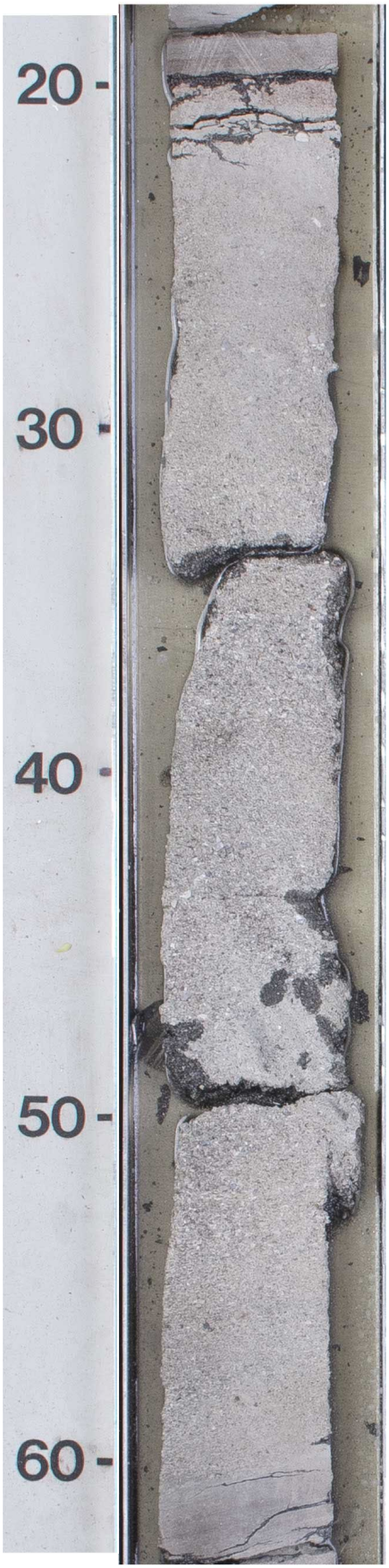


Figure 42: Core photo showing a grain flow deposit with the base of the flow at 162.60 m depth.

### 4.3.3 Slump deposits

Slumps get into motion due to liquefaction of accumulated sediments on the delta front (Postma, 1984). Slumps are laminar and move as a plug with shearing of a cohesive body of sediment. The sediments are not thoroughly mixed, and it is possible to observe distorted beds being folded. Due to the small amount of deformation, it is assumed that the sediments are only transported small distances.

#### 4.3.3.1 Description

The slumps observed in this core are relatively thin, with a thickness from 10 to 50 cm. Some of the slumps have a very high mud content with coarser material in what appear to be patches, see Figure 43 (159 m). These slumps are assumedly the result of several beds of varying texture that have been destabilized. The other type of slumps as seen in Figure 44 (108m) is sandier with distorted lamination.

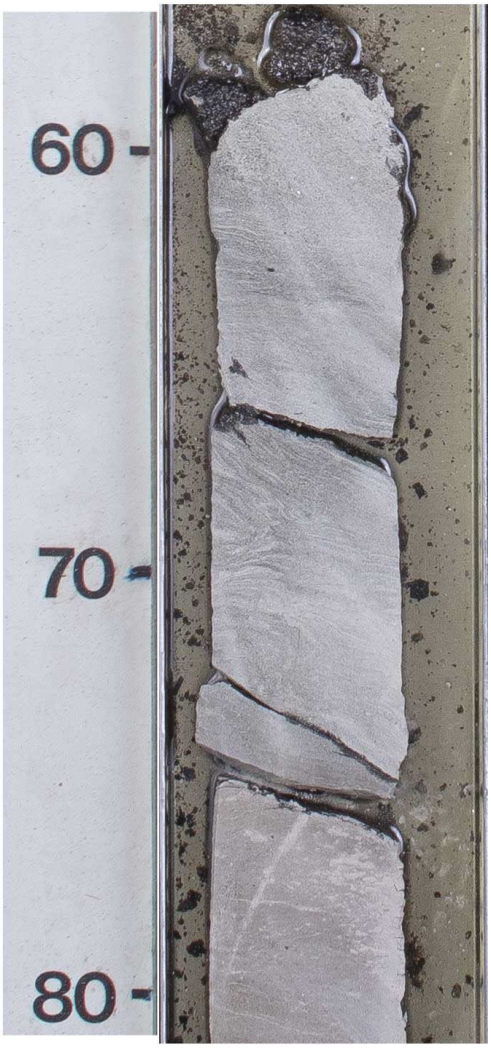


Figure 43 (Right): Core deposit showing patchy slump with chaotic texture. The picture is from the depth of 159.30 to 159.85 m.

Figure 44 (Left): Core deposit showing a sandy slump with distorted lamination with the top boundary of the deposit at 108.62 m depth.

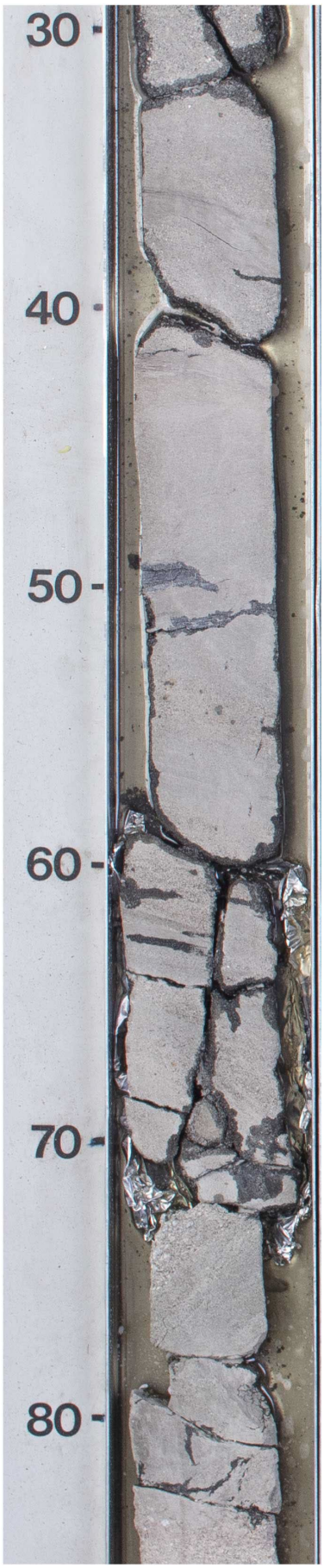

## 4.4 Flow transformation

As previously stated, turbidity currents and debris flows are two end members, while many flows can be placed somewhere in between. Throughout the span of a flow, the composition may change, which causes the flow mechanisms to evolve throughout the flow. This can occur both laterally and vertically and is defined by Haughton et al. (2009) as follows. "Flow transformation describes changes in flow state between laminar and turbulent states with or without intervening "transitional flow" conditions, or vice versa". The range of flows and their deposits are shown in Figure 45 (Haughton et al., 2009).

### 4.4.1 Hybrid event beds

Hybrid event beds, as described by Haughton et al. (2009), are observed throughout the core. They represent a flow transformation from non-cohesive to cohesive up the unit. Haughton et al. (2009) divided the beds into five facies, as shown in Figure 46. The flow starts as a high-density turbidity current and erodes muddy sediments from shallower parts of the slope. As more and more mud is incorporated into the flow, the cohesiveness increases, and the flow goes from turbulent to laminar.

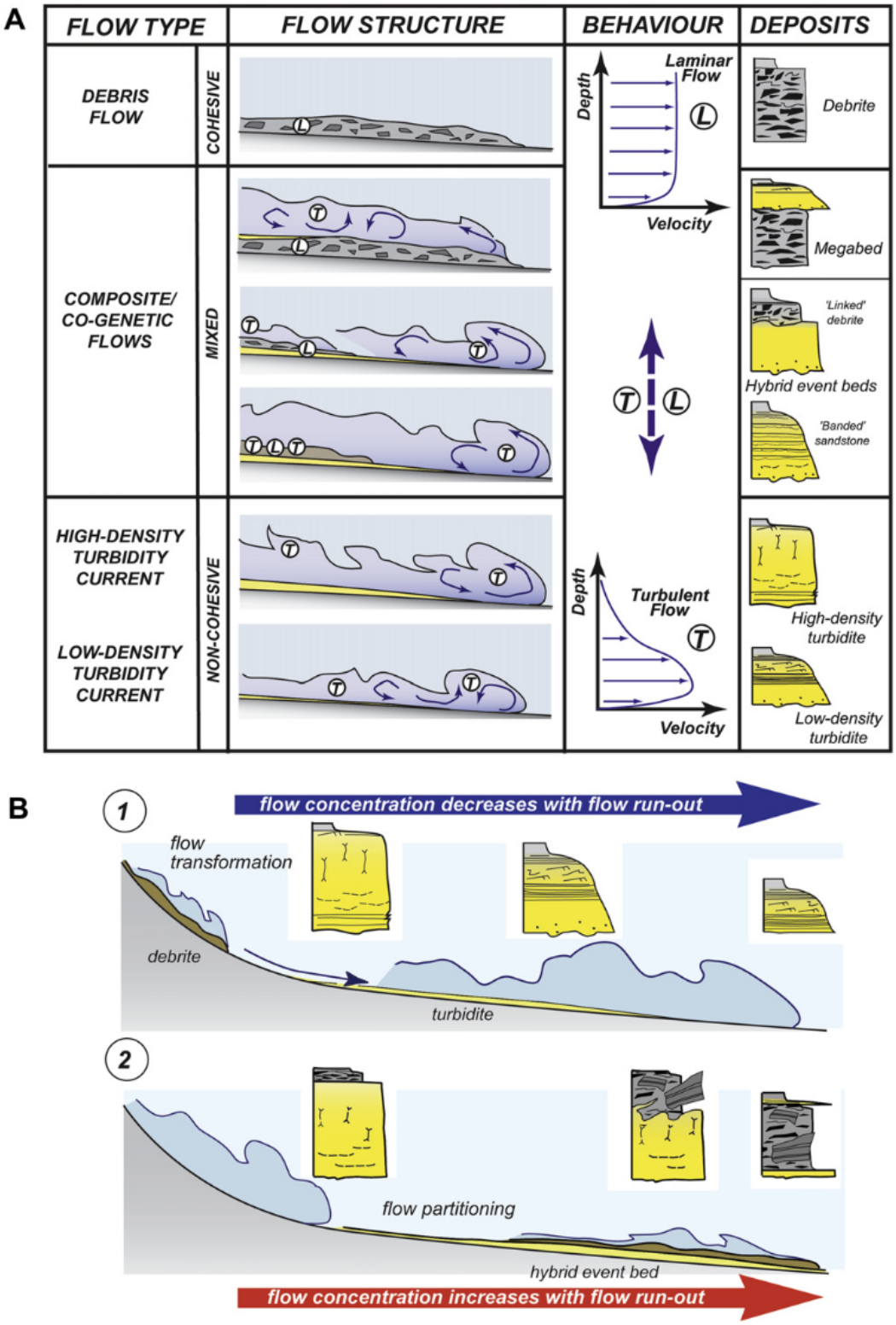


Figure 45: A) Diagram showing the relation between flow type, flow structure, behavior and deposit. B) Diagram showing the flow transformation evolution with the increasingly transformed deposits of dense to dilute (1) and hybrid event beds (2). From Haughton et al., (2009).

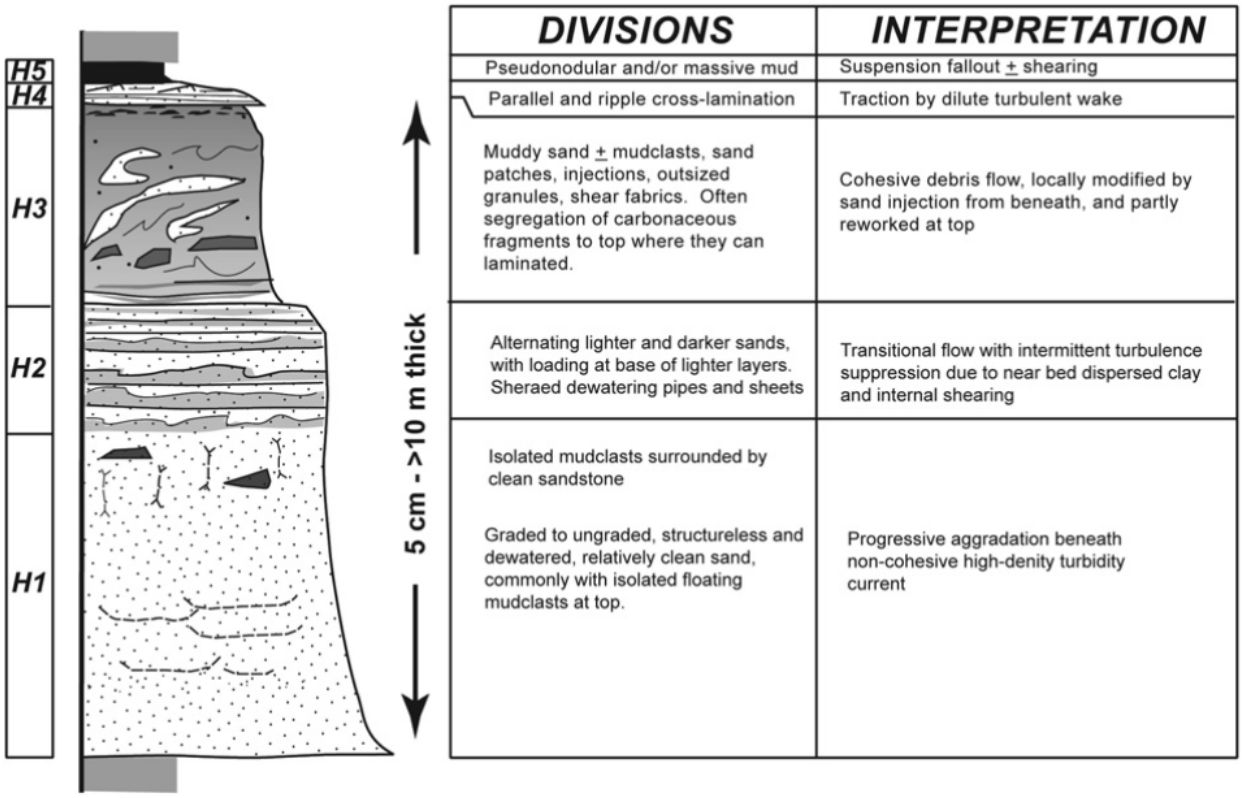


Figure 46: Diagram showing the ideal hybrid event bed sequence with description of the facies and the interpreted depositional mechanism. From Haughton et al., (2009).

#### 4.4.1.1 Description

The hybrid event beds have a sharp lower boundary, with the base of a high density turbidite sequence (H1 = $T_A$). There are two main variations of hybrid beds observed in the core. The first is a high-density turbidite that has a smaller, muddy, fine-grained mudflow-like deposit on top. The turbidite shows several pars of Lowes sequence for high density turbidites ($S_1$, $S_2$, $S_3$), see Figure 31, and the mudflow contains few clasts and larger grains. The other type has a massive sandstone at the base with some planar lamination ($T_A$, $T_B$), overlain by a thicker, structureless debrite, often containing larger mud clasts, and coarser grains up to pebble size. All the different parts of Haughton et al.'s (2009) facies model for hybrid beds are observed in the core, but a complete sequence has not been observed. The thickness of the observed hybrid beds is difficult to determine, as H5 cannot be separated from the hemipelagic suspension fallout. Example of hybrid bed is shown in Figure 47.

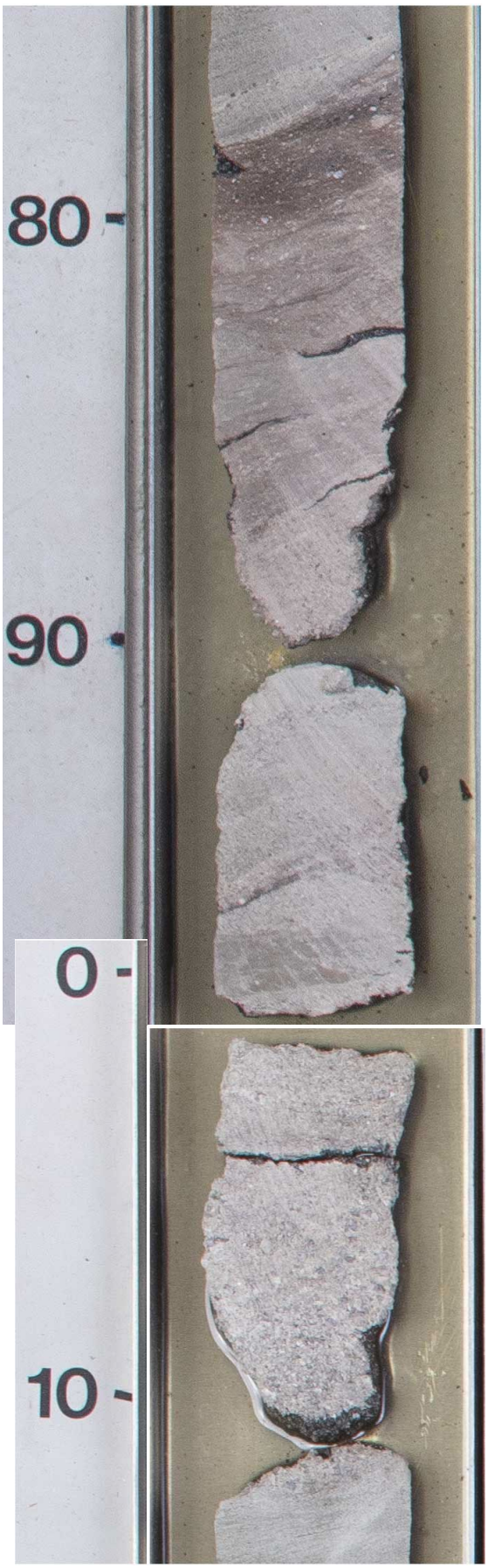


Figure 47: Core photo showing a hybrid event bed, at 141.13 to 140.78 m depth.

### 4.4.2 Dense to dilute flow

The dense to dilute flow deposits show flow transformation from debris flow to turbidity current through the process of dilution. If the dense debris flow has a high yield strength, the flow will not shear at the top nor the nose, and will therefore not be diluted, but if the yield strength is lower, part of the debris flow will rip apart and create a turbulent cloud (Felix and Peakall, 2009). The stratification of the flow, where the concentration is higher near the bed than towards the top of the flow, allows for a higher density underflow and a low density overflow to form (Felix et al., 2006).

Two forms of dense to dilute flow transformation are observed in the core, and what separates them is how the flow is diluted. The dilution can occur due to mixing of water into a cohesive flow, making it less cohesive, and therefore transforming into a diluted turbulent cloud. The transformation can also be from a non-cohesive laminar flow, referred to as a grain flow, to a turbulent non-cohesive flow. Both flow transformations create a less dense flow in the end, but the deposits vary significantly, depending on whether the starting material was cohesive or not.

Transformation from cohesive debris flow to a turbulent, non-cohesive turbidity current is observed several times throughout the core.

#### 4.4.2.1 Description

The deposits are up to 1.8 m thick, with the debritic part of the sequence often forming the majority of the bed.

These deposits often show a muddy, chaotic segment with a patchy and poorly mixed conglomerate or sandstone with a very muddy matrix at the base of the deposit. The deposits appear patchy, which could be explained by larger, somewhat consolidated clasts of sediments have been ripped up and transported with the flow without being fully resuspended. A turbidite overlies the debritic material, showing one or several parts of the Bouma sequence and fining up into hemipelagic suspension fallout.

The other observed version of dense to dilute flow is a change from high concentration to low concentration. The result of a high to low concentration flow transformation can be observed, where the low density is deposited before the high density. The nose of the flow is diluted, depositing rippled and planar laminated sandstone. The concentration as the main body of the flow is deposited, the higher concentrated part of the flow is deposited, giving the unit a coarsening up trend.

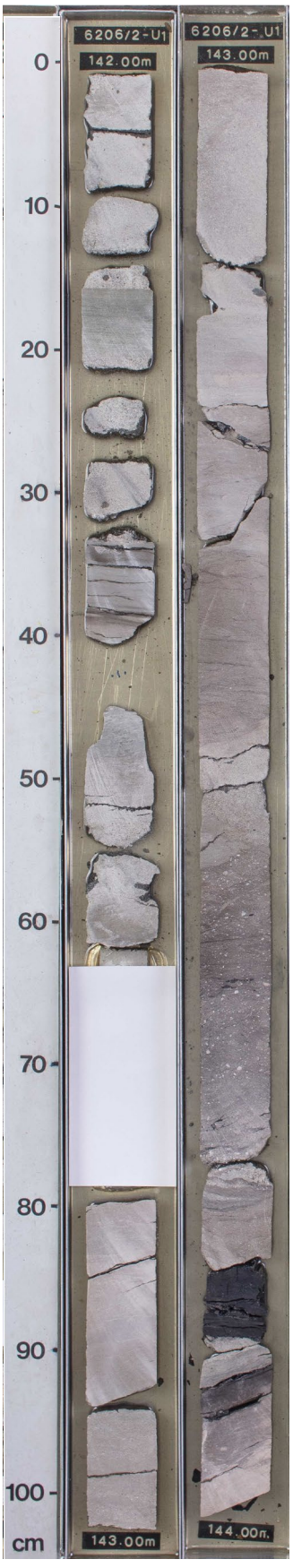


Figure 48: Core photo showing deposits of dense to dilute flow transformation.The base of the bed is at 143.78.

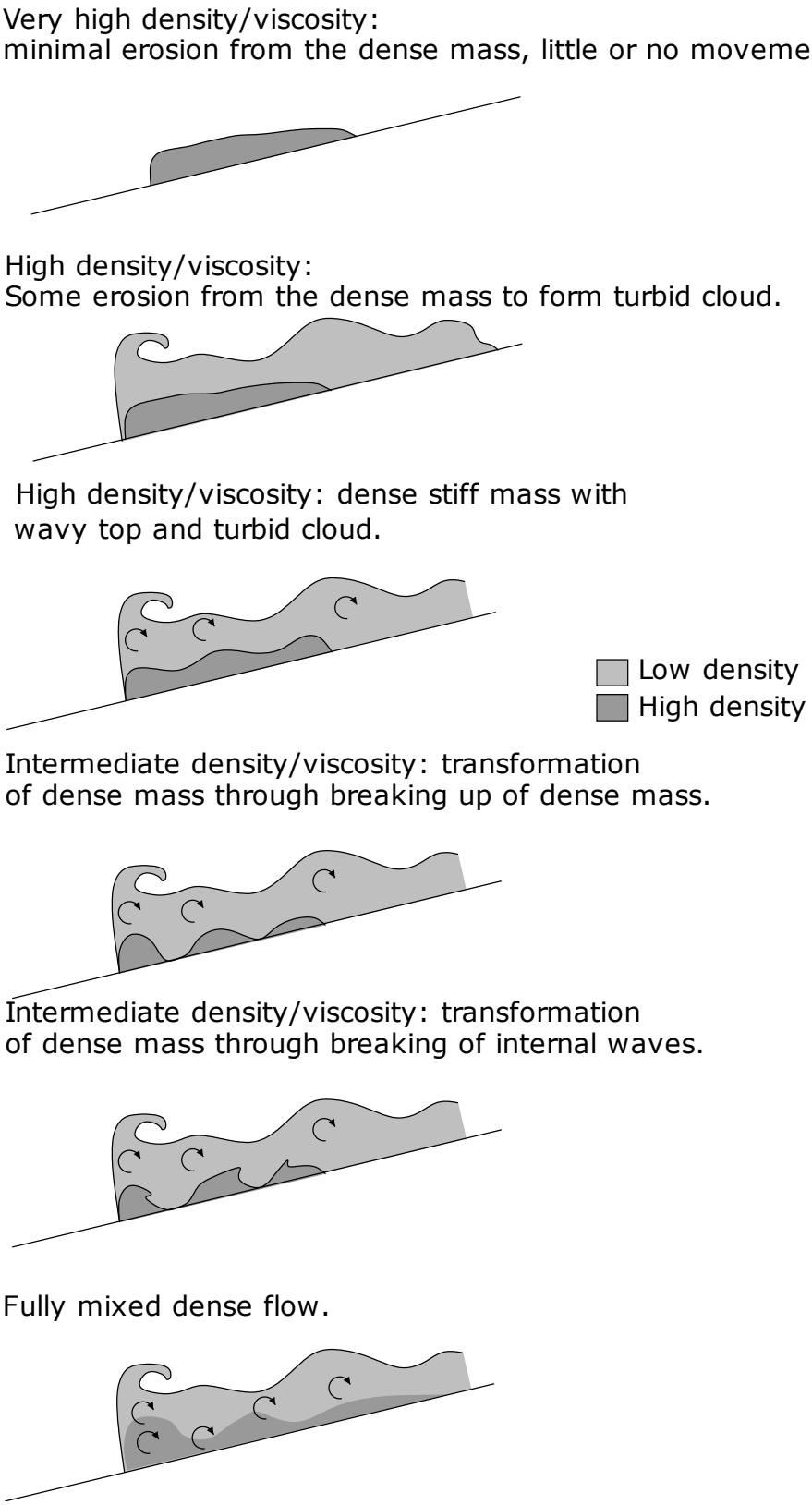


Figure 49: Diagrams showing a flow model of the evolution for the dilution of dense flows, where the least diluted is at the top and most diluted is at the bottom of the figure. From (Felix and Peakall, 2006).

### 4.4.3 Complex flow transformation beds

Some beds show flow transformation from dense to dilute to dense and back to dilute again. This may be due to the cohesive part of the flow breaking up, with turbulent flow in between, as described by Felix et al. (2009), see Figure 49. They use the term broken-apart flow where the internal waves of the flow reached an amplitude where the dense part breaks apart and separates, see Figure 49. The deposit shows debritic lenses in a turbidite, with either sharp or gradual boundaries (Felix et al. 2009). The turbiditic and debritic deposits of a complex flow appear similar to the standard turbidites and debrites described in chapter 4.3.1 and 4.3.2.

#### 4.4.3.1 Description

In the core, it is difficult to identify this type of flow transformation, as flow transformation often shows lateral transformation, rather than vertical. The event bed in Figure 50 shows the alternating debritic and turbiditic sediments with both gradual and sharp boundaries.

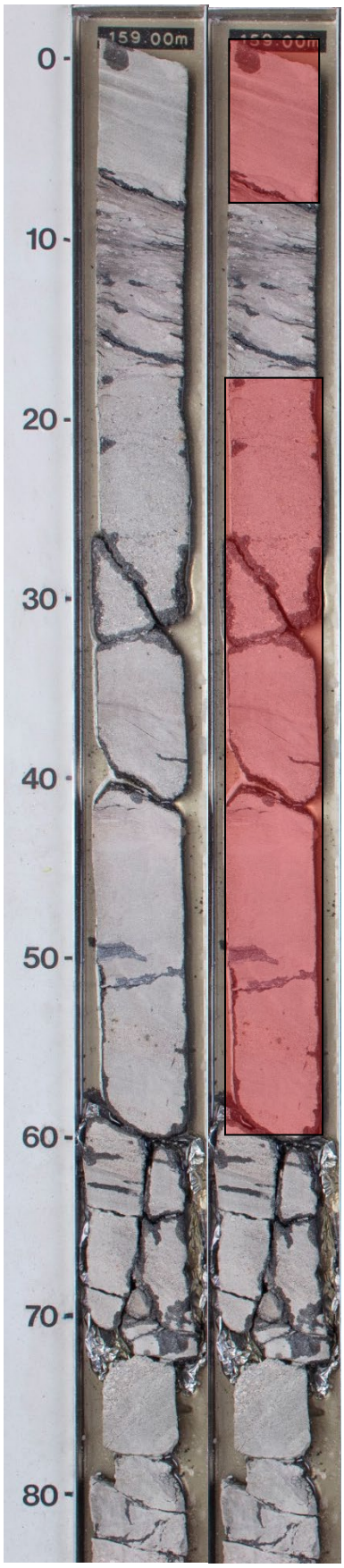


Figure 50: Core photo showing complex flow deposits, with alternating dense and dilute deposits. The dilute deposits are marked with red.

## 4.5 Hyperpycnal flows

Hyperpycnal flows occur when a river flows into a water body of lower density than the river water, and the flow travels along the seabed under the water body as an underflow (Felix et al., 2006), see Figure 51. The cause of the density difference can be salinity, temperatures or suspended sediments. According to Bhattacharya (2006), hyperpycnal flows in marine settings are dependent on the sediment concentration being greater than the density of the saline waterbody the flow travels into. These conditions occur in deltas and hyperpycnal flows are a mechanism for sediment transport out to the deeper shelf. The deposits are described as either a fluid mud, a turbidite, but can also be massive fining/coarsening up if the flow is either waxing or waning (Bhattacharya, 2006). Hyperpycnal flows have the potential to transform into turbidity currents, as discussed in chapter 4.3.1. Such flows may be erosive and can remove mud from the seabed (Bhattacharya, 2006), thus increasing the flow concentration. If the flow is not strong enough, the flow might not transform into a larger flow, e.g., a turbidity current.

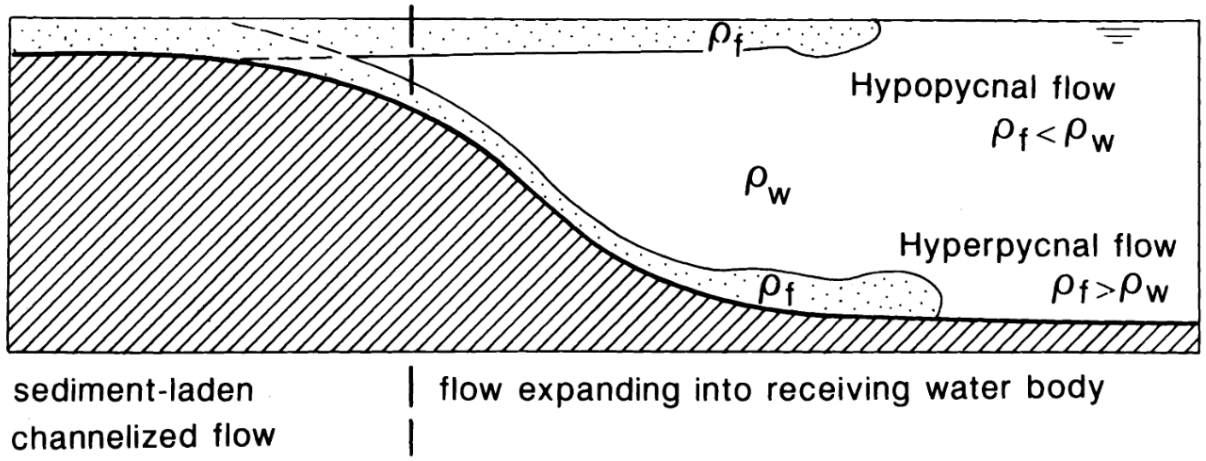


Figure 51: Diagram illustrating a hyperpycnal and a hypopycnal flow. Here $\rho_f$ is the density of the flow and $\rho_w$ is the density of body of water. From Mulder and Alexander (2001).

Mulder and Alexander (2001) characterise a hyperpycnal flow as a quasi-steady concentrated density flow forming at a river mouth, which travels a short distance carrying a relatively small sediment volume. The deposit of a hyperpycnal flow is called a hyperpycnite and several possible deposit sequences are shown in Figure 52. Different types of hyperpycnites have been found in the core.

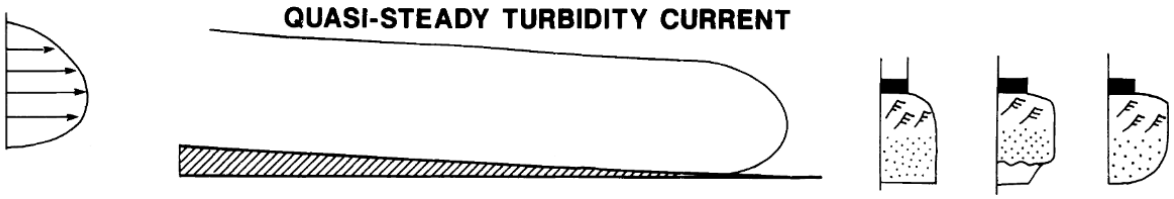


Figure 52: Diagram showing the velocity profile, an idealized flow shape and schematic logs of the deposit of a quasi-steady turbidity current. From Mulder and Alexander (2001).

Description

The hyperpycnal deposits in this core often show both inverse and normal graded sandstone (i.e. the sequence shown on the right-most side in Figure 52); an example is shown in Figure 33. The bed thickness varies greatly, and it is difficult to distinguish the thinner hyperpycnites from massive turbidite sandstone ($T_A$ or $S_3$). The hyperpycnites also lack larger clasts. In between events, hemipelagic sedimentation dominates. These sediments are often structureless or show some planar lamination, see Figure 33.

## 4.6 Hemipelagic sedimentation

When the river flow carries little sediment, it can transform into a hypopycnal (see Figure 51) or homopycnal plume at the river mouth, resulting in suspended sediment in the upper part of the water column. As the discharge decreases, the suspended muds may flocculate and settle as mud drapes on the sea floor over vast areas (Bhattacharya, 2006). As these muds settle, they have a very low concentration, and the muds can therefore be transported further out if a gravity flow sweeps the sea floor.

Hemipelagic sedimentation is observed in the core as mudstones or finer sandstones in between the event beds (Figure **53**). The suspension fallout from hypopycnal plumes is hard to distinguish from the muddy events and turbidite caps.

The river input in between events varies greatly in grain size and grading. The variation of grain size in the hemipelagic deposits is interpreted to be caused by the waxing and waning of the river's capacity and competence.

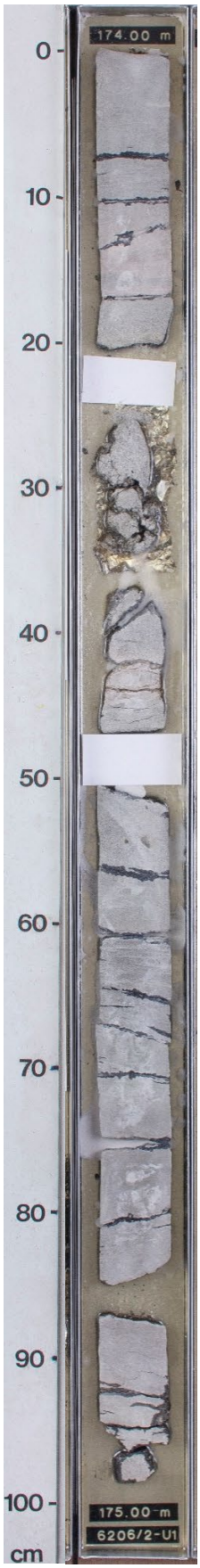


Figure 53: Core photo of hemipelagic sedimentation.

# 5 Discussion

This work agrees with Smelror et al. (1994) regarding the depositional environment being a deltaic setting. They suggest the lower part of the core to have formed in a terrestrial, distal fan setting with marine influence, while the upper part of the core was interpreted as inner shelf/prodelta to open marine at the top.

The first part of this discussion examines the depositional environment and compares this with the interpretation of Smelror et al. (1994), while in the second part the flow processes of event beds are discussed in more detail.

## 5.1 Depositional environment and evolution

Throughout the core, both the elemental composition of the deposits and the type of deposit change significantly. The elemental measurements indicate terrestrial input as the dominant supply of sediment in the lower part of the core. At 98.3 m there is a notable reduction in concentration of proxies related to terrestrially derived material (Zr, Th, Cu, Zn, Al, K, Ti). In contrast, the concentrations of proxies for marine influence (Sr and Ca) increase from 98.3 m and towards the top. Below 98.3 m depth, the deposits are dominated by event beds and detrital, continentally derived sediments while above 98.3 m, the deposition is dominated by low-density turbidity currents and hemipelagic fallout.

Bioturbation levels and proxies for redox conditions indicate that deposition took place under oxic conditions throughout.

### 5.1.1 Lower part of the core: flood-dominated delta

As the event beds are interpreted to be mainly triggered by hyperpycnal flows from the river outlet (see further discussion below), or storms, the suggested delta type for this delta is a flood-dominated delta. The pulsing flow deposits observed in the core may be indicative of the deposition mainly taking place under major flooding periods, often associated with storms. Bhattacharya (2006) argues that this sort of dominant depositional mechanism can be categorized as a flood-dominated delta. According to Mutti et al. (2000), flood-dominated fluvio-deltaic systems are an important part of alluvial and shallow marine, tectonically active basins on active margins, which fits with the suggested geological setting in the study area of Brekke et al. (2001).

Glauconite is found in event beds in both the lower and upper parts of the core, which indicates marine conditions in both parts. Although there is only one glauconite bed in

the lower part, this still indicates marine conditions just before the hiatus as well as after the 80 Ma gap in deposition. The redeposition of glauconite indicates that the deposits cannot have formed in very shallow water, or there would be no space for redeposition. On the other hand, the deposits cannot have formed in very deep water either, as indicated by the hummocky cross stratification and the deposition of short-travelled hyperpycnites linked to a river mouth.

Thus, although the overall interpretation of the depositional environment is in agreement with Smelror et al. (1994), the deposits are interpreted here to have formed in a more constant marine environment with regular fluvial input.

### 5.1.2 Transition and upper part of the core

The transition from fluvial dominated to marine dominated indicates a reduction in fluvial input which can occur due to several reasons. As the boundary between the fluvially dominated and marine dominated deposits is a hiatus of 80 million years (Smelror et al., 1994), the transition is not observed and the mode of change cannot be determined with certainty.

One explanation is a transgression, and therefore a change in depositional environment from near the river outlet to more distal on the delta front or prodelta. Another hypothesis for change in energy conditions is lobe switching of the river outlet. In this scenario, the water depth of deposition would not change throughout the entire depositional period of the core, but the river influence would reduce drastically when the river switched outlet. Given the time gap of 80 Ma, it is perhaps less likely that the water depth would remain constant, suggesting that a transgression is a likelier explanation.

Either way, the energy is decreased, and the environment has changed from a high energy environment at the delta front to a more quiescent environment. Regardless of which depositional environment the upper part of the core is, the dominant influence has changed from fluvial to marine. For the purpose of this thesis, that is the most interesting change. The event beds ceased when the fluvial input reduced, indicating that the event beds are dependent on fluvial input to occur. The fluvial influence in the lower part is also indicated by the hyperpycnites, which disappear in the upper part of the core, again indicating a link between event beds and fluvial processes.

## 5.2 Flow processes interpretation

As described above, various types of sediment gravity flow deposits have been interpreted in the deltaic part of the core. The flows responsible for these deposits can all form in deltas, either linked to river input through hyperpycnal flows or from destabilisation of the delta front. Flow types such as debris flows, turbidity currents, and transforming flows from dense to dilute flow are expected in delta deposits. Hyperpycnal flows can transform into such sediment gravity flows in two processes, as described by Bhatthacharya (2006) and Mulder and Alexander (2001). A hyperpycnal turbidity current can flow directly out from the river into the basin, often showing thicker deposits due to a sustained flow. These flows are termed quasi-steady turbidity currents by Mulder and Alexander (2001). If the sediment concentration is not high enough to flow directly into the basin, the sediments may deposit rapidly, resulting in an unstable slope, which could fail and flow out into the basin. Dense flows caused by slope instability may transform into more dilute flows (Felix and Peakall, 2006).

More unexpected in deltas are hybrid beds. The literature suggest that the deposition of hybrid beds occur in distal fan deposits (Fonnesu et al., 2018; Haughton et al., 2009; Pierce et al., 2017; Talling, 2013) or mid-fan (Fonnesu et al., 2018; Hussain et al., 2020) deposits in a larger, deeper marine environment. Haughton et al.'s (2009) figure (Figure 45) illustrates the processes for formation of a hybrid event bed. These processes can also take place in the deltaic environment envisioned in the current work.

Here, two alternative flow transformation processes are suggested. According to Bhattacharya (2006), extensive mud drapes may form during more quiet periods in between flooding events and hyperpycnal flows. Bhattacharya (2006) suggests the possibility for mud drapes to be resuspended during flooding events. As mud is mixed into the hyperpycnal flow, the flow may become increasingly cohesive, creating a laminar underflow which can deposit as a hybrid bed, see Figure 54.

A second flow mechanism is as follows. As the river flows into the basin, the fluid may have a very high sediment concentration in the case of a flood. As the flow meets the more still-standing water in the basin, in addition to the space of the flow increasing significantly from a confined river channel to a delta, the sediment-laden water will slow down, and the competence of the flow will decrease. Due to the rapid deposition, the slope may destabilise and flow further out into the delta as a flow with a changed composition compared to the original fluvial input. The speed of the river input in addition to the high sediment concentration may erode into the seafloor, changing the composition of the flow.

These two flow mechanisms show that deposition of hybrid beds may also occur in a shallow, flood-dominated delta environment, and care should be taken when hybrid event beds are found. The results from this work show that it cannot be assumed that such event beds are confined to distal fans.

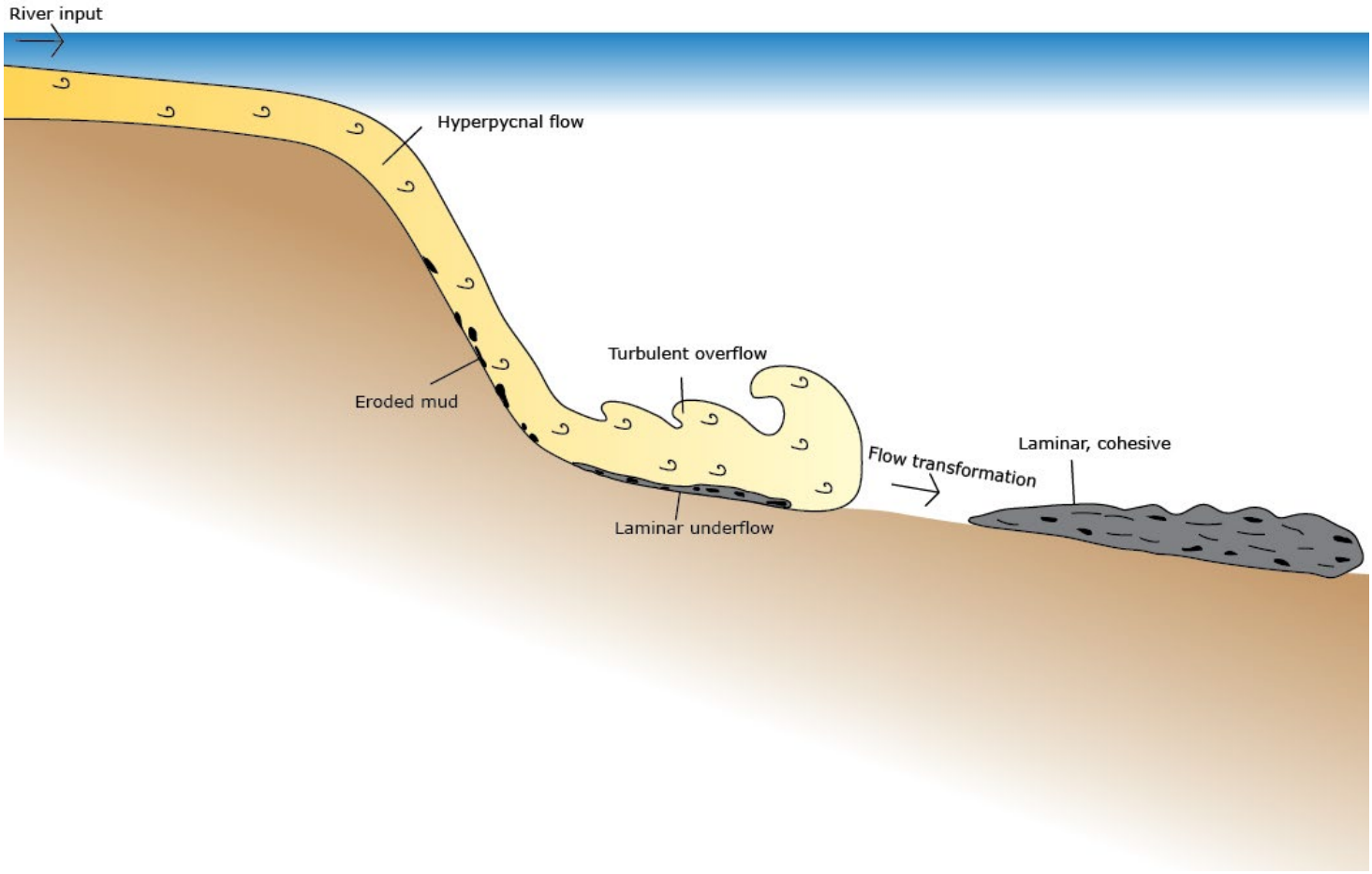


Figure 54: Diagram showing the inferred flow processes of the transformation from hyperpycnal flow to hybrid event bed.

## 5.3 Further work

This study presents the possibilities for the use of XRF on event beds and in deltaic setting. It is recommended to further investigate the possibilities regarding small scale XRF on event beds and related to flow transformation to determine any possible elemental signatures in these deposits for a more reliable interpretation. It is also necessary to investigate depositional environments for flow types and flow transformation, as e.g., hybrid beds do not only form in the previously suggested mid fan or deep marine environment. Investigate depositional environments for flow types, as e.g. hybrid beds do not only form in deep marine, mid fan. Investigate other deltaic deposits for these flow processes.

Several of the elemental measurements (Ti, K, Al, Si, Zn, Zr, S, Sr, Ba and possibly Ca) show cyclicity on various scales in this core. This is something that should be looked into for further research, as it is outside the scope of this thesis. A time series analysis of the cyclicity in the core would provide a better understanding of the timing of the events.

# 6 Conclusions

The aim of this study was to reinterpret the depositional environment and flow processes of the deposits in core 6206/02-U-01. The sediments in the lower part of the core show a large range of sediment gravity flow deposits, and are formed from low density turbidites, high density turbidites, mudflows, grain flows, slumps, dense to dilute flows, hybrid event flows and hyperpycnal flows. The flow transformation processes described in this work include dense to dilute flow transformation and hybrid event transformation.

In the lower Jurassic deposits in the lower part of the core (below 98.3 m depth), elemental proxies and event beds indicate a depositional environment dominated by fluvial processed and with an influx of continentally derived sediments. The Lange and Kvitnos formations in the upper part of the core (above 98.3 m) show few, small scale, event beds, as opposed to the underlying lower part of the core. Elemental proxies, along with the lack of event beds indicate an environment dominated by marine processes.

Based on the proxies and the event beds (including common hyperpycnites), the depositional environment of the lower part of the core is interpreted as a flood-dominated delta. The presence of possible hummocky cross stratification and resedimented glauconite suggest a prodelta setting.

The hybrid beds found in this deltaic setting are interpreted to have formed from transformation of hyperpycnal flows, either by incorporation of mud eroded from the delta bed, or by slowing down of mud-laden hyperpycnal flows resulting in increasingly cohesive and laminar flows.

# References


Algeo, T.J., and Maynard, J.B., 2004, Trace element behaviour and redox facies in core shales of Upper Pennsylvanian Kansas type cyclothems: Chemical Geology, v. 206, p. 289-318.

Allen, J.R.L., 1985, Priciples of physical sedimentology, Chapman & Hall, 272 p.

Bhattacharya, J.P., 2006, Deltas, *in* Posamentier, H.W., and Walker, R.G., eds., Facies Models Revisited, SEPM, p. 237-292.

Bianchette, T.A., McCloskey, T.A., and Liu, K.-b., 2016, Re-evaluating the Geological Evidence for Late Holocene Marine Incursion Events along the Guerrero Seismic Gap on the Pacific Coast of Mexico: PLoS ONE, v. 11.

Blystad, P., Brekke, H., Færseth, R.B., Larsen, B.T., Skogseid, J., and Tørudbakken, B., 1995, Structural of the Norwegian continental shelf. Part II: The Norwegian Sea Region: NPD-Bulletin, v. 8, p. 45.

Bouma, A.H., 1962, Sedimentology of some flysch deposits: A graphic approach to facies interpretation: Elsevier, p. 168.

Brekke, H., Sjulstad, H.I., Magnus, C., Williams, R.W., Martinsen, O.J., and Dreyer, T., 2001, Sedimentary environments offshore Norway - an overview. Sedimentary Environments Offshore Norway - Palaeozic to Recent: Elsevier, v. 10, p. 7-37.

Calvert, S., and Pedersen, T.F., 2007, Chapter Fourteen Elemental Proxies for Palaeoclimatic and Palaeoceanographic Variability in Marine Sediments: Interpretation and Application: Developments in Marine Geology, v. 1, p. 567-644.

Chamley, H., 2001, Clay Mineralogy, *in* Cochran, J.K., Bokuniewicz, H.J., and Yager, P.L., eds., Encyclopedia of Ocean Sciences, Academic Press, p. 74-81.

Felix, M., Leszczynski, S., Slaczka, A., Uchman, A., Amy, L., and Peakall, J., 2009, Field expressions of the transfromation of debris flows into turbidity currents, with examples from the Polish Carpathians and the French Maritime Alps: Marine and Petroleum Geology, v. 26, p. 2011-2020.

Felix, M., and Peakall, J., 2006, Transformation of debris flows into turbidity currents: mechanisms inferred from laboratory experiments: Sedimentology, v. 53, p. 107-123.

Felix, M., Peakall, J., and McCaffrey, W.D., 2006, Relative importance of processes that govern the generation of particulate hyperpycnal flows: Journal of Sedimentary Research, v. 76, p. 382-387.

Fonnesu, M., Felletti, F., Haughton, P.D.W., Patacci, M., and McCaffrey, W.D., 2018, Hybrid event bed character and distribution linked to turbidite system sub-environments: The North Apennine Gottero Sandstone (north-west Italy): Sedimentology, v. 65, p. 151-190.

Friis, H., Poulsen, M.L.K., Svendsen, J.B., and Hamberg, L., 2007, Discrimination of density flow deposits using elemental geochemistry - Implications or subtle provenance differentiation in a narrow submarine canyon, Palaeogene, Danish North Sea: Marine and Petroleum Geology, v. 24, p. 221-235.

Halland, E.K., Gjeldvil, I.T., Johansen, W.T., Magnus, C., Meling, I.M., Mujezinovic, J., Riis, F., Rød, R.S., Pham, V.T.H., and Tappel, I., 2014. Structural elements in the Norwegian Sea. Retrieved 10.12. 2022 from http://npd.no/contentassets/aa14c3079a47451c88268166ba4e61aa/chapter-5.pdf

Haughton, P., Davis, C., McCaffrey, W., and Barker, S., 2009, Hybrid sediment gravity flow deposits - Classification, origin and significance: Marine and Petroleum Geology, v. 26, p. 1900-1918.

Hesse, R., and Schacht, U., 2011, Chapter 9 - Early Diagenesis of Deep-Sea Sediments, *in* Hüneke, H., and Mulder, T., eds., Deep-sea Sediments: Developments in Sedimentology, Elsevier, p. 557-713.

Hiscott, R.N., 1994a, Loss of capacity, not competence, as the fundamental process governing deposition from turbidity currents: Journal of sedimentary research, v. A64, p. 209-214.

Hiscott, R.N., 1994b, Traction carpet stratification in turbidites - fact or fiction: Journal of sedimentary research, v. A64, p. 204-208.

Hussain, A., Haughton, P.D.W., Shannon, P.M., Turner, J.N., Pierce, C.S., Obradors-Latre, A., Barker, S.P., and Martinsen, O.J., 2020, High-resolution X-ray fluorescence profiling of hybrid event beds: Implications for sediment gravity flow behaviour and deposit structure: Sedimentology, v. 67, p. 2850-2882.

Jongepier, K., Rui, J.C., and Grue, K., 1996, Triassic to Early Cretaceous stratigraphic and structural development of the northeastern Møre Basin margin, off Mid-Norway: Norsk Geologisk Tidsskrift, v. 76, p. 199-210.

Leeder, M.R., 2011, Sedimentology and sedimentary basins: from turbulence to tectionics, Wiley-Blackwell, 784 p.

Lowe, D.R., 1976, Grain flow and grain flow deposits: Journal of Sedimentary Research, v. 46, p. 188-199.

Lowe, D.R., 1982, Sediment gravity flows: II Depositional Models with Special Reference to the Deposits of High-Density Turbidity Currents: Journal of sedimentary research, v. 52, p. 279-297.

Mueller, P., Patacci, M., and Giulio, A.D., 2017, Hybrid event beds in the proximal to distal extensive lobe domain of the coarse-grained and sand-rich Bordighera turbidite system (NW Italy): Marine and Petroleum Geology, v. 86, p. 908-931.

Mulder, T., and Alexander, J., 2001, The physical character of subaqueous sedimentary density flows and their deposits: Sedimentology, v. 48, p. 269-299.

Mutti, E., Tinterri, R., di Biase, D., Fava, L., Mavilla, N., Angella, S., and Calabrese, L., 2000, Delta-front facies associations of ancient flood dominated fluvio-deltaic systems: Rev. Soc. Geol. España, v. 13, p. 165-190.

Mørk, M.B.E., Vigran, J.O., Smelror, M., Fjerdingstad, V., and Bøe, R., 2003, Mesozoic mudstone compositions and the role of kaolinite weathering - a view from shallow cores in the Norwegian Sea (Møre to Troms): Norwegian Journal of Geology, v. 83, p. 61-78.

Pierce, C.S., Haughton, P.D.W., Shannon, P.M., Pulham, A.J., Barkers, S.P., and Martinsen, O.J., 2017, Variable character and diverse origin of hybrid event beds in a sandy submarine fan system, Pennsylvanian Ross Sandstone Formation, western Ireland: Sedimentology, v. 65, p. 952-992.

Postma, G., 1984, Slumps and their deposits in fan delta front and slope: Geology, v. 12, p. 27-30.

Poulsen, M.L.K., Friis, H., Svendsen, J.B., Jensen, C.B., and Bruhn, R., 2007, The Application of Bulk Rock Geochemistry to Reveal Heavy Mineral Sorting and Flow Units in Thick, Massive Gravity Flow Deposits, Siri Canyon Palaeocene Sandstones, Danish North Sea: Developments in Sedimentology, v. 58, p. 1099-1121.

Rosenthal, Y., 2007, Chapter Nineteen Elemental Proxies for Reconstructing Cenozoic Seawater Paleotemperatures from Calcareous Fossils, *in* Hillaire-Marcel, C., and Vernal, A.D., eds., Developments in Marine Geology, Elsevier, p. 765-797.

Smelror, M., Jacobsen, T., Rise, L., Skarbø, O., Verdenius, J.G., and Vigran, J.O., 1994, Jurassic to Cretaceous stratigraphy of shallow cores on the Møre Basin Margin, Min-Norway: Norsk geologisk tidsskrift, v. 74, p. 89-107.

Talling, P.J., 2013, Hybrid submarine flows comprising turbidity current and cohesive debris flow: Deposits, theoretical and experimental analyses, and generalized models: Geosphere, v. 9, p. 460-488.

Tamura, T., and Masuda, F., 2003, Shallow-marine fan delta slope deposits with large scale cross-stratification: the Plio-Pleostocene Zaimokuzawa formation in the Ishikari Hills, northern Japan: Sedimentary geology, v. 158, p. 195-207.

Tanaka, K., Akagawa, F., Yamamoto, K., Tani, Y., Kawabe, I., and Kawai, T., 2007, Rare earth element geochemistry of Lake Baikal sediment: its implication for geochemical response to climate change during the Last Glacial/Interglacial transition.: Quarternary Science Reviews, v. 26, p. 1362-1368.

ThermoFisher, 2018. How does XRF work? Retrieved 31.10. 2022 from https://www.thermofisher.com/no/en/home/industrial/spectroscopy-elemental-isotope-analysis/spectroscopy-elemental-isotope-analysis-learning-center/elemental-analysis-information/xrf-technology.html

Tribovillard, N., Alego, T.J., Lyons, T., and Riboulleau, A., 2006, Trace metals as paleoredox nd paleoproductivity proxies: An update: Chemical Geology, v. 232, p. 12-32.

Turner, B.W., Tréanton, J.A., and Slatt, R.M., 2016, The Use of Chemostratigraphy to Refine Ambiguous Sequence Stratigraphic Correlations in Marine Shales: An Example From the Woodford Shale, Oklahoma: Journal of the Geological Society, v. 173, p. 854-868.

Velde, B., 2014, 9.12 - Green clay minerals, *in* Holland, H.D., and Turekian, K.K., eds., Treatise on Geochemistry, Elsevier, p. 315-364.

# Appendix 1

# Graphical sedimentary log

Location 6206/2-01

Scale 1:20

Date

Sheet no. 26 of 26

samples, photos | relief | lithology | grain size & bedding | sedimentary structures, fossils, palaeocurrents | colour | description

grain size & bedding

carbonates: mud | W | P | G | R | F | B

clastics: c | s | vf | f | m | c | vc | G

50

51

52

53

54

55

END OF CORE

c s vf f m c vc G
mud W P G R F B

**Graphical sedimentary log**

Location

Scale 1:20

Date

Sheet no. 25 of 26

samples, photos | relief | lithology | grain size & bedding (carbonates: mud | W | P | G | R | F | B; clastics: c | s | vf | f | m | c | vc | G) | sedimentary structures, fossils, palaeocurrents | colour | description

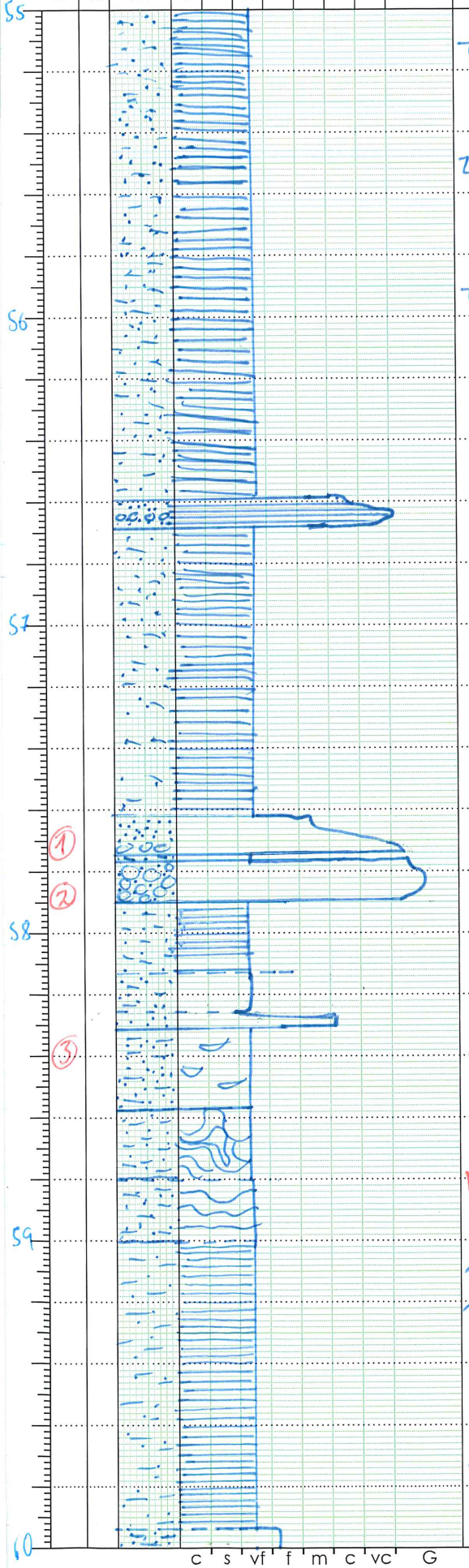


Hard to determine if loading/flame or burrowing.

All thicker sand laminae (0.3 mm) are disturbed/bioturb

Lenticular → sand laminae

Same as below cong at 56.6

Mud ripples

HDT green sand facies, some larger mud clasts ~3 mm

T_t T_B

sand in burrows is white, green, black

Mud ripples

Sand laminae

some more sandy intervals → more bioturb

green sand facies, mud clasts from 0.1-4 cm subangular-subrounded

HDT green conglomerate, poly clasts up to 2 cm in middle & coarsening-fining up

+ green sand

several clear sand burrows in lam mudst + mud ripples

Heavily bioturbated green sand facies + mud + white sand

Green sand facies, dense → Debris flow mudchips - rip up

Green sand facies, sparse mud rip ups, flattened yellow green clasts

Mud flow

coal clast

Deformed sand patch, poorly mixed

sand laminae

Brown/oxidized.

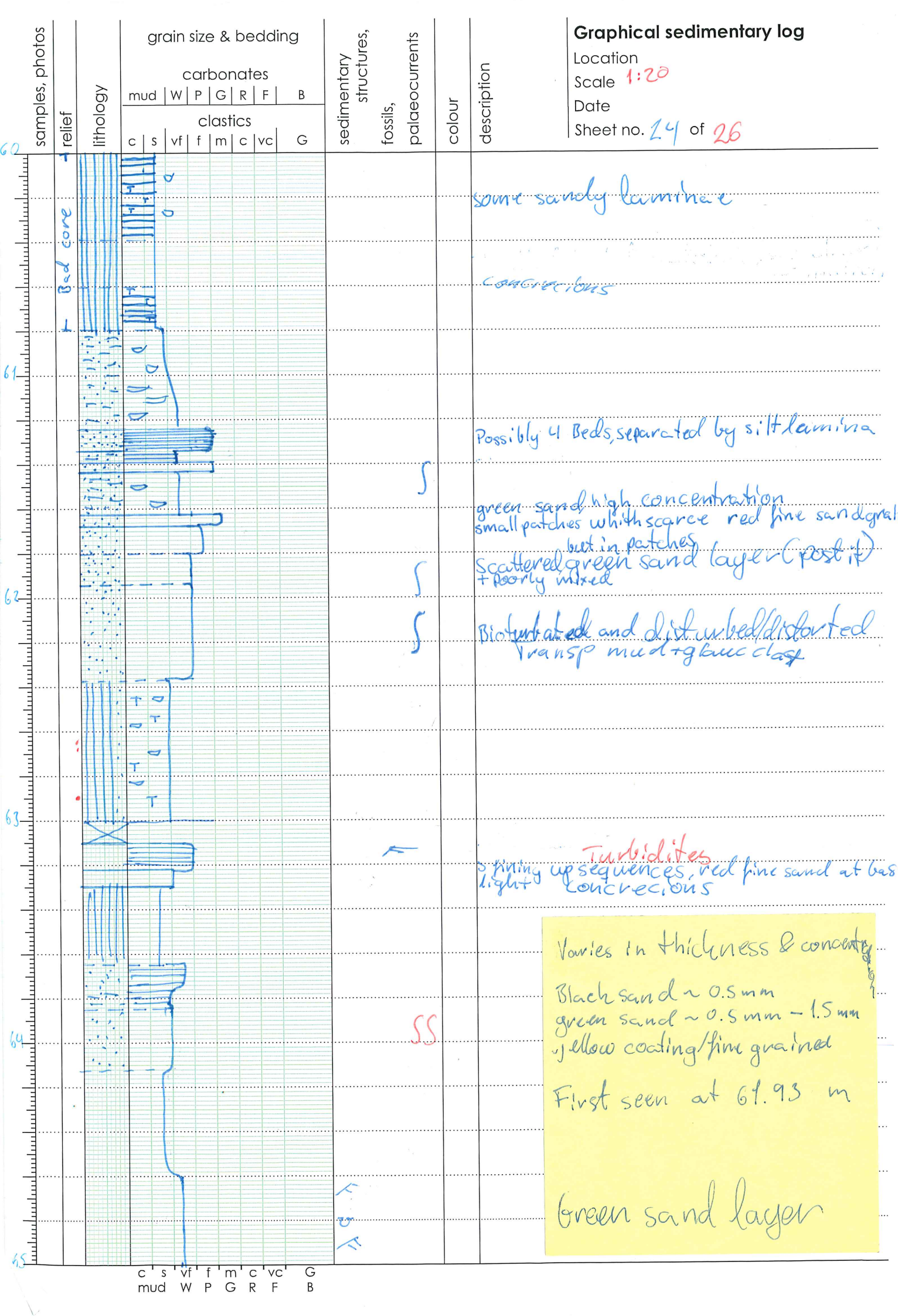
samples, photos
relief
lithology
grain size & bedding
carbonates
mud W P G R F B
clastics
c s vf f m c vc G
sedimentary structures, fossils, palaeocurrents
colour
description
Graphical sedimentary log
Location
Scale 1:20
Date
Sheet no. 24 of 26
60
61
62
63
64
65
Bad core
some sandy laminae
Concretions
Possibly 4 Beds, separated by silt lamina
green sand high concentration
small patches whith scarce red fine sand grains
but in patches
Scattered green sand layer (post it)
+ poorly mixed
Bioturbated and disturbed/distorted
Transp mud + glauc clast
Turbidites
fining up sequences, red fine sand at base
light + Concrecions
Varies in thickness & concentration
Black sand ~ 0.5 mm
green sand ~ 0.5 mm – 1.5 mm
yellow coating/fine grained
First seen at 61.93 m
Green sand layer
c s vf f m c vc G
mud W P G R F B

**Graphical sedimentary log**

Location

Scale 1:20

Date

Sheet no. 23 of 26

samples, photos | relief | lithology | grain size & bedding (carbonates: mud | W | P | G | R | F | B; clastics: c | s | vf | f | m | c | vc | G) | sedimentary structures, fossils, palaeocurrents | colour | description

65

66

67

68

69

70

Mudstone with sand laminae.
Laminae is either thin (0.1–0.3 cm) continous, horizontally or lens shaped.
Ripples are observed in some of the laminae/lenses.

Traction tapering

Mud ripples, silt tapering

Fixed – angle contact?

c mud | s | vf W | f P | m G | c R | vc F | G B

**Graphical sedimentary log**

Location

Scale 1:20

Date

Sheet no. 22 of 26

samples, photos | relief | lithology | grain size & bedding (carbonates: mud | W | P | G | R | F | B; clastics: c | s | vf | f | m | c | vc | G) | sedimentary structures, fossils, palaeocurrents | colour | description

70

sand laminae - discontinous

Disturbed clasts of clay, sand, some oxidized clasts of basal cong? poly (red, green, white clasts) yellow/ tm some clasts oxidizing mudflow matrix-

71

brown with some green/yellow first 20cm of bed

undisturbed 2cm

Heavily disturbed some green material

72

non heterolithic - mud

Disturbed

0.1 - 2cm thick laminae rusty, [clay?] very fine some sand grains observed uneven to even intervals most: 0.1-0.3 mm, one 2cm

First apperance at 74.74

concretion

coarser lamination

2cm

73

74

some sand laminae are horizontal lam, other cross

some lenticular lamination

↳ sand as very thin, uneven or discontinous laminae

scarse

Possible sand ripples ⇒ varying paleocurrent

75

c mud | s W | vf P | f G | m R | c F | vc | G B

• rusty layer - see post it

**Graphical sedimentary log**

Location

Scale 1:20

Date

Sheet no. 21 of 26

samples, photos | relief | lithology | grain size & bedding (carbonates: mud | W | P | G | R | F | B; clastics: c | s | vf | f | m | c | vc | G) | sedimentary structures, fossils, palaeocurrents | colour | description

75

Fod

lighter clast draped (1cm)

Darker or varnish?

76

Partly poorly mixed → debris

clasts up to 3cm

Ichnogenetic pyrite

Partly poorly mixed

77

glauconitic 1cm laminar/boundary

Partly poorly mixed

some glauconitic sand

§§

white, hard, silt

78

Dark grey

Darker than older sediments,

sandy laminations

79

some glauconitic clasts

80

c mud | s W | vf P | f G | m R | c F | vc B | G

**Graphical sedimentary log**

Location

Scale 1:20

Date

Sheet no. 20 of 26

samples, photos | relief | lithology | grain size & bedding (carbonates: mud | W | P | G | R | F | B; clastics: c | s | vf | f | m | c | vc | G) | sedimentary structures, fossils, palaeocurrents | colour | description

80

light brown → Radinite carb

clasts of sandstone

Poorly mixed → SS

some white more cemented laminae esp. to the top

81

SS

SS

white cemented

(4)

82

Not so much SS

some horizontal lamination

some glauconitic laminae

SS

83

SS

bioturbation

some whiter more cemented beds/laminae

poorly mixed

(5)

one ~1cm thick laminae of more cemented SS

84

some lamination

(6)

Fully bioturbated

85

c mud | s | vf W | f P | m G | c R | vc F | G B

**Graphical sedimentary log**

Location

Scale 1:20

Date

Sheet no. 19 of 26

samples, photos | relief | lithology | grain size & bedding (carbonates: mud, W, P, G, R, F, B; clastics: c, s, vf, f, m, c, vc, G) | sedimentary structures, fossils, palaeocurrents | colour | description

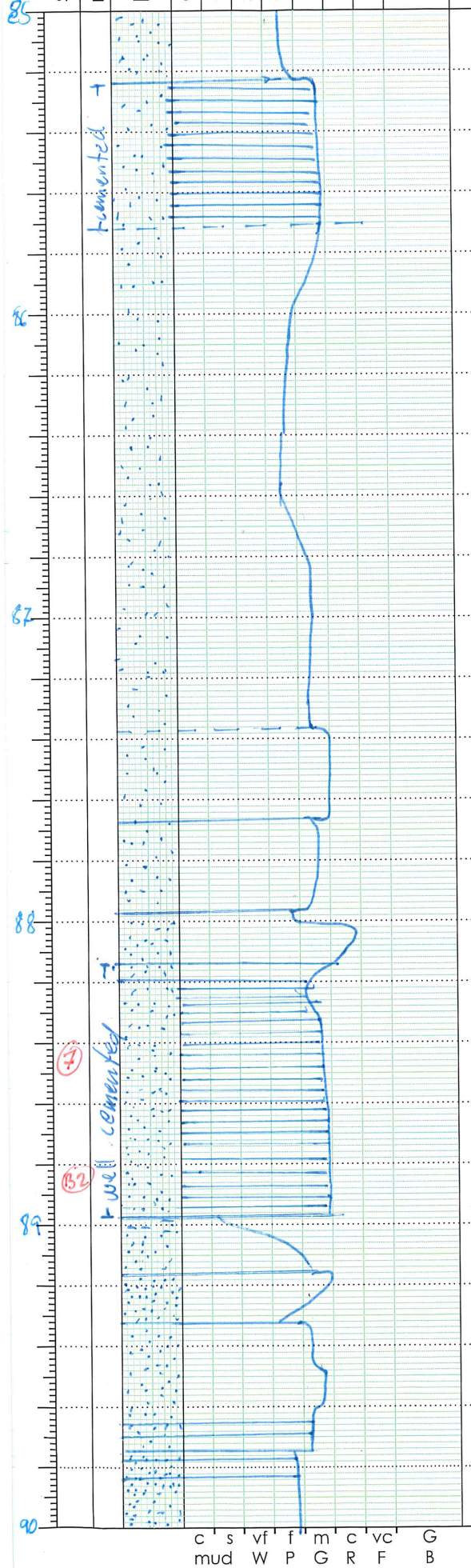


white & green stops

browner towards top
similar to m89-85
more white (quartz?)
green, white, red
poorly mixed?
wavy

not as green
glauco nerals ?

Poorly mixed somewhat
some wavy lamination
silt in sand

green gradually declines (not fully) over 10cm

mainly green, gray clasts of sand/silt varying colour
↓mica
green, white, gray, black specs
Poorly mixed

silt/fine sand clasts towards top
some browner parts, uneven
some lamination, but unclear
one metallic clast ≈2mm (pyrite? detrital?)
continous traction

green white
clasts of sand or massive quartz cemented
+glauconitic sand clasts
0.5 - 5cm
green, white, black grains
Diagenetic glaucon
Pulsation

Poorly mixed
more green
river input

Sheared
Some scattered up to 0.5 cm pebbles
Dilute turbidite
LDT

Poorly mixed
shells fragments
flat boundary
green coating on sand
LDT

Green patches toward top
river input
LDT

**Graphical sedimentary log**

Location

Scale 1:20

Date

Sheet no. 18 of 26

samples, photos | relief | lithology | grain size & bedding (carbonates: mud | W | P | G | R | F | B; clastics: c | s | vf | f | m | c | vc | G) | sedimentary structures, fossils, palaeocurrents | colour | description

90

Poorly mixed Muddy debrite

Poly, up to 0.6cm clast supp Poorly mixed

Polymict up to 4cm clasts, subangular

Sand patches matrix supp

3cm intervals x2 with blasts, green, red

mud flows

wedge with fossils & clasts ~ 1cm thick

91

Rip up ? green patches, angular, reel clasts

green sand clasts

Poorly mixed, green sand patches

carbonate clast at top ? 0.4cm long

greenish clasts 5cm marlish mess, crusted clasts

outlaw, lighter

Poorly mixed

(33)

Cracked iron concretion

92

carbonate, black mudstone river

injectite input

(8)

ripup

mudflow

Poorly mixed ?, green clasts

Diagenetic iron

Nicely filled furrow

93

Poly,

River input

94

clasts, mudflow

Sand blobs - round >3cm

Rusty clasts, greener patches w/corona ~0.5cm

calcite laminae

green towards top

95

c s vf f m c vc G

mud W P G R F B

# Graphical sedimentary log

Location

Scale 1:20

Date

Sheet no. 17 of 26

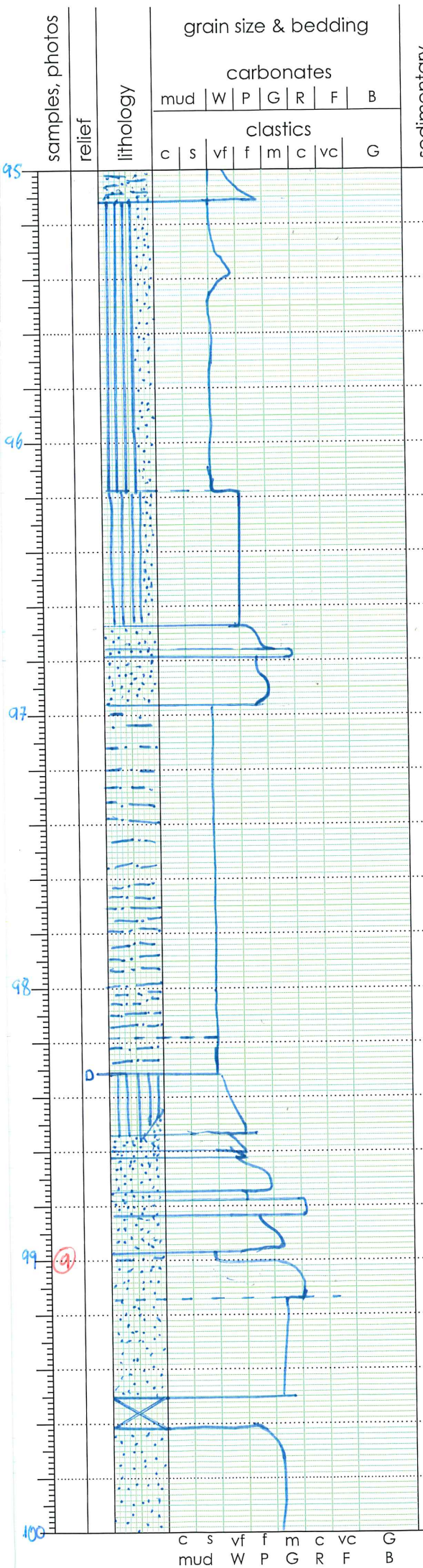


green

Red coating on clasts 0.5 - 2 cm

green patches

Red coated clast ~0.8 cm

event concretion

river input

Red and green coated patches - clasts

Hemipelagic

green coated sand in patch

Brownen, sandy silt

# Graphical sedimentary log

Location

Scale 1:20

Date

Sheet no. 16 of 26

samples, photos | relief | lithology | grain size & bedding | sedimentary structures, fossils, palaeocurrents | colour | description

grain size & bedding

carbonates: mud | W | P | G | R | F | B

clastics: c | s | vf | f | m | c | vc | G

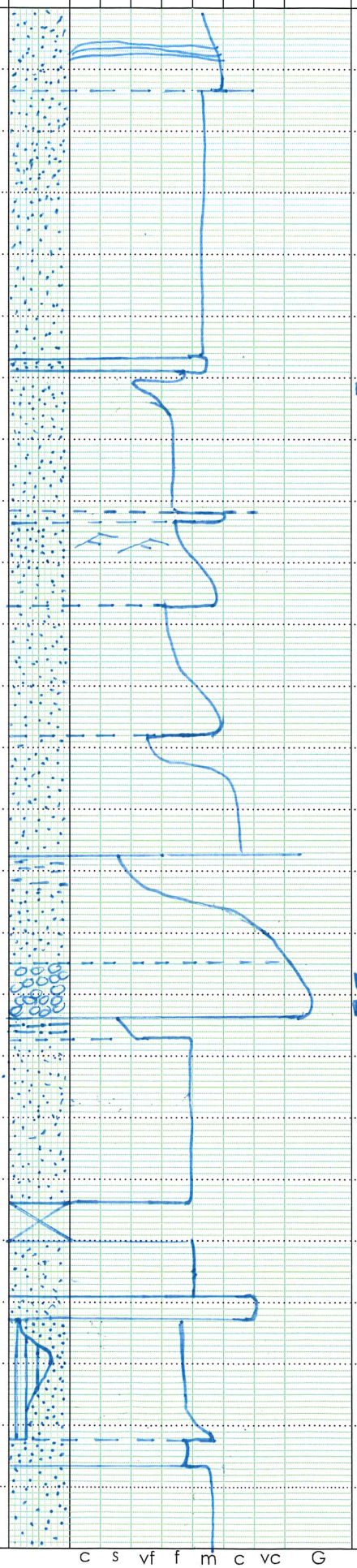


Green Brown — LDT Green med sand laminae in white f sand → Discontinuous; pyrite coated

HDT

HDT

HDT
1 clast ~ 5 cm, Immature, poorly sorted

HDT

coal clasts ~ 3 cm, matrix supported/pebbly sandstone

Brown, browner upwards from 103.40

Pyrite coated clasts ~ 4 mm

river input

S

Immature HDT

Poorly mixed mud/ss hemipelagic

Turbidite, $T_4$

**Graphical sedimentary log**

Location

Scale 1:20

Date

Sheet no. 15 of 26

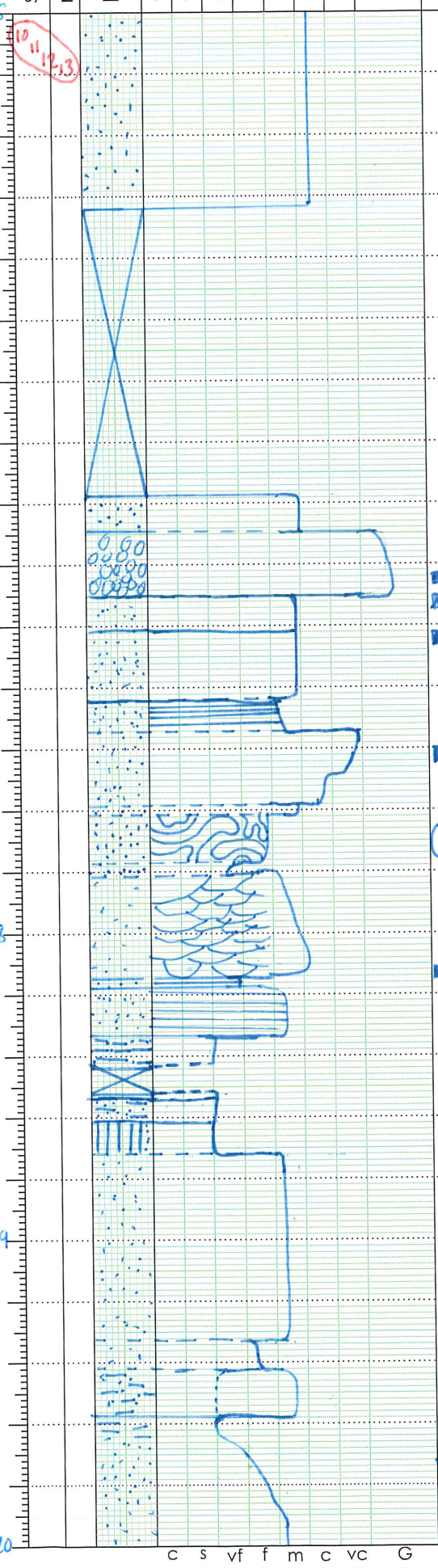


Well cemented
gradual transition from gray to brown at ~ 105.40

HDT
~1 cm clasts, pdy, poorly consolidated
4cm coal clast
Brown coal clasts and specks
coal, 3cm thick river input

LDT

Immature texturally, grain size silt to vc sand
coal layer - clast, metallic clast 1.5 cm
HDT +specks

Turbidite, cut & fill
Park, from f/m to c sand

coal

Brown, sandy siltstone

Pyrite

Brown, sdy silt/silty sand, poorly mixed? mudflow?
green, gray towards topp mudflow
Poorly mixed

input dependent (river)

**Graphical sedimentary log**

Location

Scale 1:20

Date

Sheet no. 14 of 26

samples, photos | relief | lithology | grain size & bedding (carbonates: mud | W | P | G | R | F | B; clastics: c | s | vf | f | m | c | vc | G) | sedimentary structures, fossils, palaeocurrents | colour | description

110

Poorly mixed
Coal laminae — input dependent

111

coal specks — Hyperpycnite

one brown 1cm laminae

Browning up — hemipelagic

112

Browning up — brown grains
coal?, thin, needles ↳ iron, pyrite coating
Rip up? / reworked? HDT

113

Darker

pebbles at boundary poorly mixed, silt to c sand
coal streaks / specks
clasts horizontally alligned at top 5cm
matrix supported, polymict, less than 2cm HDT
clast supported at base

114

Poorly mixed, clay size to vc sand

Patchy sandstone

coarse sand scattered

115

Wearly mixed debris

c s vf f m c vc G
mud W P G R F B

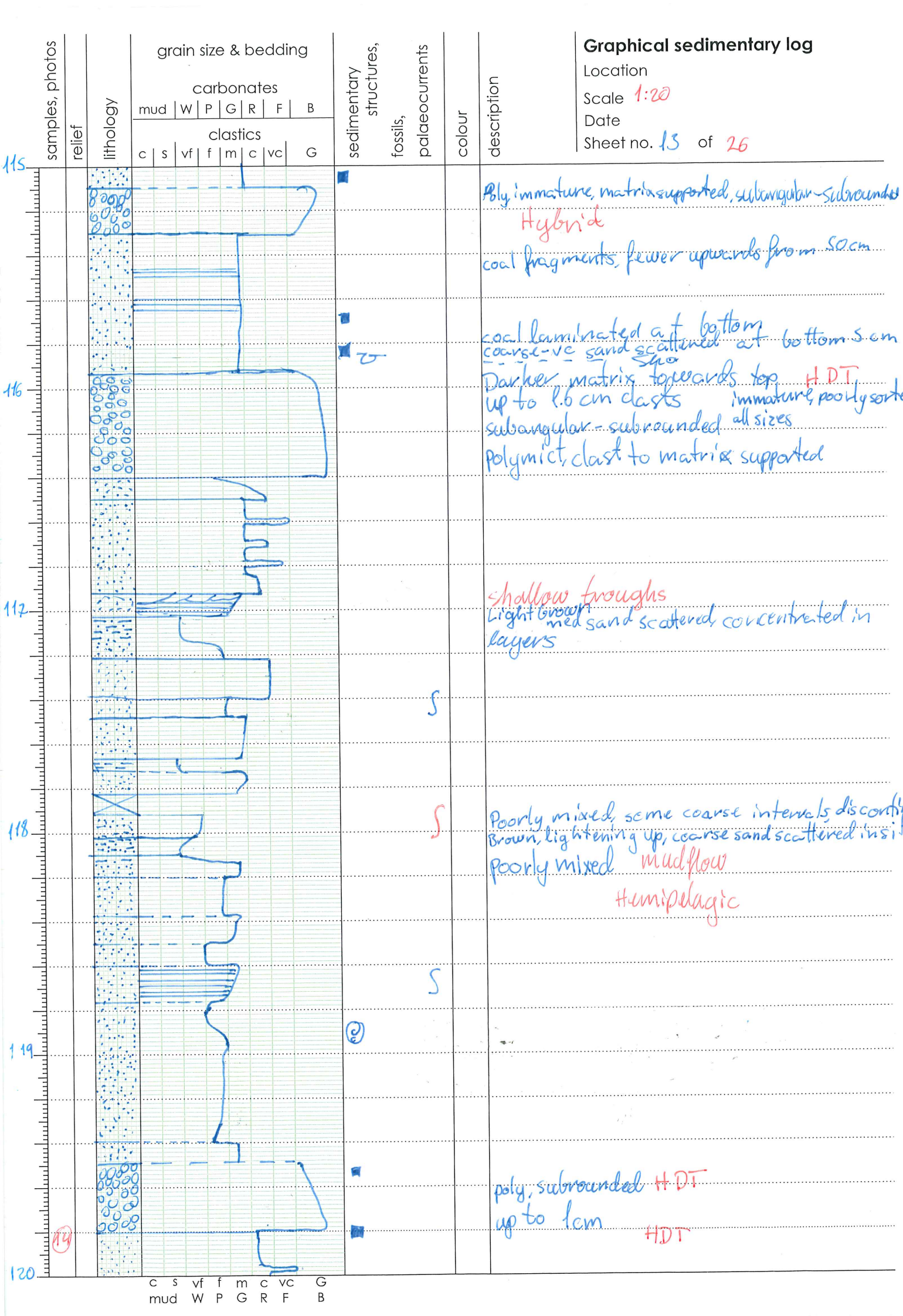
samples, photos
relief
lithology
grain size & bedding
carbonates
mud W P G R F B
clastics
c s vf f m c vc G
sedimentary structures, fossils, palaeocurrents
colour
description
Graphical sedimentary log
Location
Scale 1:20
Date
Sheet no. 13 of 26
115
116
117
118
119
120
Poly; immature, matrix supported, subangular-subrounded
Hybrid
coal fragments, fewer upwards from 50cm
coal laminated at bottom
coarse-ve sand scattered at bottom 5cm
Darker matrix towards top
HDT
up to 1.6 cm clasts
immature, poorly sorted
subangular-subrounded
all sizes
polymict, clast to matrix supported
shallow troughs
Light brown
med sand scattered, concentrated in layers
Poorly mixed, some coarse intervals disorder
Brown, lightening up, coarse sand scattered in sit
poorly mixed
mudflow
hemipelagic
poly, subrounded
HDT
up to 1cm
HDT
c s vf f m c vc G
mud W P G R F B

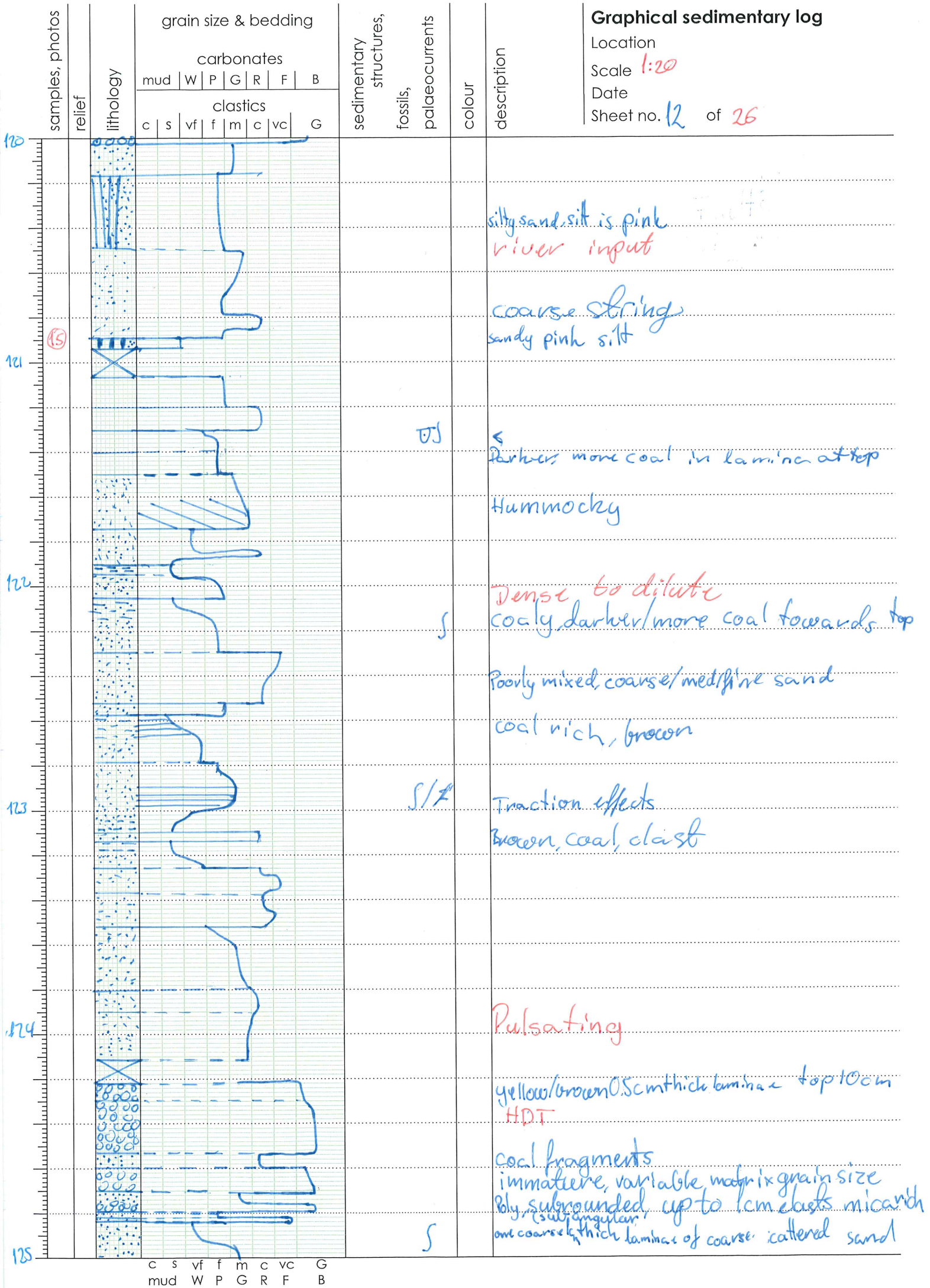
samples, photos
relief
lithology
grain size & bedding
carbonates
mud W P G R F B
clastics
c s vf f m c vc G
sedimentary structures, fossils, palaeocurrents
colour
description
Graphical sedimentary log
Location
Scale 1:20
Date
Sheet no. 12 of 26
120
121
122
123
124
125
15
silty sand, silt is pink
river input
coarse string
sandy pink silt
UJ
darker, more coal in lamina at top
Hummocky
Dense to dilute
coaly, darker/more coal towards top
Poorly mixed, coarse/medium sand
coal rich, brown
S/T
Traction effects
brown, coal, clast
Pulsating
yellow/brown 0.5cm thick laminae top 10cm
HDT
coal fragments
immature, variable matrix grain size
poly, subrounded, (sub) angular, up to 1cm clasts mica rich
one coarse, thick laminae of coarse scattered sand
S
c s vf f m c vc G
mud W P G R F B

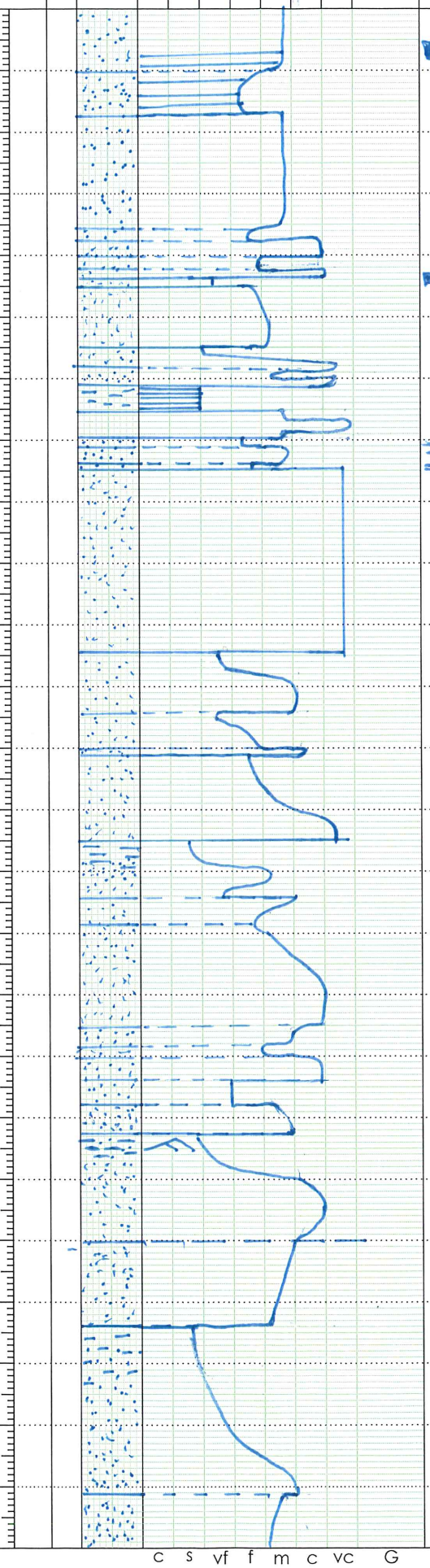


**Graphical sedimentary log**

Location

Scale 1:20

Date

Sheet no. 11 of 26

one cm thick laminae with coarse sand

one cm thic laminae with coarse, angular sand

Poorly mixed

coaly laminae

Debrite

Poorly mixed med sand/fine sand

Brown/pink

Turbidites

HDT

Browner towards top

Porous, silt inbetween, poorly concolidated

Browner, mud flow

Poorly mixed (slump-debris)

Debritic underflow

coal fragments

Dense to dilute

coal fragments

somewhat laminated Hemipelagic

coaly-fragments

Debris flows

Brown top 8 cm

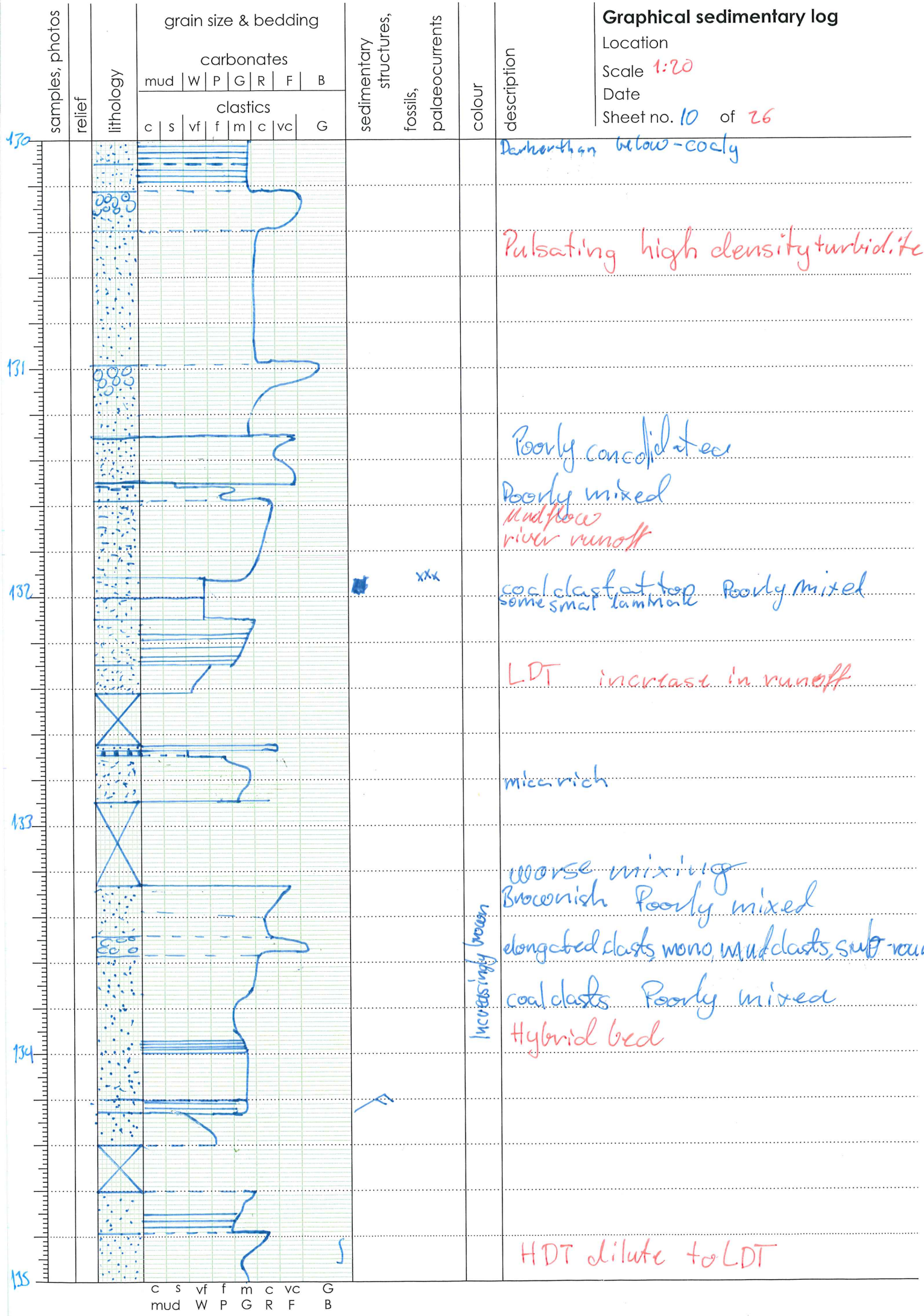
samples, photos
relief
lithology
grain size & bedding
carbonates
mud W P G R F B
clastics
c s vf f m c vc G
sedimentary structures, fossils, palaeocurrents
colour
description
Graphical sedimentary log
Location
Scale 1:20
Date
Sheet no. 10 of 26
130
131
132
133
134
135
Darker than below - coaly
Pulsating high density turbidite
Poorly consolidated
Poorly mixed
Mudflow
river runoff
xxx
coal clast at top
some small laminae
Poorly mixed
LDT
increase in runoff
mica rich
worse mixing
Brownish
Poorly mixed
elongated clasts mono, mudclasts, sub-rounded
coal clasts
Poorly mixed
Hybrid bed
HDT dilute to LDT
increasingly brown
c s vf f m c vc G
mud W P G R F B

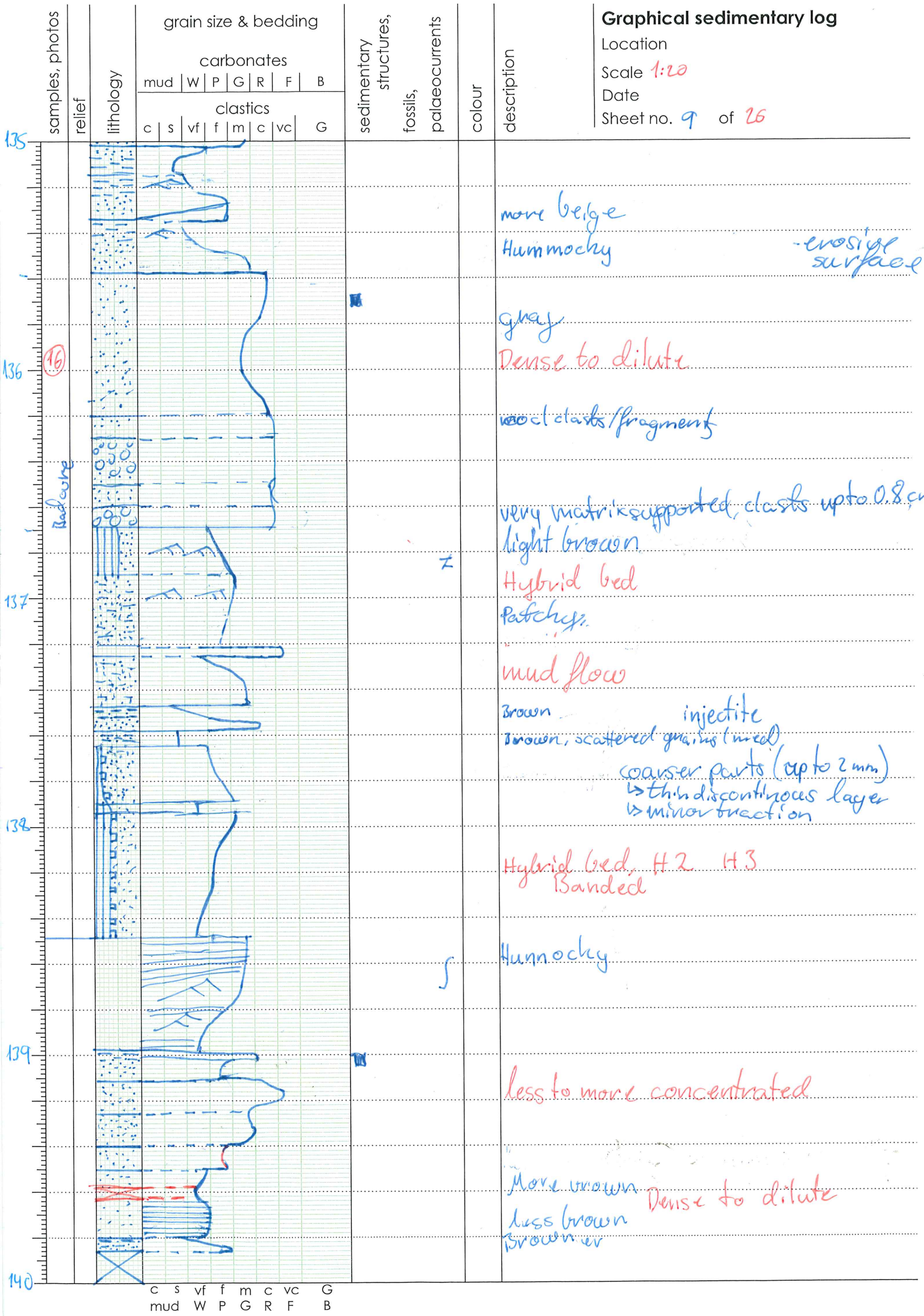
samples, photos
relief
lithology
grain size & bedding
carbonates
mud W P G R F B
clastics
c s vf f m c vc G
sedimentary structures, fossils, palaeocurrents
colour
description
Graphical sedimentary log
Location
Scale 1:20
Date
Sheet no. 9 of 26
135
136
137
138
139
140
16
Radiolaria
more beige
Hummocky
-erosive surface
gray
Dense to dilute
rare clasts/fragments
very matrixsupported, clasts up to 0.8 cm
light brown
Hybrid bed
Patchy
mud flow
Brown
injectite
Brown, scattered grains (mixed)
coarser parts (up to 2 mm)
→ thin discontinous layer
→ minor fraction
Hybrid bed, H2 H3
Banded
Hummocky
less to more concentrated
More brown
Dense to dilute
less brown
brownier
c s vf f m c vc G
mud W P G R F B

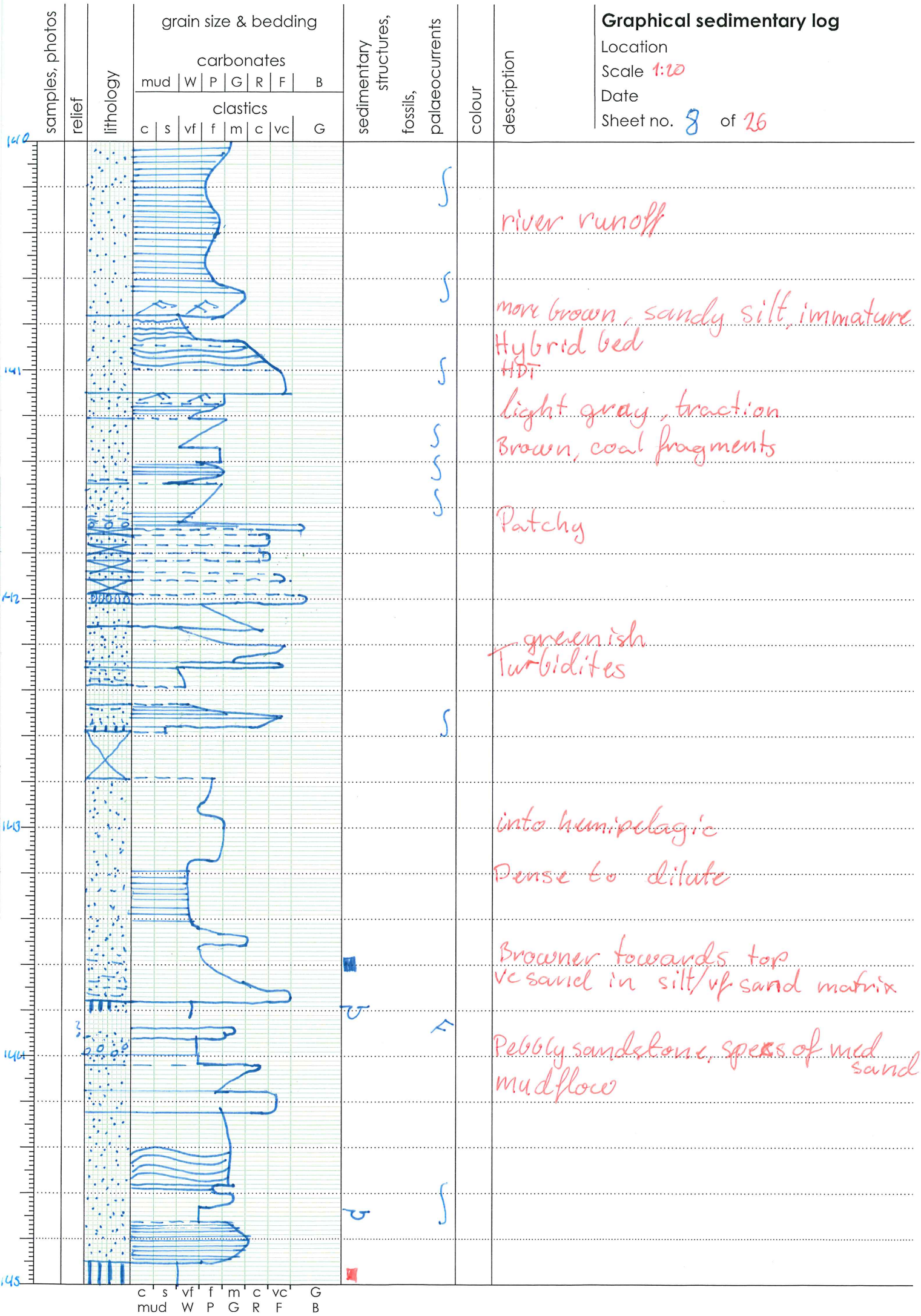
samples, photos
relief
lithology
grain size & bedding
carbonates
mud W P G R F B
clastics
c s vf f m c vc G
sedimentary structures, fossils, palaeocurrents
colour
description
Graphical sedimentary log
Location
Scale 1:20
Date
Sheet no. 8 of 26
140
141
142
143
144
145
river runoff
more brown, sandy silt, immature
Hybrid bed
HBT
light gray, traction
Brown, coal fragments
Patchy
greenish
Turbidites
into hemipelagic
Dense to dilute
Browner towards top
vc sand in silt/vf sand matrix
Pebbly sandstone, specks of mud
sand
mudflow
c s vf f m c vc G
mud W P G R F B

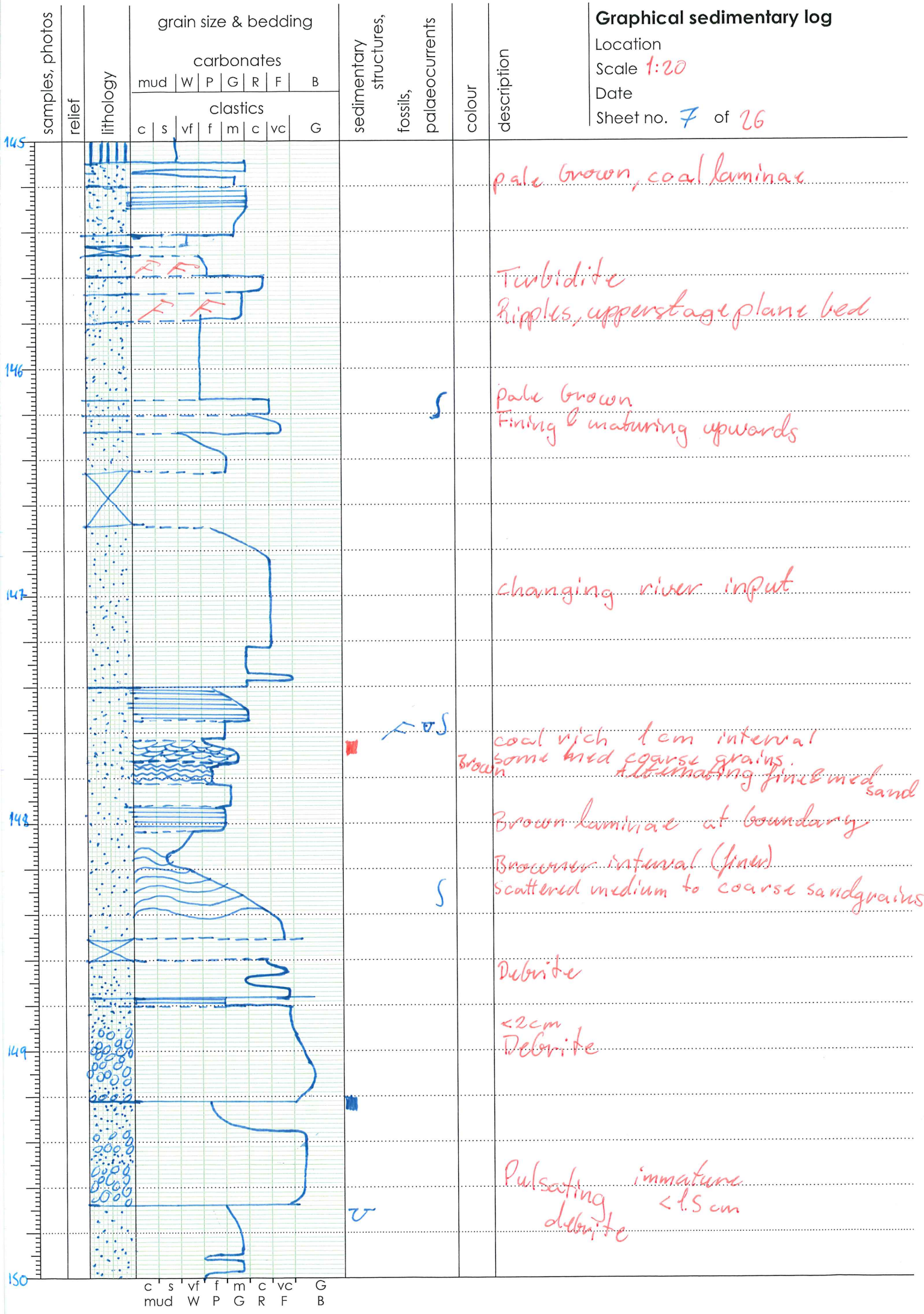
samples, photos
relief
lithology
grain size & bedding
carbonates
mud W P G R F B
clastics
c s vf f m c vc G
sedimentary structures, fossils, palaeocurrents
colour
description
Graphical sedimentary log
Location
Scale 1:20
Date
Sheet no. 7 of 26
145
146
147
148
149
150
pale brown, coal laminae
Turbidite
Ripples, upper stage plane bed
pale brown
Fining & maturing upwards
changing river input
coal rich 1cm interval
some med coarse grains
brown
alternating fine med sand
Brown laminae at boundary
Brown inter val (finer)
scattered medium to coarse sandgrains
Debrite
<2cm
Debrite
Pulsating debrite
immature
<1.5cm
c s vf f m c vc G
mud W P G R F B

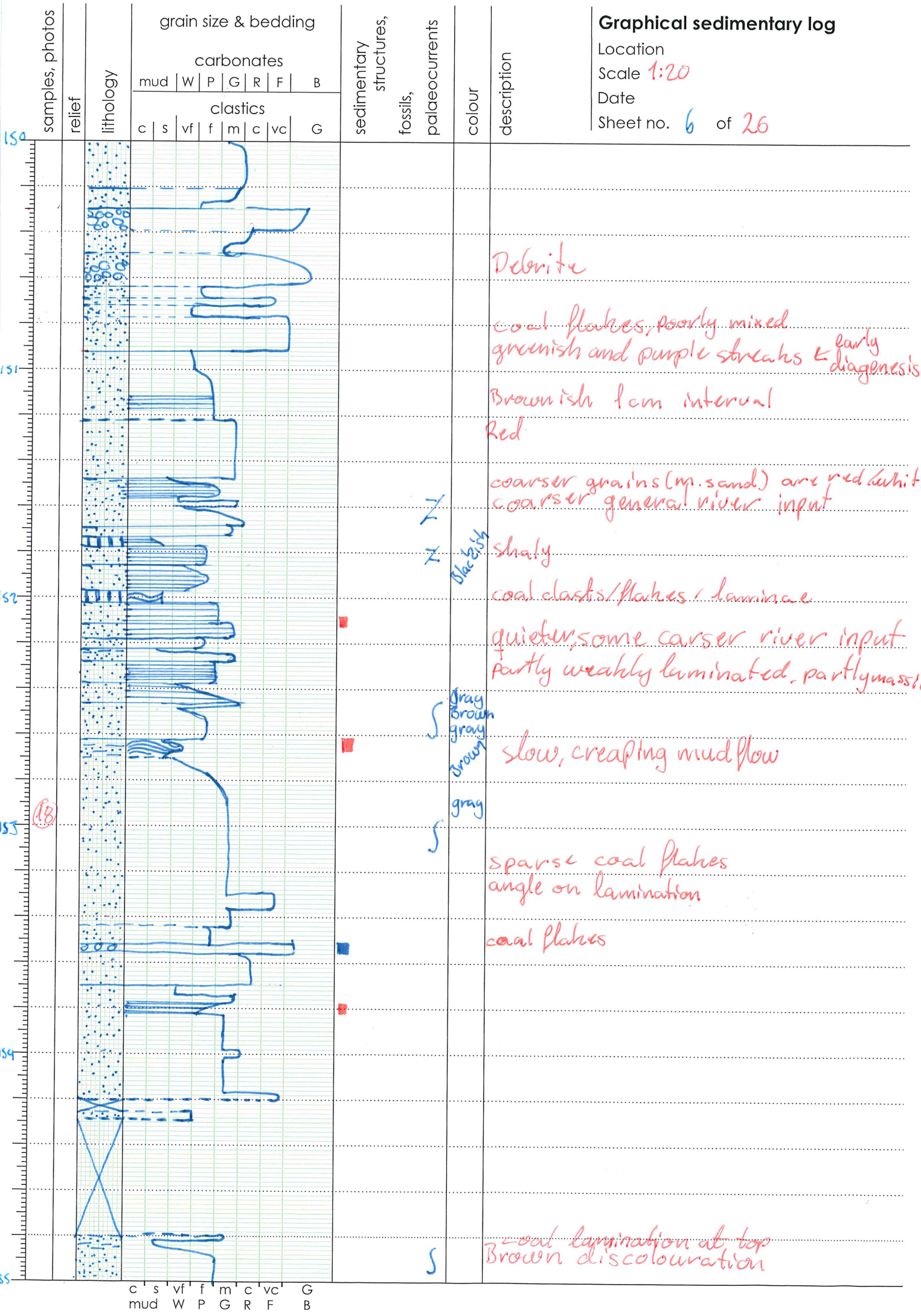
samples, photos
relief
lithology
grain size & bedding
carbonates
mud W P G R F B
clastics
c s vf f m c vc G
sedimentary structures, fossils, palaeocurrents
colour
description
Graphical sedimentary log
Location
Scale 1:20
Date
Sheet no. 6 of 26
150
151
152
153
154
155
18
Debrite
coal flakes, poorly mixed
greenish and purple streaks ← early diagenesis
Brownish 1cm interval
Red
coarser grains (m. sand) are red/white
coarser general river input
shaly
Blackish
coal clasts/flakes / laminae
quieter, some carser river input
partly weakly laminated, partly massive
gray
brown
gray
brown
gray
slow, creaping mud flow
sparse coal flakes
angle on lamination
coal flakes
coal lamination at top
Brown discolouration
c s vf f m c vc G
mud W P G R F B

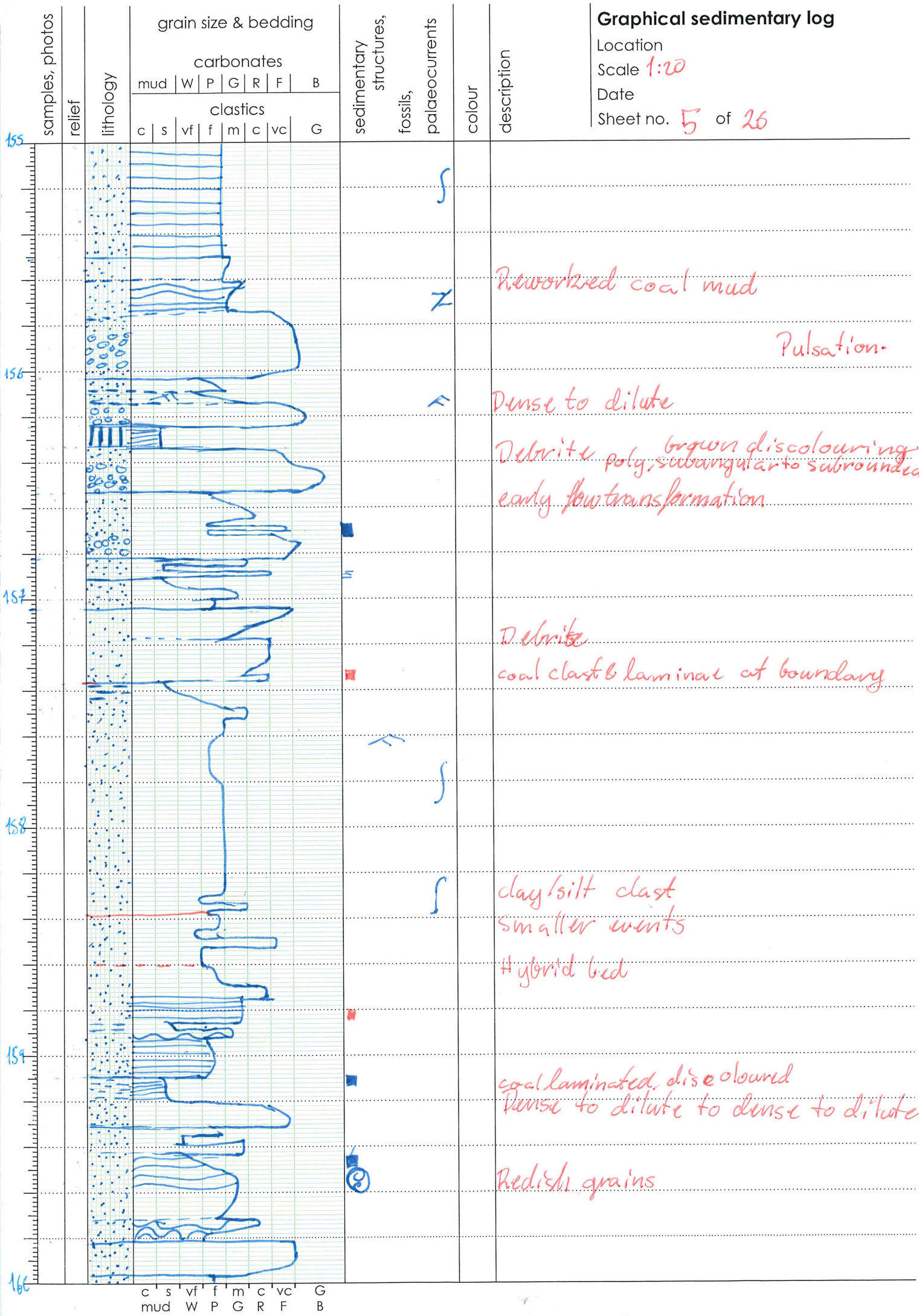
samples, photos
relief
lithology
grain size & bedding
carbonates
mud W P G R F B
clastics
c s vf f m c vc G
sedimentary structures, fossils, palaeocurrents
colour
description
Graphical sedimentary log
Location
Scale 1:20
Date
Sheet no. 5 of 26
155
156
157
158
159
160
Reworked coal mud
Pulsation.
Dense to dilute
Debrite poly, brown discolouring subangular to subrounded
early flow transformation
Debrite
coal clast & laminae at boundary
clay/silt clast
smaller units
Hybrid bed
coal laminated, discoloured
Dense to dilute to dense to dilute
Reddish grains
c s vf f m c vc G
mud W P G R F B

**Graphical sedimentary log**

Location

Scale 1:20

Date

Sheet no. 4 of 26

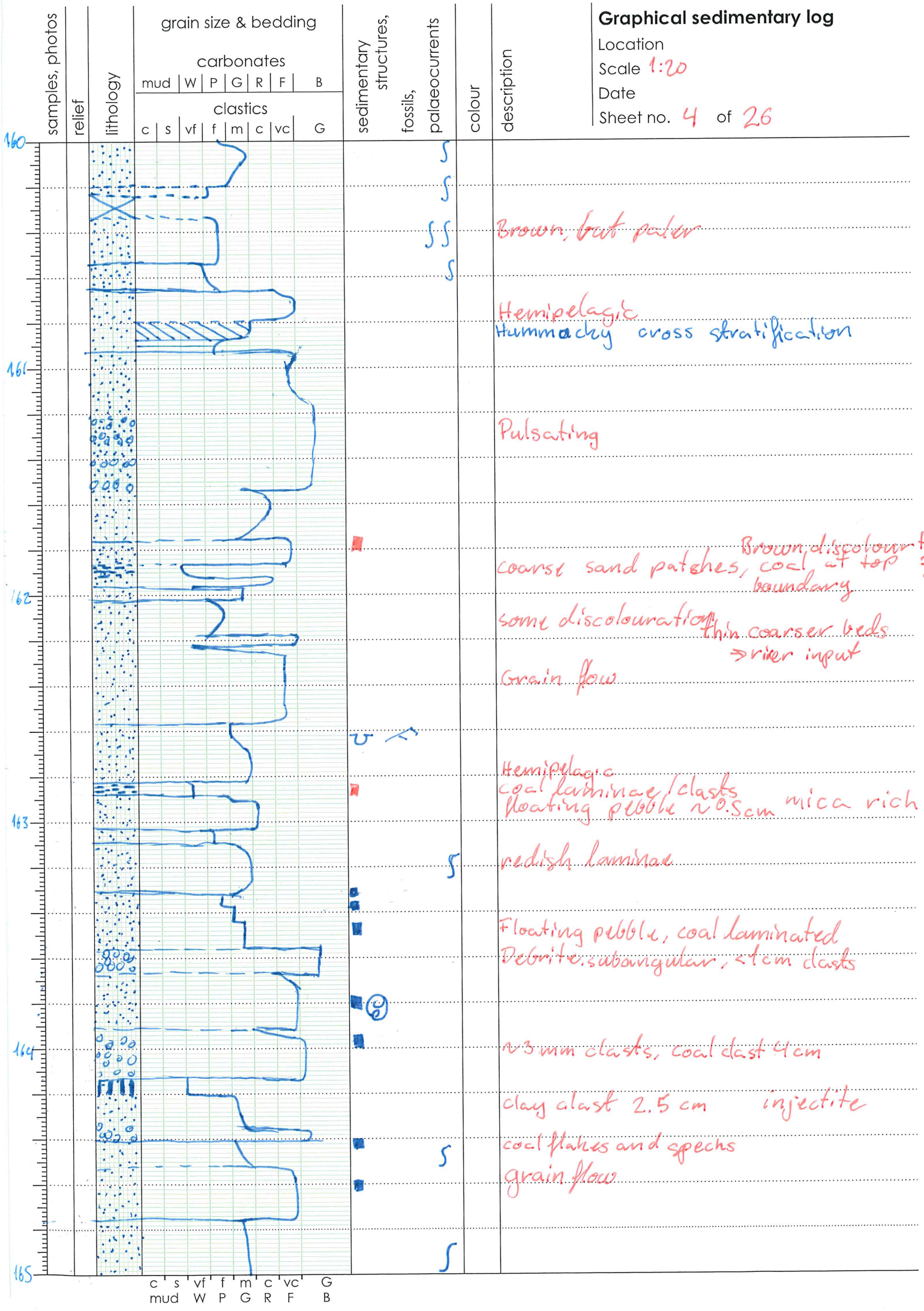

**Graphical sedimentary log**

Location

Scale 1:20

Date

Sheet no. 3 of 26

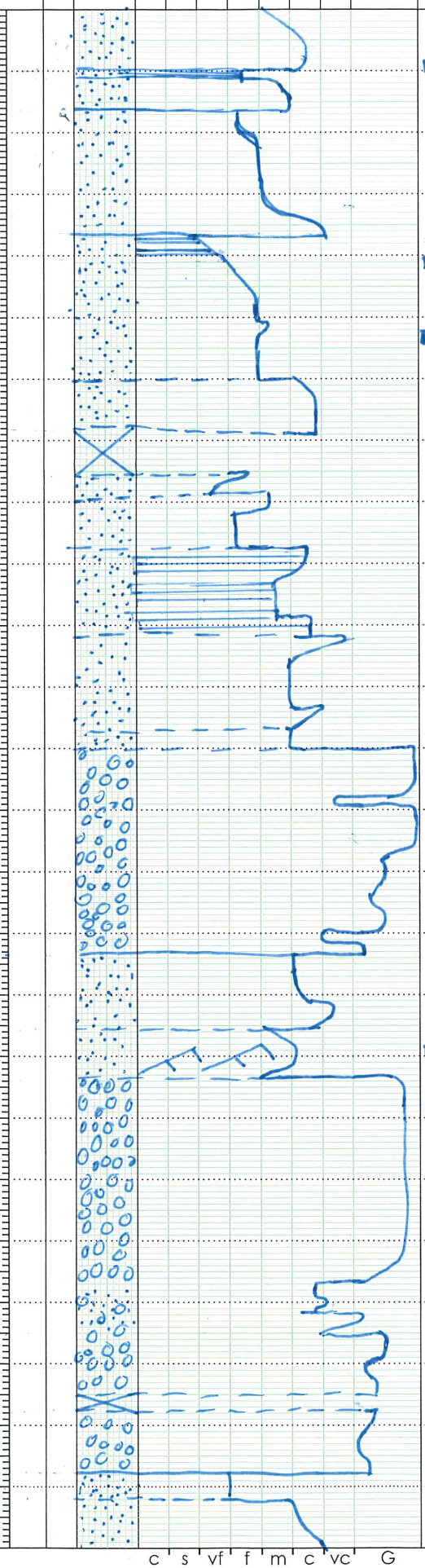


turbidites, repeated events
coal fragment and laminae

colour varies between redish, dark gray and light gray

some coal laminae, discontinous

gray

Redish

Debrite to dilute
well concollidated

alternating clast-matrix dominated
polymict clasts up to 3 cm

coal clasts and laminae

Large coal clast 2cm

Debrite with dilute upper part

polymict, angular to subangular
coal fragments
some clasts (up to 2cm), well rounded

Alternating clast-matrix dominated
polymict, rounded to subangular

micarich, some lamination

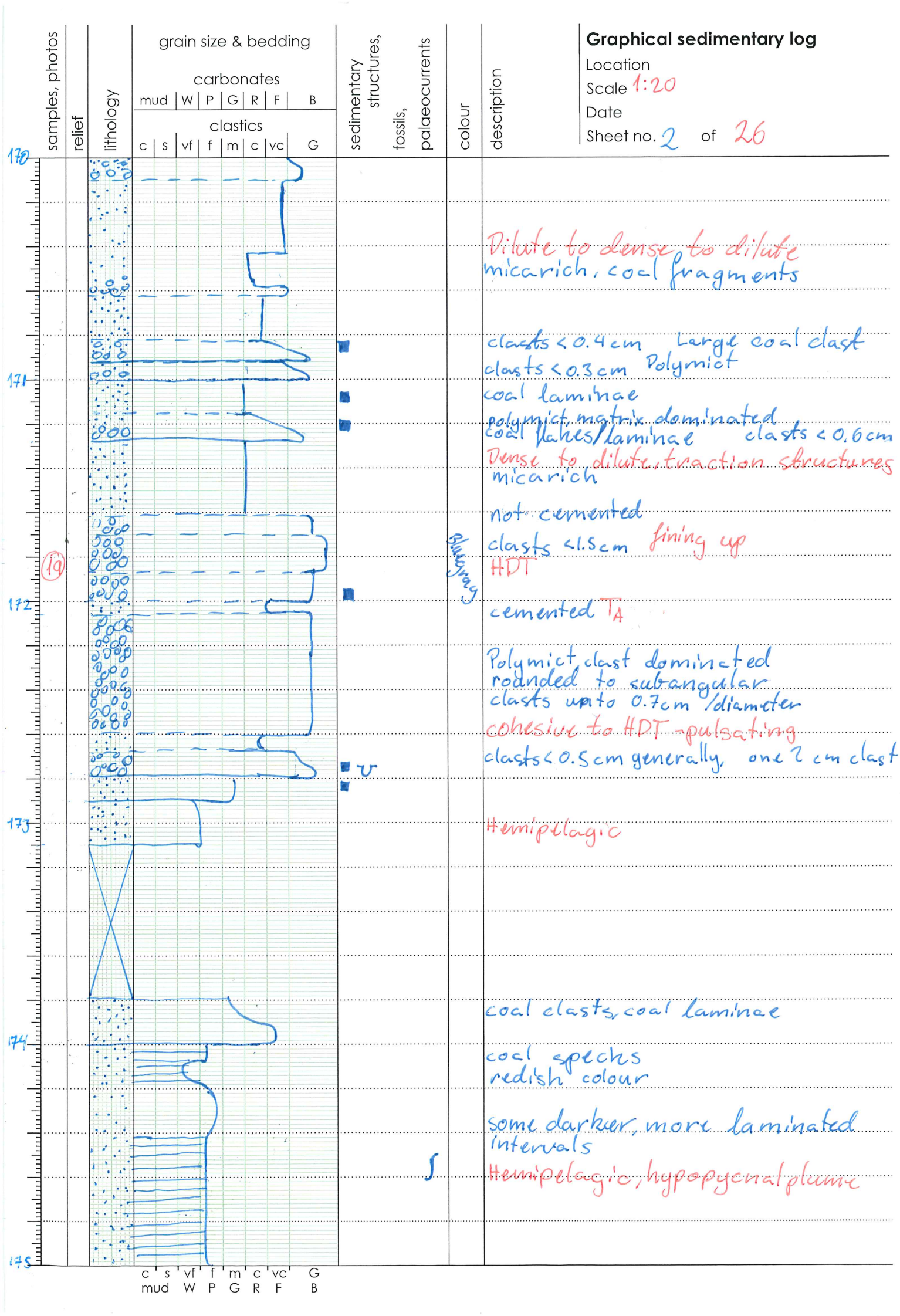
samples, photos
relief
lithology
grain size & bedding
carbonates
mud W P G R F B
clastics
c s vf f m c vc G
sedimentary structures, fossils, palaeocurrents
colour
description
Graphical sedimentary log
Location
Scale 1:20
Date
Sheet no. 2 of 26
170
171
172
173
174
175
19
Dilute to dense to dilute
micarich, coal fragments
clasts < 0.4cm Large coal clast
clasts < 0.3cm Polymict
coal laminae
polymict matrix dominated
coal flakes/laminae clasts < 0.6cm
Dense to dilute, traction structures
micarich
not cemented
clasts < 1.5cm fining up
HDT
Blue-grey
cemented TA
Polymict clast dominated
rounded to subangular
clasts up to 0.7cm /diameter
cohesive to HDT - pulsating
clasts < 0.5cm generally, one 2 cm clast
Hemipelagic
coal clasts, coal laminae
coal specks
redish colour
some darker, more laminated
intervals
Hemipelagic, hypopygenal plume

**Graphical sedimentary log**

Location 2606/2-U1

Scale 1:20

Date

Sheet no. 1 of 26

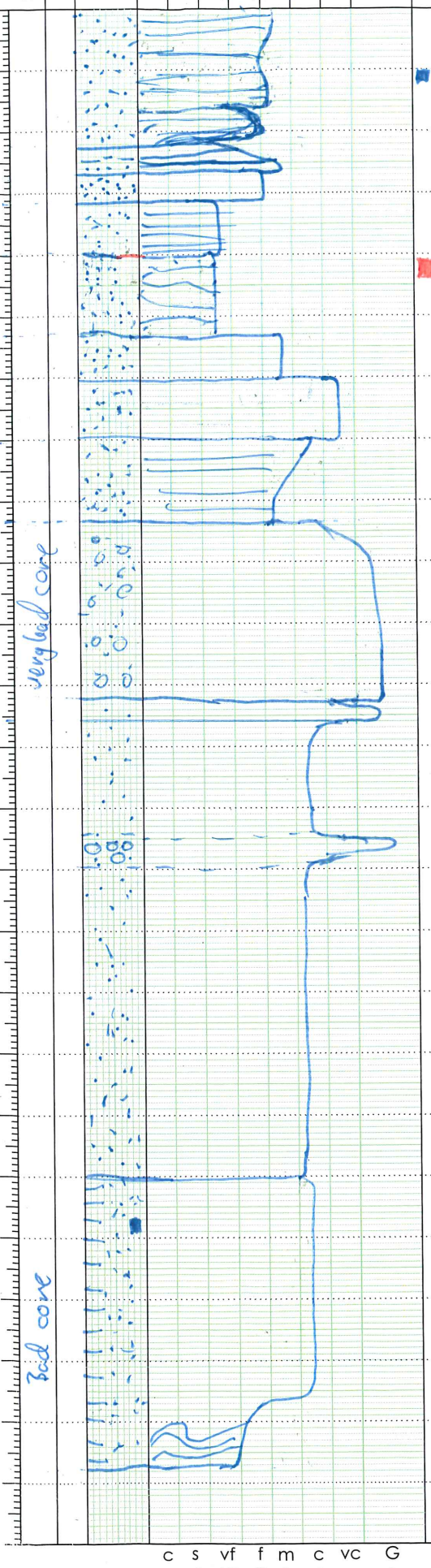


coal fragments, clasts <1mm & 1.5 x 0.2cm

Pulsating turbidite, $T_D$

coal towards top, brown discolouring

some strange structures

draping

pebbles on bottom

coal clast at top

coal laminae

some coarser grains

More red towards the top

some black clasts

very porous - less fine fraction

higher angle on lamination

HDT

unconsolidated, polymict

sandy with some pebbles

some coarser intervals, no clear boundary

some pebbles, polymict

HDT

very varying grain size mud to vcs

coal clast, wood

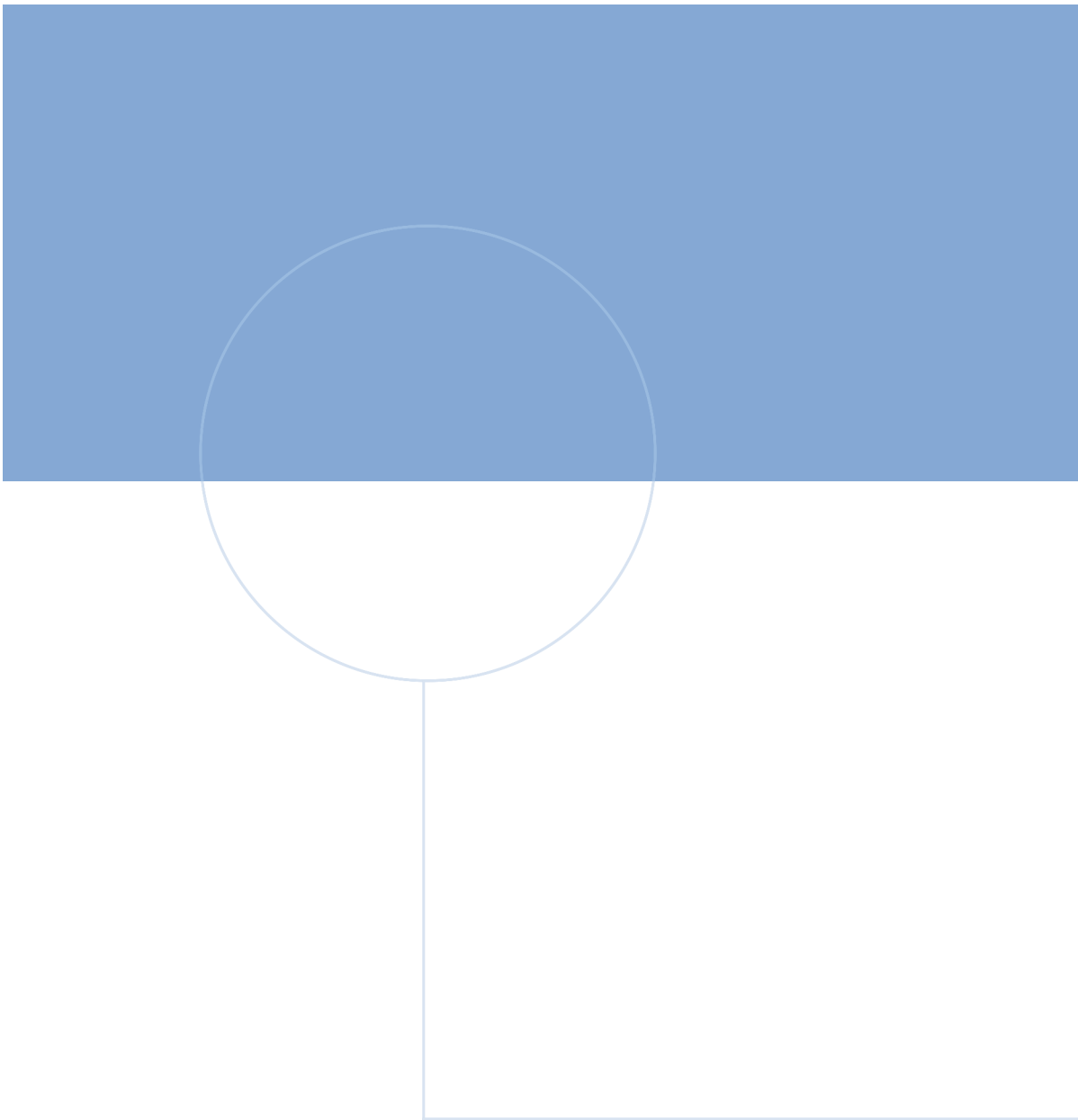

NTNU

Norwegian University of
Science and Technology